NANOPARTICLES AS REACTIVE PRECURSORS: SYNTHESIS OF ALLOYS, INTERMETALLIC COMPOUNDS AND MULTI-METAL OXIDES THROUGH LOW-TEMPERATURE ANNEALING AND CONVERSION CHEMISTRY

A Dissertation

by

JOHN CHRISTOPHER BAUER

Submitted to the Office of Graduate Studies of
Texas A&M University
in partial fulfillment of the requirements for the degree of

DOCTOR OF PHILOSOPHY

May 2009

Major Subject: Chemistry

NANOPARTICLES AS REACTIVE PRECURSORS: SYNTHESIS OF ALLOYS, INTERMETALLIC COMPOUNDS AND MULTI-METAL OXIDES THROUGH LOW-TEMPERATURE ANNEALING AND CONVERSION CHEMISTRY

A Dissertation

by

JOHN CHRISTOPHER BAUER

Submitted to the Office of Graduate Studies of
Texas A&M University
in partial fulfillment of the requirements for the degree of

DOCTOR OF PHILOSOPHY

Approved by:

Co-Chairs of Committee,	Raymond Schaak
	Abraham Clearfield
Committee Members,	Marcetta Darensbourg
	Joseph Ross
Head of Department,	David H. Russell

May 2009

Major Subject: Chemistry

ABSTRACT

Nanoparticles as Reactive Precursors: Synthesis of Alloys, Intermetallic Compounds, and Multi-Metal Oxides Through Low-Temperature Annealing and Conversion Chemistry. (May 2009)

John Christopher Bauer, B.S., Louisiana Tech University

Co-Chairs of Advisory Committee: Dr. Raymond E. Schaak
Dr. Abraham Clearfield

Alloys, intermetallic compounds and multi-metal oxides are generally made by traditional solid-state methods that often require melting or grinding/pressing powders followed by high temperature annealing (> 1000 °C) for days or weeks. The research presented here takes advantage of the fact that nanoparticles have a large fraction of their atoms on the surface making them highly reactive and their small size virtually eliminates the solid-solid diffusion process as the rate limiting step. Materials that normally require high temperatures and long annealing times become more accessible at relatively low-temperatures because of the increased interfacial contact between the nanoparticle reactants.

Metal nanoparticles, formed via reduction of metal salts in an aqueous solution and stabilized by PVP (polyvinylpyrrolidone), were mixed into nanoparticle composites in stoichometric proportions. The composite mixtures were then annealed at relatively low temperatures to form alloy and intermetallic compounds at or below 600 °C. This method was further extended to synthesizing multi-metal oxide systems by annealing

metal oxide nanoparticle composites hundreds of degrees lower than more traditional methods.

Nanoparticles of Pt (supported or unsupported) were added to a metal salt solution of tetraethylene glycol and heated to obtain alloy and intermetallic nanoparticles. The supported intermetallic nanoparticles were tested as catalysts and PtPb/Vulcan XC-72 showed enhanced catalytic activity for formic acid oxidation while Pt_3Sn/Vulcan XC-72 and $Cu_3Pt/\gamma\text{-}Al_2O_3$ catalyzed CO oxidiation at lower temperatures than supported Pt.

Intermetallic nanoparticles of Pd were synthesized by conversion chemistry methods previously mentioned and were supported on carbon and alumina. These nanoparticles were tested for Suzuki cross-coupling reactions. However; the homocoupled product was generally favored. The catalytic activity of $Pd_3Pb/\gamma\text{-}Al_2O_3$ was tested for the Heck reaction and gave results comparable to $Pd/\gamma\text{-}Al_2O_3$ with a slightly better selectivity.

Conversion chemistry techniques were used to convert Pt nanocubes into Pt-based intermetallic nanocrystals in solution. It was discovered that aggregated clusters of Pt nanoparticles were capable of converting to $FePt_3$; however, when Pt nanocubes were used the intermetallic phase did not form. Alternatively, it was possible to form PtSn nanocubes by a conversion reaction with $SnCl_2$.

ACKNOWLEDGEMENTS

I would like to thank my advisor and committee co-chair Dr. Schaak for his guidance and support throughout my research. I would also like to extend thanks to my committee co-chair Dr. Clearfield, my committee members Dr. Darensbourg and Dr. Ross for their useful insight and sponsorship.

I am also thankful for my professors in The Chemistry Department at Texas A&M who helped to give me a strong foundation and basic knowledge to succeed. I would especially like to thank Xiaole (Joy) Chen for help in performing the cyclic voltammetry experiments, Qingsheng Liu for his help in constructing our CO oxidation reaction system, and Ting-Hao Phan for his help in running some CO oxidation experiments. A great appreciation is also owed to the faculty and staff of the Texas A&M Chemistry Department X-ray Laboratory and the Microscopy and Imaging Center for providing their help and expertise.

I am very grateful for all the help Yatsandra has offered and the encouragement she has given me. The encouragement and support that I have also received from my friends and family made it possible for me to succeeded and I am thankful.

NOMENCLATURE

XRD	X-ray diffraction
SAED	selective area electron diffraction
TEM	transmission electron microscopy
EDS	energy dispersive spectroscopy
XPS	X-ray photoelectron spectroscopy
EG	ethylene glycol
TEG	tetraethylene glycol
dppf	1,1'-Bis(diphenylphosphino)ferrocene
acac	acetylacetonate
HDD	1,2-hexadecanediol
HDA	hexadecylamine
ACA	1-adamantanecarboxylic acid
PVP	Polyvinylpyrrolidone

TABLE OF CONTENTS

Page

LIST OF FIGURES

FIGURE Page

FIGURE Page

FIGURE Page

LIST OF TABLES

1. INTRODUCTION: NANOCRYSTALS AS REACTIVE TEMPLATES FOR LOW-TEMPERATURE SYNTHESIS OF ALLOY AND INTERMETALLIC COMPOUNDS

Metals are an important component of everyday modern life; however, in their pure (elemental) form they can be ductile, soft, and very reactive making them limited in their use. The addition of one or more elements to a metal can form a solid solution, also known as an alloy, and can often improve some of its physical properties. One well known example of such a case is the addition of tin to copper to produce a bronze alloy that is superior in hardness and corrosion resistance to iron and was vital in the development of tools, weapons, armor, and building materials in the ancient world. Alloys are often found to have a disordered crystal structure where each element is randomly placed in a crystal lattice and it was believed that this was the only form in which alloys could exist.

In 1839 a German chemist, Karl Kartsten, published the first account that metal alloys could exist as compounds when he noticed that "a discontinuity occurred in the action of acids on alloys of copper and zinc at equiatomic compositions".[1] The first alloy compound he discovered was CuZn and eventually led the way for a new class of alloys called intermetallic compounds. Intermetallic compounds differ from the definition of a "traditional" alloy due to the fact that their crystal structure is ordered. In fact, they are phases where two or more elements, in stoichiometric proportions, are arranged in

---

This dissertation follows the style of the *Journal of the American Chemical Society*.

specific crystallographic locations in a crystal lattice. Intermetallic compounds are often associated with being harder and having higher melting temperatures than their elemental components, but tend to be very brittle.

The formation of solid-state compounds generally relies on the elements of the reactive components to diffuse into each other and crystallize. The process of breaking the reactant's elemental bonds across an extended crystal structure requires a large amount of energy provided by high temperatures, pressure, or a combination of the two. One way to assist the diffusion process is to increase the interfacial contact between the reactants to reduce diffusion distances. Many solid-state synthetic methods try facilitating atomic diffusion by improving the degree of intimate contact.

Alloy and intermetallic compounds are most commonly formed by melting two or more components and this allows a maximum mixing to obtain a homogenous product. A very traditional solid-state chemistry method is to mix powdered reactants, press them into a pellet to increase the interfacial contact, and heat at high temperatures for a period of time. Another method is using low-melting metals that can be used as a solvent, or co-function as a reactant, to dissolve the elements and eventually crystallize them to an alloy. An additional method that can be used to form alloys and intermetallic compounds are gas phase reactions in which elements are transferred into a gas phase and are deposited onto a substrate to form a thin film. One version of this method involves physically removing the elements from a metal source by a high energy beam and is generally referred to as physical vapor deposition (PVD). The second version is called chemical vapor deposition (CVD) in which a thin film is formed through the

decomposition of a gaseous metal species and is deposited onto a substrate. The thin films can be transformed to alloys or intermetallic compounds by an additional annealing step. Some of these examples given for the formation of alloy and intermetallic compounds usually require high temperature or harsh conditions that favor thermodynamically stable products. While other methods may be able to form metastable products, they may still lack general control over crystallite size, morphology, crystal-structure, surface-composition, etc. Furthermore, producing alloy and intermetallic nanomaterials becomes challenging because the high temperatures needed to drive the reaction would cause small particles to agglomerate and sinter.

The ability to produce alloys and intermetallic compounds at lower temperatures would prove to be advantageous because it could not only allow the formation of dispersed nanocrystals, but it would also enable one to gain more control in designing materials for new applications. For instance, the simultaneous decomposition of $Fe(CO)_5$ and reduction of platinum (II) acetylacetonate ($Pt(acac)_2$) form nearly monodisperse self assemblies of FePt alloy nanocubes[2, 3] and nanorods[4, 5] in a polyol-type reaction. Similarly, the simultaneous reduction of $Pt(acac)_2$ and $Pb(acac)_2$ using *tert*-butylamineborane complex as a reducing agent forms intermetallic PtPb nanorods.[6, 7] Though these examples do show a fairly high degree of control in design, the results are very challenging to obtain because one must simultaneously rely on multiple elements nucleating at the same location, with the proper composition, and structure, while considering the effect of surface stabilizers, solvents, temperature, etc. Not to

mention applying the same conditions to a different system of metals usually does not guarantee the same results.

Over the last decade the synthesis of single metal nanoparticles has matured to a level where there is a large library of materials to access, uniform size and shape can be obtained, and the particles can self-assemble. Researchers have come to realize that in the synthesis of single metal nanoparticles, which are well understood, multiple parameters are much easier to control than multi-metal systems. Many have begun to use single metal nanoparticles as reactive precursors to make more complex multi-metal systems that can potentially exhibit new or enhanced physical properties. One such example can be seen for producing monodisperse Fe nanoparticles and oxidizing them with trimethylamine oxide to form γ-Fe_2O_3.[8] Alivisatos and co-workers converted Co nanocrystals into hollow CoO nanoparticles (by introducing an O_2/Ar mixture into the reaction system), hollow Co_3S_4 and hollow Co_9S_8 nanoparticles (by injecting a solution of sulfur in *o*-dichlorobenzene), and hollow CoSe (by injection of selenium in a solution of *o*-dichlorobenzene).[9, 10] The particles became hollow through a diffusion based mechanism called the Kirkendall effect where the inward diffusion of O, S, and Se was slower than the outward diffusion of Cobalt in each case. Trioctylphosphine (TOP) has been used as a source of phosphorus to convert In powder and Ni nanocrystals into InP and hollow Ni_2P nanoparticles.[11-13] Xia and co-workers formed alloy AgAu nanoboxes,[14] nanocages,[15] and multi-walled nanotubes[16] by first forming Ag nanostructures and reacting $HAuCl_4$ in an aqueous solution via a galvanic replacement reaction. Multi-walled AgAu-AgPd nanotubes,[17] AgPd, and AgPt alloy nanoboxes[14]

could be formed by adding Pd or Pt salts into the reaction systems. Their previous studies only used single-crystalline Ag nanoparticles; however, when multiply-twinned particles of Ag capped with oleylamine in chloroform were used they were converted into hollow nanoring and nanocage alloy structures.[18] These are only a few examples demonstrating that single metal nanoparticles can serve as reactive templates to form new multi-metal nanoparticle systems while preserving their uniform size and shape.

Our group has pioneered the synthesis of alloy and intermetallic nanocrystals at relatively low-temperatures by applying "conversion chemistry" methods to single metal nanoparticles. Our first example of nanoparticle conversion began by forming Co nanoparticles, stabilized by PVP, followed by a galvanic replacement reaction with K_2PtCl_6 to form hollow alloy CoPt nanoparticles with superparamagnetic properties.[19] In another case, $HAuCl_4 \cdot 3H_2O$, $Cu(C_2H_3O_2)_2$, and $SnCl_2$ salts were reduced in a polyol reaction to form a ternary intermetallic phase of $AuCuSn_2$.[20] It was found that Sn^{2+} was oxidized to Sn^{4+} for the formation of Au nanoparticles stabilized by PVP. A solution of $NaBH_4$ was added for the reduction of excess Sn^{2+} and upon heating at 70 °C AuSn intermetallic (NiAs structure-type) nanoparticles were formed. Additional heating allowed the Cu to diffuse into the system finally forming a $AuCuSn_2$ system.[21] The same procedure was adapted by replacing Cu with Ni to form $AuNiSn_2$.[21]

The diffusion mediated synthesis of intermetallic nanoparticles in solution paved the way by taking the conversion chemistry concept a step further. In one such case, preformed β-Sn nanocrystals were converted in a polyol solution to form Sn-based intermetallic nanocrystals that still maintained the original morphology.[22] The reaction

of $FeCl_3$ with β-Sn under reducing conditions could form a variety of $FeSn_2$ shapes such as spheres, cubes, hollow squares, U-shaped structures, nanorods, and nanorod dimmers. It is believed that the anisotropic structure of β-Sn and different diffusion rates along its different axes facilitated the variety of morphologies. Similar methods can form single crystalline intermetallic systems starting from β-Sn nanocrystals such as $CoSn_3$, Ni_3Sn_4, Cu_6Sn_5, Ag_4Sn, AuSn, PtSn, and $RuSn_2$.[23] This process is also capable of generating intermetallic materials (α-$CoSn_3$, $NiSn_3$, and $RuSn_2$) that are considered difficult to make by traditional bulk methods and in most cases are newly discovered. In a separate study, diethylzinc was reacted with dendritic Pd nanoparticle networks and multifaceted and polydispersed Cu nanoparticles to form PdZn and Cu_6Zn_5 respectively, while maintaining the same morphology.[24] Monodisperse spherical Au nanoparticles were also converted to Au_3Zn (with the same morphology and size dispersity) using diphenylzinc.[24] Conversion chemistry techniques were also applied to transform segments of Pt nanowires (formed by electrodeposition in anodic alumina membranes) into intermetallic compounds (PtPb, PtBi, PtSb, and Pt_3Co).[25]

In addition to the concept of using single metal nanoparticles as reactive templates it was also found that intermetallic nanoparticles could be just as reactive. For example, when PtSn nanoparticles were reacted with $SnCl_2$ in tetraethylene glycol $PtSn_2$ was formed.[26] Similarly, reacting PtSn with K_2PtCl_6 could form Pt_3Sn which could be further reacted with $SnCl_2$ to yield PtSn.[26] This process has potential to be used as a method of obtaining phases that are initially difficult to obtain directly. Similar reactivities were seen in the conversion of AuSn to $AuCuSn_2$ intermetallic

nanoparticles.[21] Bi2Pd and BiPt intermetallic nanoparticles were used as precursors in a mild heat treatment in air (350-400 °C) to form Bi_2O_3/Pd and Bi_2O_3/Pt followed by additional annealing (700-800 °C) for the transformation into Bi_2PdO_4 and $Bi_2Pt_2O_7$.[27]

It was also demonstrated that the phosphorus from trioctylphosphine (TOP) could be cleaved from the P-C bond and diffuse into the metal nanoparticles forming metal phosphides.[28, 29] Taking advantage of the P-C cleavage a variety of phosphide systems could be formed (FeP, CoP, Ni_2P Cu_3P) and including systems of the 4d and 5d transition metals that often were difficult to synthesize under normal methods (Rh_2P, Pd_5P_2, PdP_2, AgP_2, PtP_2, and Au_2P_3).[30, 31] This process is also useful for the conversion of bulk powders, Ni nanocrystals supported on graphite and thin foils.[31] It was also shown that shape-controlled Rh nanocrystals could be converted to Rh_2P while still retaining the original shape (cube/octahedron, triangle, and multipods).[32]

It has been shown through a number of examples that conversion chemistry methods are able to produce a large variety of multi-element nanoparticle systems while simultaneously maintaining a large degree of control over the structure (composition, nanocrystal shape, size, crystal structure, etc.). However, this concept is still in the early stages of development and its full potential toward applications has not been fully realized. For instance, metal nanoparticles have been widely used in catalytic applications in hydrogenations[33], NO_x reduction[34], CO oxidation[35], alcohol oxidation[36], carbon-coupling[37], and many more reactions. The advantage that nanoparticle catalysts offer is that a large fraction of atoms are located on or near the surface. Therefore, the majority of the atoms are involved in the catalytic reaction resulting in a higher catalytic

activity as compared to their bulk counterparts. Unfortunately, unwanted by-products can form and strongly bind to the catalyst's surface to deactivate the catalyst (as seen with coke formation in hydrogenation[38] reactions and CO poisoning in methanol electro-oxidation reactions[39]). A common method to reduce poisoning effects and even enhance catalytic activity is to use alloy[40] or intermetallic[41] compounds. However, current synthetic methods for forming alloy and intermetallic nanoparticle catalysts are problematic.

The problem of forming alloy and intermetallic nanoparticles for catalytic applications begins with the synthesis of nanocrystals in general. Nanoparticles have very reactive surfaces due to "dangling bonds" that can drive the particles to grow to bulk sizes to increase stability. Surface-stabilizers (e.g. – polymers or surfactants) are needed to stabilize the surface and keep the particles in the nanoregime. When using these particles as catalysts it can be imagined that the surface stabilizers, that are bound to and wrap around the surface of the particles, may inhibit contact with the chemical reactants and slow the reaction down.

One solution is to immobilize the particles to a solid support such as carbon, Al_2O_3, TiO_2, CeO_2, SiO_2, zeolites, and other types of materials. The particles are then stabilized on the surface of the supports and no longer require surface-stabilizers that can block access to the catalysts. The formation of alloy and intermetallic nanoparticles directly on a support material becomes difficult when one considers that multiple elements would have to reduce, nucleate and grow uniform sized particles with the same composition simultaneously at multiple locations on the support. Currently, co-

reduction of metal salts onto the support followed by high temperature treatment can obtain supported alloy and intermetallic nanoparticles, but this often results in particle sintering that reduces the surface-area and lowers catalytic activity.

It is believed that the large surface-area to volume ratio of nanoparticles exposes most atoms to the surface, which cuts down on diffusion distances resulting in less energy needed for a reaction. This results in nanoparticles themselves becoming reactive components in a reaction. Therefore, conversion chemistry techniques can be applied for the synthesis of alloy and intermetallic nanoparticle catalysts immobilized on a solid support by using preformed nanoparticles as reactive templates to preserve their small uniform size and dispersion. In addition, conversion chemistry can be used as a method in developing and designing new catalytic materials for a variety of reactions. Eventually, conversion methods can make their way toward designing multi-element materials where it is important that many parameters can simultaneously be controlled such as crystal-structure, size, shape, and surface composition.

2. LOW-TEMPERATURE SYNTHESIS OF ALLOYS, INTERMETALLIC COMPOUNDS AND MULTI-METAL OXIDES USING NANOPARTICLES AS REACTIVE PRECURSORS

2.1 Introduction

Alloys, intermetallic compounds and transition metal oxide materials have many physical properties including ferromagnetism[42-44], shape-memory effects[45], hydrogen storage[46, 47], corrosion resistance[48], magnetism[49], superconductivity[50-53], ferroelectricity, nonlinear optical behavior[54], ionic conductivity[55], and catalysis[41, 56-64]. Taking advantage of these properties for technological applications requires control over composition, morphology, crystallite size, and crystal structure. Unfortunately, current synthetic methods for these materials often involve harsh reaction conditions, involving high temperatures, which can make it difficult to control all of these parameters.

Traditional syntheses of alloys and intermetallic compounds often use methods of arc-melting and annealing metal powders at temperatures over 1000 °C for days or even weeks. The synthesis of ternary and quaternary transition metal oxides are also traditionally produced by "heat and beat" methods where oxide powders are ground together, pressed into pellets, and heated to high temperatures (~1000 °C) for long periods of time, with the process being repeated several more times until a pure product is made. The high temperatures and long reaction times are required to provide enough energy to break bonds across the entire extended crystal structure and also to allow atomic diffusion. The diffusion of the elements to create the product is considered the

rate-limiting step. Since these conditions require high temperatures, they tend to form thermodynamically favored products, which can limit the access to metastable phases.

Alternative methods to synthesize alloys, intermetallic compounds, and transition metal oxides do exist that are able to produce nanostructured materials. Mechanical alloying is one example of a method that uses high pressures to produce alloy nanoparticle powders, but is unable to have much control over crystal morphology.[65] A multistep technique was also developed using a process known as mechanically activated, field activated pressure-assisted synthesis (MAFAPAS) that involves milling the powders together at the nanoscale, applying a high density alternating current and uniaxial pressure to obtain dense FeAl intermetallic compounds with a crystallite size range between 50-150 nm.[66-68] Other common examples of forming intermetallic nanostructures include thermolysis[69], chemical vapor deposition[70], gas-phase condensation[71], and high-temperature/high-pressure processing[72]. There are also a variety of methods that have been successfully used to synthesize simple metal oxides at low-temperatures such as coprecipitation[73], hydrothermal synthesis[74], topochemical reactions[75, 76], and the sol-gel process[77].

A new process has been developed where transition metal or metal oxide nanoparticles, stabilized by poly(vinyl pyrolidone) (PVP), were used as reaction precursors for fast low-temperature reactions to form alloys, intermetallic compounds and multi-metal oxide materials. The idea is that available metal or metal oxide nanoparticles can be combined in known ratios to form a nanoparticle composite mixture. At this scale the interfacial contact between the reactants becomes much more

intimate and more atoms are in contact with each other as compared to traditional grinding and pressing methods. The nanoparticle composite effectively reduces the solid-solid diffusion distance from the micrometer to the nanometer scale. The reduced diffusion distances allow the reaction to happen much more quickly at lower temperatures than traditional methods. The advantage of this method using less harsh reaction conditions is the possibility that new structures can be generated that are not normally stable for bulk systems formed at high temperatures. In addition, one could potentially study low-temperature phase formation and kinetically control the reaction pathway of these materials. This method of rapid low-temperature annealing of nanoparticle composites can prove to be versatile when one takes into account the availability of all the metal and metal oxide nanoparticles that could potentially serve as precursors.

2.2 Experimental

2.2.1 Using metal nanoparticles as precursors for the formation of alloy and intermetallic compounds

The synthesis of intermetallic CoPt began by making a nanoparticle composite of Co and Pt by dissolving $CoCl_2$ (10.1 mg, 0.042 mmol), K_2PtCl_6 (20.6 mg, 0.042 mmol), and PVP (MW = 40000, 100 mg) into 15 mL of NANOpure water (18.2 MΩ). After the solution stirred under bubbling Ar for 20 minutes the metal salts were reduced by a drop wise addition of 5 mL of $NaBH_4$ (0.061 M) and the solution was aged for 2-3 h. The particles were isolated by centrifugation and washed with NANOpure water and ethanol (three times each). The Co:Pt nanoparticle composite was annealed in a tube furnace

under flowing Ar at 600 °C for 90 minutes. Transition metal alloys were made using the same procedure where $Ni(C_2H_3O_2)_2$ (28.2 mg, 0.038 mmol) and K_2PtCl_6 (18.3 mg, 0.038 mmol) were reduced with 0.061 M solution of $NaBH_4$ in the presence of PVP and a Ni:Pt nanoparticle composite was formed where it was annealed at 600 °C for 90 minutes. For the synthesis of a Ag_3Pt alloy, $AgNO_3$ (19.4 mg, 0.114 mmol) and K_2PtCl_6 (15.5 mg, 0.037 mmol) were mixed into a composite using the previous mentioned procedures and heated at 600 °C for 90 minutes. Au_3Pd was made similarly by starting with $HAuCl_4 \cdot 3H_2O$ (38.4 mg, 0.098 mmol) and $PdCl_2$ (6.7 mg, 0.038 mmol) and annealing the Au:Pd nanoparticle composite at 600 °C for 90 minutes. The nanoparticle composite of Ag:Pd was made using $AgNO_3$ (6.4 mg, 0.038 mmol) and $PdCl_2$ (6.7 mg, 0.038 mmol) and reducing with $NaBH_4$ in the presence of PVP was only needed to form the alloy at room temperature.

2.2.2 Synthesis of metal oxide nanoparticle precursors

Nanoparticles of Cu_2O and CoO were synthesized by dissolving the appropriate metal salts into 15 mL of NANOpure water (18.2 MΩ) along with 100 mg of PVP (MW = 40,000). The metal salts that were used were $Cu(C_2H_3O_2)_2 \cdot H_2O$ (19.0 mg, 0.0952 mmol) and $CoCl_2 \cdot 6H_2O$ (18.9 mg, 0.0794 mmol). The metal salts were reduced to form metal nanoparticles, in the presence of PVP, by adding $NaBH_4$ (10 mg, 0.2645 mmol) while stirring with a magnetic stir bar. Stirring under air was continued for 30-60 min to allow the particles to oxidize (CoO required 3-4 h of stirring). The oxide nanoparticles were separated from solution by centrifugation at 13,000 rpm, washed at least 3 times with ethanol, and then dried under ambient conditions. TiO_2 nanoparticles were synthesized

by adding titanium isopropoxide (2.0 mL, 0.0351 M in 2-propanol) to 20 mL of H_2O and 100 mg of PVP to initiate the hydrolysis reaction. The solution was stirred for 15-30 min and then centrifuged at 13,000 rpm. Bi_2O_3 nanoparticles were synthesized based on a procedure developed by Feldmann and a brief description is given.[78] $Bi(NO_3)_3 \cdot 5H_2O$ (1.66 g) was dissolved in 50 mL of diethylene glycol with sonication. NaOH (1 mL, 0.1 M) was added and the solution was heated to 140 °C for 1 h followed by raising the temperature to 180 °C for 2 h. The solution was cooled to room temperature, and the Bi_2O_3 nanoparticles were separated by centrifugation at 13,000 rpm and washed several times with ethanol and dried under ambient conditions.

2.2.3 Characterization details

Powder X-ray Diffraction (XRD) data were collected using a Bruker GADDS three-circle X-ray diffractometer (Cu Kα radiation, 40 mV, 40 mA) using microdiffraction powder techniques.[79, 80] The large background at low angles is due to air scattering because the beam size is larger than the sample for the microdiffraction experiments.[79, 80] Transmission electron microscopy (TEM) images, energy dispersive X-ray spectroscopy (EDS), and selected area electron diffraction (SAED) patterns were collected on a JEOL 2010 TEM operating at 200 kV. Samples were prepared by re-suspending the isolated and cleaned nanoparticles in ethanol and dropping the solution on a carbon-coated Cu or Ni grid (chosen to avoid EDS interface with constituent elements in the samples).

2.3 Synthesis of alloy and intermetallic compounds through nanoparticle precursors

The synthesis of the CoPt intermetallic compound began by dissolving $CoCl_2$ and K_2PtCl_6 (molar ratio of 1.9) in deionized (DI) H_2O with PVP (MW = 40,000). The solution was reduced with $NaBH_4$, under bubbling Ar gas, to nucleate and form Co and Pt nanoparticles in about 20-30 minutes. After isolating the nanoparticle composite by centrifugation, the samples were annealed in a tube furnace under flowing Ar at up to 600 °C. XRD data, as seen in Figure 2.1, shows a face-centered cubic pattern that is shifted to the right of where the simulated Pt peaks are located and indicates that an

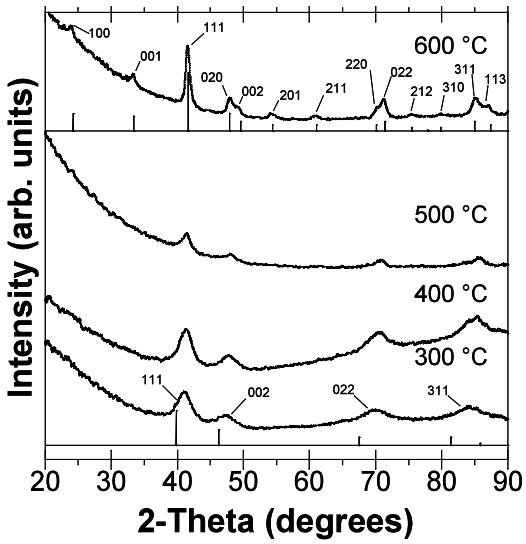

Figure 2.1. Powder XRD patterns showing annealed Co:Pt nanocomposites that formed alloys at 300 °C, 400 °C, and 500 °C and are compared to Pt simulated peaks. At 600 °C, CoPt ordered into an intermetallic structure (AuCu structure-type) and is compared to the CoPt simulated peaks.

alloy was formed by 300 °C. An intermetallic structure is formed at 600 °C within 90 minutes. In other work, similar results were observed for the AuCu and $AuCu_3$ systems where it was found that the intermetallic structures were formed within 5-10 minutes at 300 °C.[81]

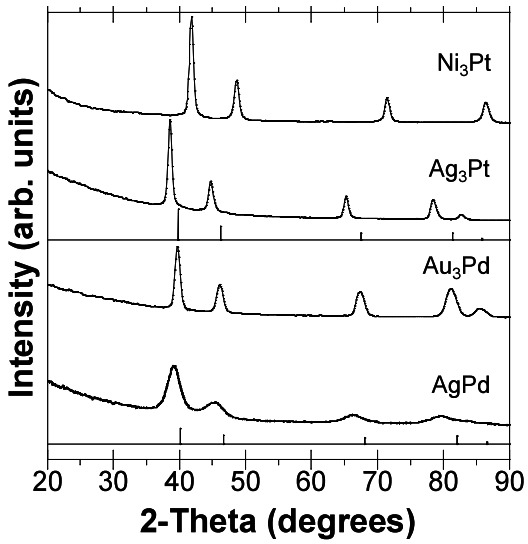

Figure 2.2. Powder XRD patterns showing Pd and Pt alloy systems synthesized by annealing the respective nanocomposites. All alloy systems exhibit a face-centered cubic pattern and are shifted from the Pd or Pt simulated peak positions.

The method of annealing nanoparticle composites was also extended to other binary metal systems to not only form intermetallic compounds but also alloys. Face-centered cubic alloys, shown in Figure 2.2, of Ni_3Pt, Ag_3Pt, and Au_3Pd were formed by annealing their nanoparticle composites at 600 °C, 800 °C, and 600 °C respectively. Interestingly, AgPd was able to form an alloy without additional annealing and the broad XRD peaks indicate the crystallite domain size remained small as shown in the bottom of Figure 2.2. In an effort to demonstrate the versatility of this method, our group

synthesized additional intermetallic compounds of Cu_3Pt, CuPt, Fe_3Pt, FePt, $FePt_3$, and Ag_2Pd_3S and alloy compounds of $AuPd_3$, AuPd, and NiPt, all synthesized at 600 °C or lower.[81]

2.4 Synthesis of ternary and quaternary complex oxides

The idea of using metal nanoparticles as precursors for alloys and intermetallic compounds was also extended to the synthesis of complex oxide materials. The procedure to make Bi_2CuO_4 was done in a similar manner as forming intermetallic compounds. In this case, Cu and Bi salts were separately dissolved in DI H_2O with PVP (MW = 40,000) and reduced with $NaBH_4$. The newly formed metal nanoparticles were oxidized in air followed by being isolated by centrifugation. The Cu_2O and Bi_2O_3

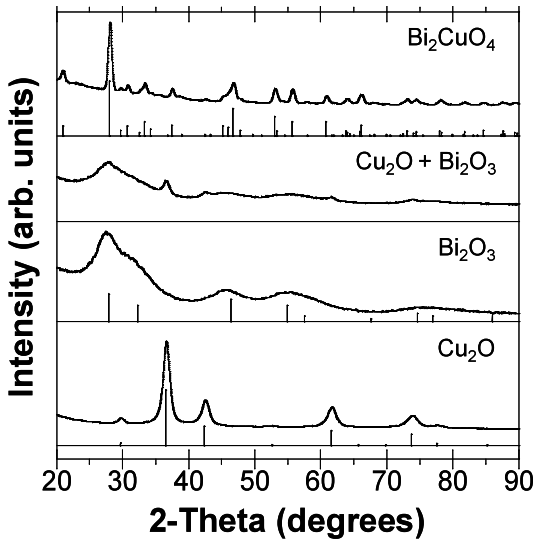

Figure 2.3. Powder XRD patterns of Cu_2O and Bi_2O_3 nanoparticles. The nanoparticle composite of Cu_2O and Bi_2O_3 shows both patterns are simultaneously present. The final product of Bi_2CuO_4 (annealing Cu_2O:Bi_2O_3 at 500 °C for 2 h) is also shown (Cu_2O converts to CuO at 500 °C). The XRD patterns are compared to the respective simulated patterns.

nanoparticles were mixed in stoichiometric proportions by re-suspending them in ethanol. After centrifuging the particles and drying in ambient conditions the Cu_2O:Bi_2O_3 nanoparticle composite was annealed in air. The XRD pattern in Figure 2.3 shows Cu_2O, Bi_2O_3, and the composite mixture confirming that both components were present. Cu_2O appears to be fairly crystalline while Bi_2O_3 exhibits broad peaks indicating the particles are small. The sample was then annealed at 500 °C for 2 h to form Bi_2CuO_4 and it matches well to the simulated peaks. As a comparison, traditional solid state methods of pressing Bi_2O_3 and CuO powders into a pellet required annealing at 800 °C for 3 days.[82] It is important to note that Cu_2O transforms to CuO upon heating at 500 °C and the metal salt ratios were based on using CuO.[83]

The TEM images in Figure 2.4(a) show that Cu_2O nanoparticles have a cubic type of morphology with an average diameter around 20 nm and the selected area electron diffraction (SAED) pattern in the inset corresponds to Cu_2O. The Bi_2O_3 nanoparticles in Figure 2.4(b) are very small, about 3-5 nm in diameter, which corresponds to the short and broad peaks in the powder XRD pattern in Figure 2.3. The SAED pattern in the inset in Figure 2.4(b) also has a similar pattern to the XRD pattern of Bi_2O_3 confirming the structure. When the nanoparticle composite of Cu_2O and Bi_2O_3 is annealed at 500 °C for 2 h to form Bi_2CuO_4, the resulting particles become sintered with an approximate diameter of 25 nm.

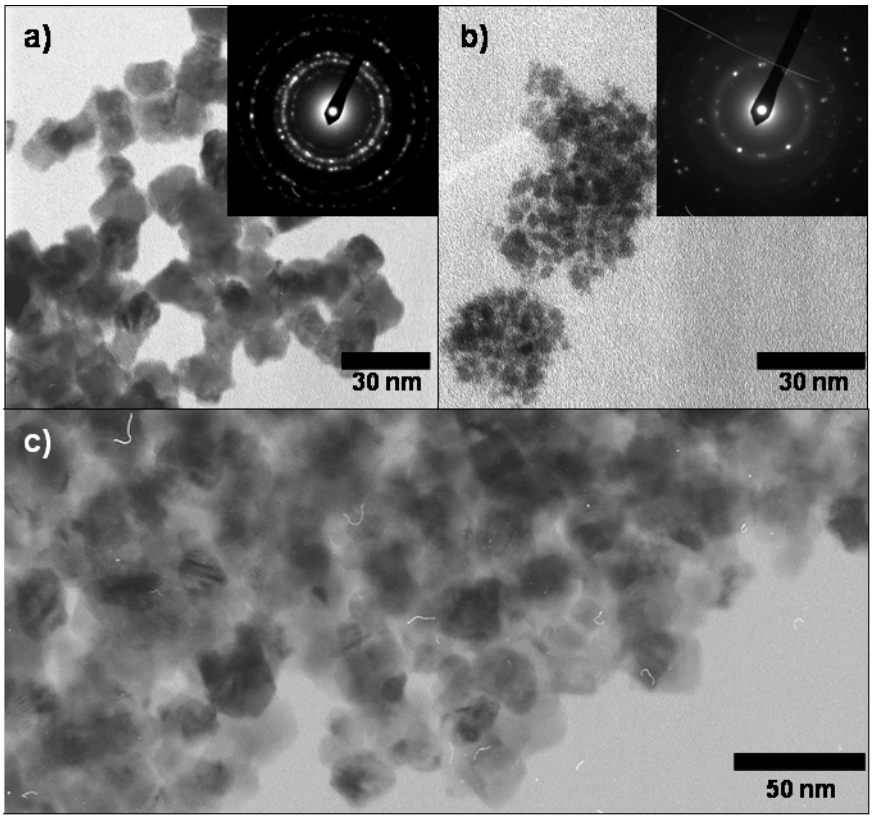

Figure 2.4. TEM images of (a) PVP stabilized Cu_2O nanoparticles, (b) PVP stabilized Bi_2O_3 nanoparticles, and (c) Bi_2CuO_4 annealed at 500 °C for 2 h. The insets are SAED patterns of the respective nanoparticles.

The same procedure was adopted to make the ilmenite-type structure of $CoTiO_3$ that is typically made by heating CoO and TiO_2 to 1200 °C for 200 h.[84] In this case, a nanoparticle composite of CoO and TiO_2 was annealed at 700 °C for 2 h (EDS results indicated a Co:Ti ratio of 1.0:1.1). As seen in Figure 2.5, quaternary metal oxides can be accessed by mixing Bi_2O_3, Fe_2O_3, and TiO_2 nanoparticles together and heating at 700 °C for 2 h to form the aurivillius-type Bi_5FeTiO_3 and is known to have ferroelectric and antiferromagnetic properties.[85-87] EDS experiment showed that the nanocomposite had a Bi:Fe:Ti ratio of 3.3:1.0:1.8, which corresponds to an average composition of

$Bi_{5.5}$ $Fe_{1.7}Ti_{3.0}O_{15}$ when normalized to Ti. When taking into account the error always present in EDS, this agrees well with the expected stoichiometry and may suggest that there is excess Bi_2O_3 and Fe_2O_3 that did not react, incorporated as inter-growths in the layered structure, or some TiO_2 did not precipitate from solution. This low-temperature method is still an improvement, in terms of energy and time required, to more traditional methods that require heating to 1050 °C.[85-87] These more gentle reaction conditions can also be adapted to produce metastable phases (not accessible at high temperatures)

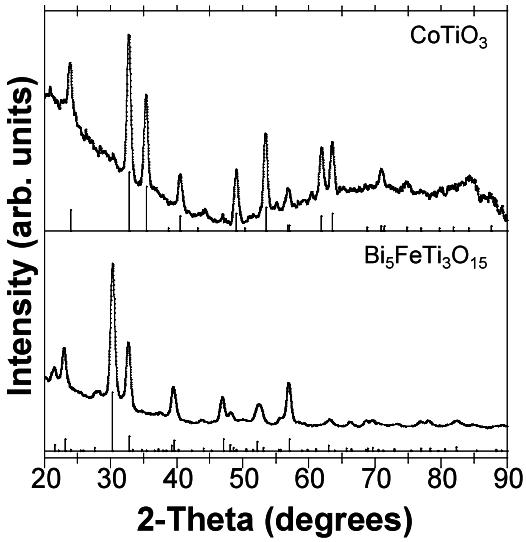

Figure 2.5. XRD pattern of $CoTiO_3$ (CoO and TiO_2 nanoparticle powders annealed at 700 °C for 2 h) and $Bi_5FeTi_3O_{15}$ (Bi_2O_3, Fe_2O_3, and TiO_2 nanoparticle powders annealed at 700 °C for 2 h). The XRD patterns are compared to their respective simulated peaks.

Our group continued this study by accessing pyrochlore-type structures of $Y_2Ti_2O_7$ (700 °C, 2h), $Eu_2Ti_2O_7$ (700 °C, 2 h), and ilemite-type $NiTiO_3$ (700 °C, 1 h) by annealing nanoparticle composites of Y_2O_3:TiO_2, Eu_2O_3:TiO_2, and NiO:TiO_2.[88] Since it

has been shown that not only ternary, but quaternary oxides can also be formed through this method it suggests that a variety of complex oxides can be formed at low temperatures using oxide nanoparticles as reaction precursors.

2.5 Conclusion

We have demonstrated that metal and metal oxide nanoparticles can be used as reaction precursors to form alloys, intermetallic compounds and multi-metal oxides within minutes at low temperatures. This method is successful because it takes advantage of increased reactivity due to the high surface-area of the nanoparticles and nanoscale mixing that increases the intimate contact effectively enough that the diffusion distances are significantly reduced. Solid-solid diffusion is no longer considered the rate-limiting step and does not require high temperature annealing. The composition of the nanoparticle composite mixture determines the product composition and therefore, more than one phase of the same system can be obtained. The procedure not only has potential, but also has proven it is capable of producing more. Previous work has shown that this simple and mild approach has potential to make these complex materials adaptable to many applications such as surface-confined thin films, free-standing films, nanomesh materials, inverse opals, and gram-scale bulk powders with dense submicrometer crystallites.[81] Not only can this procedure be applicable to processes but, since the solid-solid diffusion is significantly decreased and high temperatures are not necessary, the nucleation phase becomes the rate-limiting step and can potentially provide access to metastable phases. The synthesis of compounds that are generally

difficult to synthesize (require high temperatures, vacuum deposition techniques, etc.) can possibly be synthesized under these mild conditions.

3. CONVERTING NANOCRYSTALLINE METALS INTO ALLOYS AND INTERMETALLIC COMPOUNDS FOR APPLICATIONS IN CATALYSIS*

3.1 Introduction

An ongoing challenge in the preparation of nanoparticle catalysts is synthesis by design where rigid standards must be met. The ability to design a good catalyst ideally requires one to simultaneously control the size, shape, composition, crystal structure, and surface chemistry of the catalytic nanoparticles, as well as the architecture of the support and its interaction with the metal. This is well known from the studies of Pt-based nanoparticle catalysts, which find widespread use in a variety of important chemical transformations, including hydrogenation[89], NO reduction[90], CO oxidation[91] and oxidation of small organic molecules (SOM's)[36]. Though Pt is considered to be the most active metal for these reactions, it does have some limitations. Aside from being very expensive, Pt is prone to CO and thiol poisoning, which can block the active sites of the catalysts, preventing further reactions from occurring.[92-95] The addition of a second metal to the catalyst to form an alloy has been known to reduce some of these negative aspects of pure Pt and, in some cases, enhance the catalytic properties.[40]

---

*Reprinted with permission from "Converting Nanocrystallline Metals Into Alloys and Intermetallic Compounds For Applications In Catalysis" Bauer, J. C.; Chen, X.; Liu, Q.; Phan, T.-H.; Schaak, R. E. **2008** *J. Mater. Chem.18*, 275 – 282 by The Royal Society of Chemistry.

Intermetallic catalysts can also show enhancements relative to pure Pt. Intermetallic compounds, which are atomically-ordered alloys that tend to have well-defined compositions and crystal structures that differ from their constituent elements, have been used as catalysts for quite some time for chemical transformations such as hydrogenation[96, 97], ammonia synthesis[98], methanol synthesis[99] and methanol oxidation[63]. In particular, recent work has shown that intermetallic alloys are potential candidates for catalysis in the electrochemical oxidation of SOM's because of their increased current densities and their improved resistance to CO poisoning.[41, 57]

Supported intermetallic catalysts are often prepared by using co-reduction, wet-impregnation or co-precipitation methods and annealing to temperatures near or above 1000 °C in a reducing atmosphere. Heating at these high temperatures causes particle sintering, but the intermetallics still tend to show improved catalytic activity despite the lower surface area.[39, 100] DiSalvo and Abruna have made unsupported intermetallic nanoparticle catalysts of BiPt at 145 °C using the polyol process, as well as PtPb using either sodium naphthalide or sodium borohydride reduction at room temperature.[58, 59, 61, 62] Using this approach, the particle surfaces are relatively clean because no extra surface stabilizers are used, although particle aggregation is observed. Electrocatalytic studies on these systems show enhanced catalytic activity and a nearly complete elimination of CO poisoning. Chemical vapor deposition methods were employed to make small and highly dispersed SiO_2-supported Ni_3Sn, Ni_3Sn_2, Ni_3Sn_4 and various Pd intermetallic nanocrystal catalysts for cyclohexane

dehydrogenation, but high temperatures were still needed and larger particle sizes were found to be inferior to smaller particles.[101, 102] Xia and Zhang synthesized Vulcan-supported intermetallic $PtBi_2$ particles with a diameter of 4 nm by aqueous co-reduction of metal salts using poly(vinylpyrrolidone) (PVP) as a stabilizer.[103]

Because intermetallic phases typically require high temperatures to form, the design of supported intermetallic nanoparticle catalysts with high surface area has proven difficult. Surface stabilizers, such as polymers and surfactants, are typically used to minimize particle growth,[56] but the capping ligands bind to the surface and tend to block the desired reactions, therefore, lower the overall catalytic activity. Organic stabilizers can be removed by oxidative heat treatment, but even low-temperature annealing can be detrimental. For example, PtRu alloys phase separate into Pt and Ru at temperatures as low as 220 °C.[104] For single-metal nanoparticle catalysts, sequestration on a high surface area support has proven very useful for nucleating and maintaining small particle sizes and keeping the particles dispersed without needing capping ligands. Unfortunately, this is much more difficult for multi-metal systems, which require co-nucleation of the elemental components at the same location on the support and in a desired ratio, as well as high-temperature annealing to nucleate ordered intermetallic compounds and many alloys.

During the past few years we have been developing low-temperature solution chemistry strategies for synthesizing intermetallic nanoparticles, including methods that permit some degree of control over particle size, size dispersity, shape, composition, and crystal structure.[20-22, 26, 105, 106] For example, we can routinely

generate nanocrystalline intermetallics in the binary Au-Cu, Pt-M (M = Sn, Sb, Fe, Bi, Pb, Cu), and M'-Sn (M' = Fe, Ni, Co, Pd) systems, as well as the ternary Au-M"-Sn (M" = Cu, Ni) system, using modifications of the polyol process. However, morphology control is limited using these techniques, and they usually use polymeric surface stabilizers. Our more recent work has focused on the idea of "conversion chemistry," where pre-formed metal nanoparticles can serve as both morphological and compositional templates for low-temperature conversion into derivative compounds.[21, 22, 26, 27, 30, 31, 106, 107]

In these cases, the shape and size dispersity defined by the metal nanoparticle precursors (which are significantly easier to control than for multi-metal systems) are generally retained in the multi-metal products, which also require a high degree of composition control to form since they tend to be line phases. Examples include nanocrystals of monodisperse Au_3Zn,[107] dendritic PdZn,[107] and hollow cube-derived $FeSn_2$,[22] as well as monodisperse and hollow nanocrystals of metal phosphides (e.g. Ni_2P).[30, 31] The advantages of these methods – rapid low-temperature nucleation of intermetallics with morphology control – complement some of the limitations of more traditional methods for intermetallic catalyst preparation. If one could apply to supported catalyst systems the methods being developed for converting metal nanoparticles into intermetallics, which facilitate control over composition and crystal structure as well as retention of the shape and size of the metal nanoparticle precursors, one could potentially design improved intermetallic catalyst systems.

Here we demonstrate that the solution-based "conversion chemistry"

strategies being developed for accessing intermetallic nanocrystals are indeed portable to supported catalyst systems. This effectively provides a strategy for modifying pre-formed supported single-metal nanoparticles to form supported multi-metal nanoparticle catalysts with controllable size, shape, composition, crystal structure, and support. Controlling these parameters is important for controlling, studying, understanding, and optimizing catalytic activity in high surface area systems. [108-111] Alloy and intermetallic nanoparticle catalysts can be prepared by a number of methods, as described above. The method described in this section differs from most other co-deposition and impregnation strategies that are used in the preparation of supported multi-metal nanoparticle catalysts. Since it involves a direct low-temperature diffusion-based process, this method does not require a post-annealing step to generate an alloy or intermetallic phase (unless the desired phase is only stable above 300 °C, e.g. $L1_0$-type FePt). The conversion from metal to alloy or intermetallic occurs directly in solution, rather than after a high-temperature annealing step that would otherwise be necessary to reduce and interdiffuse sequentially-deposited metal precursors. As such, it minimizes sintering and particle growth, provides access to hollow and other morphology-controllable nanostructures, and can provide access to multiple stable line phases in a single binary system.

3.2 Experimental

3.2.1 Chemicals

The following metal reagents were used: K_2PtCl_6 (40.11% Pt), $SnCl_2$ (anhydrous,

99% min.), $Pb(C_2H_3O_2)_2 \cdot 3H_2O$ (ACS, 99.0-103.0 %), $SbCl_3$ (99.9 % min.), $CuCl_2$ (anhydrous, 99%), $FeCl_3 \cdot 6H_2O$ (ACS, 97.0-102.0%), $Bi(NO_3)_3 \cdot 5H_2O$ (Mallinckrodt Chemical Works), and $Ce(NO_3)_3 \cdot 6H_2O$ (99.5%). Several commercial catalysts were used: Pt/Al_2O_3 (Strem Chemicals, Platinum 5 % on alumina), Pt/Vulcan XC-72 (E-TEK, C1-20 20 % HP Platinum on Vulcan XC-72), and PtRu/Vulcan XC-72 (E-TEK,C13-20 20 % HP Pt:Ru Alloy (1:1 a/o) on Vulcan XC-72). Solvents were ethylene glycol (EG, 99+%) and tetraethlyene glycol (TEG, 99+%). All chemicals were purchased from Alfa Aesar unless otherwise noted.

3.2.2 Synthesis of unsupported Pt nanoparticles

K_2PtCl_6 (60 mg, 0.124 mmol) was dissolved in 20 mL of ethylene glycol. After purging with Ar for 15 min, the temperature was raised to 160 °C and the color turned from yellow to dark brown, and the solution was removed from the heat. The Pt nanoparticles were collected by centrifugation and washed with ethanol.

3.2.3 Conversion of unsupported Pt nanoparticles to intermetallics

Alloy and intermetallic nanoparticles were synthesized by dispersing an appropriate amount of unsupported Pt nanoparticles in 20 mL of a metal salt solution in tetraethylene glycol (TEG). After purging the solution with Ar for 20 min, the temperature was increased to the temperature necessary to form the desired product. Specifically, PtSn (1:4.3; Pt:$SnCl_2$ molar ratio) was heated to 235 °C for 30 min; PtPb (1:1.1; Pt:$Pb(C_2H_3O_2)_2 \cdot 3H_2O$ molar ratio) was heated to 190 °C for 30 min; BiPt (1:1; Pt:$Bi(NO_3)_3 \cdot 5H_2O$ molar ratio) was heated to 220 °C for 30 min; and $FePt_3$

(0.5:1.1 Pt: $FeCl_3 \cdot 6H_2O$ molar ratio) was heated to 308 °C for 60 min to obtain the alloy and then annealed under flowing Ar at 550 °C for 30 min to obtain the $L1_2$-type intermetallic.

3.2.4 Synthesis of Pt nanoparticles supported on γ-Al_2O_3 and CeO_2

Pt nanoparticles (3.2 wt% loading) were supported on γ-Al_2O_3 and CeO_2 using the polyol method. The CeO_2 support was synthesized by thermally decomposing $Ce(NO_3)_3 \cdot 6H_2O$ at 500 °C for 5 h in air while γ-Al_2O_3 was purchased from Strem Chemicals and used as received. The support [CeO_2, 300 mg; Al_2O_3, 300 mg] was added and stirred into a solution of K_2PtCl_6 [23.9 mg] in 7 mL of EG. The mixture was purged with Ar for 20 min and the temperature was increased to 110 °C and held for 1 h, during which time the color changed from yellow to brown. The supported Pt nanoparticles were collected by centrifugation and washed with acetone.

3.2.5 Conversion of supported Pt nanoparticles to intermetallics

Supported intermetallic nanoparticles (PtSn, PtPb, PtSb, Pt_3Sn, and Cu_3Pt) were synthesized in a similar manner as described for the unsupported particles. The previously synthesized supported Pt nanoparticles with a 3.2 wt% Pt loading were used as the Pt source, as well as commercial Pt/γ-Al_2O_3 (5 wt% Pt, Strem Chemicals) and Pt/Vulcan XC-72 (20 wt% Pt, E-TEK). The supported intermetallic nanoparticles were made as follows: PtSn (1:8; Pt:$SnCl_2$ molar ratio) was heated to 235 °C for 1 h,; PtPb (1:1.1; Pt: $Pb(C_2H_3O_2)_2 \cdot 3H_2O$ molar ratio) was heated to 190 °C for 1 h; and PtSb (1:1; Pt:$SbCl_3$ ratio) was heated to 275 °C for 1 h, Pt_3Sn was

synthesized by mixing supported Pt and $SnCl_2$ (3:1; Pt:$SnCl_2$ molar ratio) in 20 mL of TEG. (Optimal molar amounts of metal reagents were determined empirically based on the formation of a phase-pure product. Excess metal, such as Sn in the formation of PtSn, likely remained oxidized and in solution as small dispersed nanoparticles, which do not readily precipitate upon centrifugation of the heavier supported intermetallic nanoparticles.) The mixture was heated to 285 °C for 1 h then removed from the heat. Supported Cu_3Pt catalysts nanoparticles were made by mixing supported Pt with $CuCl_2$ (1:3 Pt:$CuCl_2$ molar ratio) in 20 mL of TEG and heating to 300 °C for 1 h followed by annealing at 500 °C for 0.5 h. The product was collected by centrifugation, washed with acetone, dried, and annealed under Ar at 500 °C for 0.5 h.

The multi-step synthesis of supported Pt_3Sn nanoparticles began with supported PtSn prepared as described above. PtSn/Vulcan was mixed with 20 mL of a K_2PtCl_6 solution in TEG (1:3; PtSn:K_2PtCl_6 molar ratio), then purged with Ar for 20 min. The temperature was then raised to 280 - 290 °C for 1 h. The reaction was removed from the heat, collected by centrifugation, and washed with acetone.

3.2.6 Catalytic testing

PtPb/Vulcan XC-72 (prepared as described above) was tested for electrocatalytic oxidation of formic acid. A suspension of the PtPb catalyst was prepared by mixing ~5 mg of catalyst, 1.6 mL of Millipore water (18 $M\Omega \cdot cm^{-1}$), 0.39 mL of isopropyl alcohol, and 10 μL of 10% Nafion solution. The mixture was sonicated for 90 min before casting onto a glassy carbon electrode (3 mm diameter, BAS). The glassy

carbon (GC) electrode was cleaned by polishing with alumina paste (1 μm, 0.3 μm, and 0.05 μm) and sonicating in Millipore water for 10 min. The volume of the suspension used to coat the GC electrode was adjusted based on the concentration of each catalyst so that the total metal loading was kept as a constant (70 $\mu g/cm^2$) for all the catalysts studied. The coated GC electrode was allowed to dry in air before further electrochemical measurements. The catalyst-coated GC electrode was activated by cycling between 0.05 V - 0.5 V (*vs*. RHE) in 0.5 M H_2SO_4 at a scanning

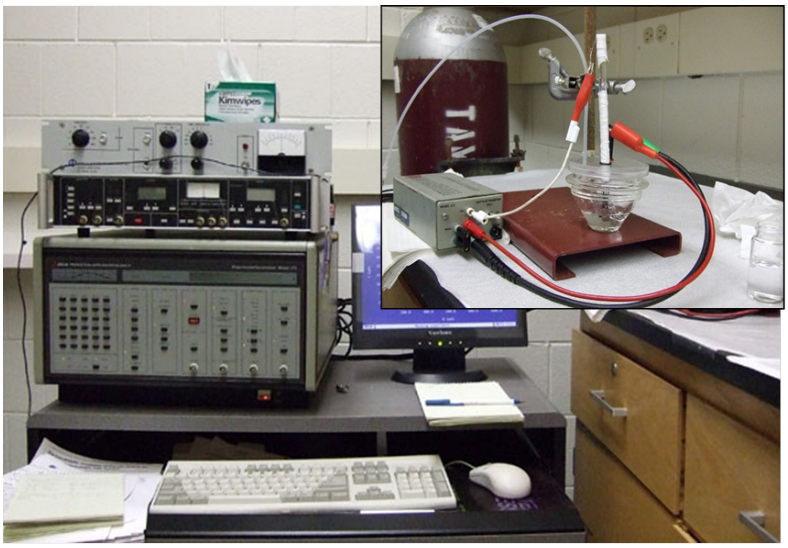

Figure 3.1. Photograph of the PAR 273 Potentiostat, M270 software package. The inset shows the three electrode sysem including the home made reference electrode (RHE), working electrode (GC), and the counter electrode (Pt foil) in a 0.5 M solution of H_2SO_4.

rate of 10 mV/s until the obtained CV shape reached a steady state. Cyclic voltammetry (using a PAR 273, EG&G shown in Figure 3.1) was carried out in 1 M formic acid with 0.5 M H_2SO_4 as the supporting electrolyte. All solutions were

prepared using Millipore water and purged with nitrogen for at least 10 min before the experiment. A homemade RHE was used as the reference electrode and Pt foil served as the counter electrode. Pt/Vulcan XC-72 (20%) and PtRu/Vulcan XC-72 (20%) were purchased from E-TEK and used as controls. PtPb/Vulcan XC-72 (~34%) was prepared in–house by converting Pt/Vulcan XC-72 (20%, E-TEK) into intermetallic PtPb as described earlier.

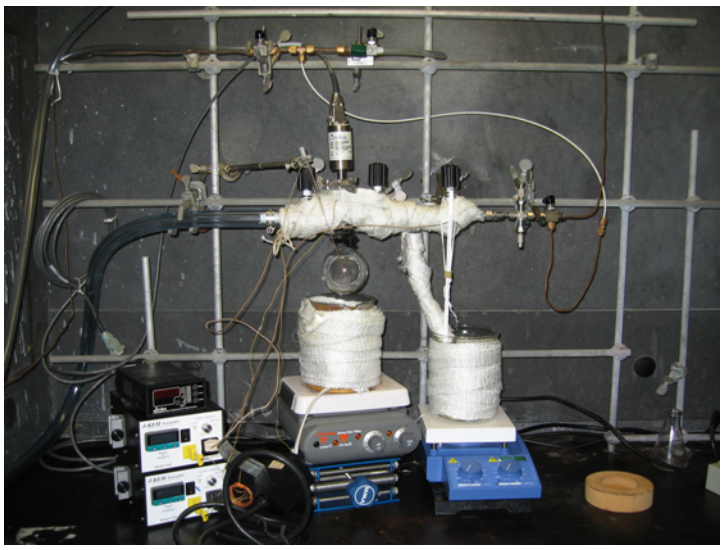

Figure 3.2. Photograph of the homemade CO oxidation reactor system. The pressure of the reactor flask was measured by a Baratron Pressure Transducer and the temperature of the oil bath and manifold were controlled by J-KEM Scientific temperature controllers.

The CO tolerance of all catalysts was studied by CO stripping voltammetry. The catalysts-coated GC electrode was immersed in a CO saturated 0.5 M H_2SO_4 solution under potential control (0.3 V vs. RHE) for 3 minutes. The solution was bubbled with nitrogen for 10 minutes at continous potential control (0.3 V) to make sure all

the CO in the solution was removed. A linear sweep was carried out at 10 mV/s starting at 0.3 V.

Preliminary CO oxidation experiments were performed in a homemade closed reactor system, shown in Figure 3.2, which was used to estimate the onset temperature for CO oxidation. O_2 and CO gases (O_2:CO = 6) were added to a vacuum chamber and allowed to mix at room temperature for 24 h. The supported catalyst was placed in a reactor and heated to 80 °C under vacuum (heating tape was used to heat the oil bath and manifold and the temperature was controlled by J-KEM Scientific temperature controllers). The O_2/CO gas mixture chamber was opened to the reaction chamber and the temperature was increased from 80 °C to 220 °C while monitoring the pressure (using a Baratron Pressure Transducer). The pressure

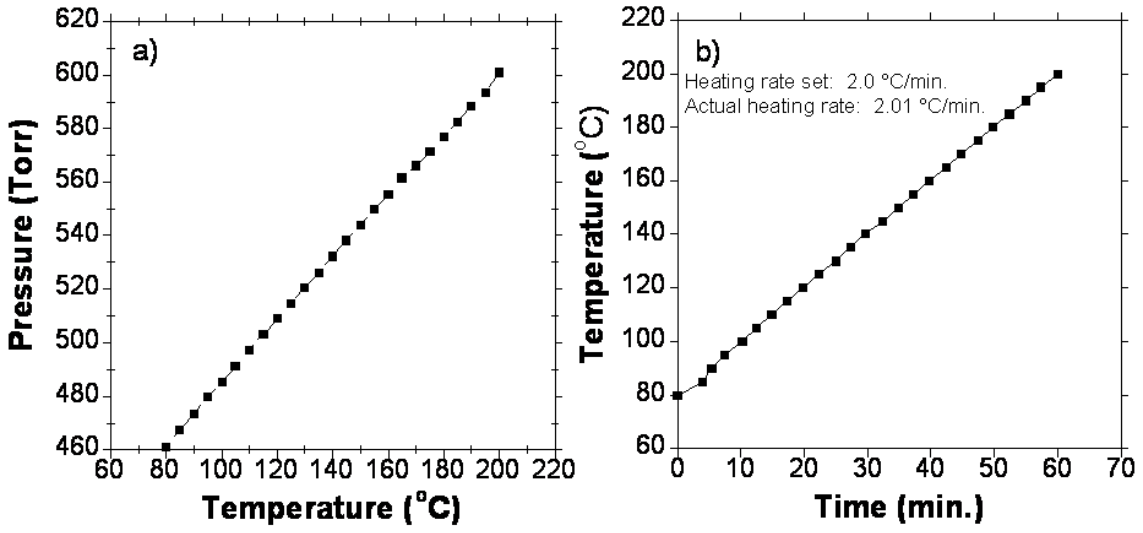

Figure 3.3. (a) Pressure vs. temperature plot showing that the pressure of O_2 was directly proportional to temperature, (b) temperature vs. time plot indicating that the J-KEM Scientific temperature controllers were capable of providing a constant heating rate.

increased at a linear (calibrated) rate as the temperature rose as shown in Figure 3.3(a). However, as soon as CO oxidation catalysis began, the pressure-temperature curve diverged from its linear progression. An approximation for the CO oxidation onset temperature could be estimated from the point of divergence. Figure 3.3(a and b) show that the CO oxidation reaction system was capable of mainting a direct relationship between pressure and temperature while being heated at a constant rate.

3.3 Converting unsupported Pt nanoparticles into intermetallics

As a first step toward accessing supported intermetallic nanoparticle catalysts, we studied the conversion of unsupported nanocrystalline Pt into Pt-*M* (*M* = Sn, Pb, Bi, Fe) alloys and intermetallic compounds in order to identify the reaction conditions necessary to carry out such transformations. Pt nanoparticles were prepared using a modified polyol process[112] without the use of PVP by heating an ethylene glycol solution of K_2PtCl_6. These Pt nanoparticles were isolated, added to a solution of an appropriate metal salt in TEG, and heated to yield intermetallic nanocrystals. Figure 3.4(a) shows the XRD patterns of the Pt nanoparticle precursors and the Pt-based intermetallics formed from them. The XRD data show nearly complete conversion to NiAs-type PtPb, PtSn, and PtBi after reaction with solutions of $Pb(C_2H_3O_2)_2 \cdot 3H_2O$ (190 °C), $SnCl_2$ (235 °C), and $Bi(NO_3)_3 \cdot 5H_2O$ (220 °C), respectively. However, the peaks in the XRD patterns of the intermetallic products are narrower than those in the Pt precursor, indicating significant particle growth during the conversion process.

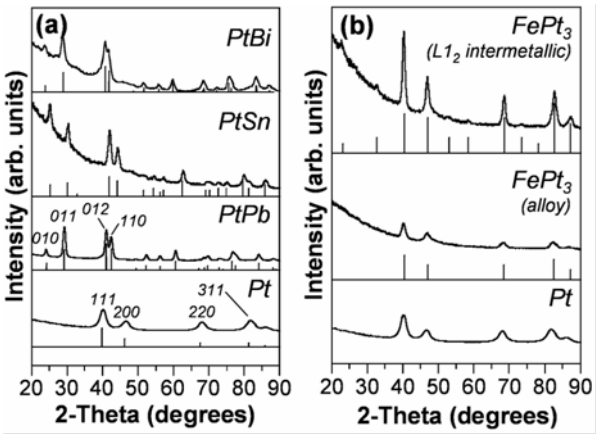

Figure 3.4. Powder XRD patterns of (a) nanocrystalline Pt and NiAs-type PtPb, PtSn and PtBi formed by reacting the Pt with appropriate metal salt solutions in TEG and (b) nanocrystalline Pt, $FePt_3$ alloy made by reacting the Pt with a TEG solution of $FeCl_3 \cdot 6H_2O$, and $L1_2$-type $FePt_3$ formed after annealing at 550 °C for 30 min. Standard reference patterns showing peak positions and relative intensities are shown below the experimental data. Characteristic peaks for fcc Pt and NiAs-type PtPb are indexed for comparison to SAED patterns shown in subsequent figures.

The TEM micrographs in Figure 3.5 confirm this by showing small Pt nanoparticles (4-5 nm) that are aggregated into spherical networks with diameters ranging from 80 to 100 nm, likely because of the absence of surface stabilizers. Converting the Pt nanoparticles to PtSn caused additional sintering of these aggregates.

This method is also useful for accessing nanocrystalline alloys. For example, Pt nanoparticles were reacted with a TEG solution of $FeCl_3 \cdot 6H_2O$ at 300 °C to form a $FePt_3$ alloy (Figure 3.4b). After annealing under Ar at 550 °C for 30 mins, intermetallic $AuCu_3$-type $FePt_3$ forms (Figure 3.4b), again with significant particle growth because of the temperature necessary to nucleate the $L1_2$ intermetallic structure.

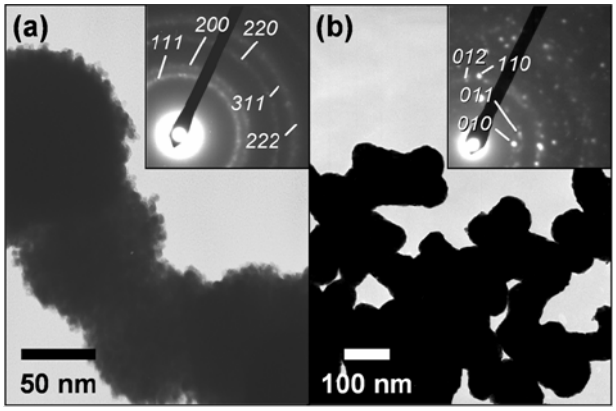

Figure 3.5. TEM micrograph showing (a) unsupported Pt nanoparticle aggregates synthesized without added surface stabilizers and (b) unsupported PtSn nanocrystals formed by reacting nanocrystalline Pt with a solution of $SnCl_2$ in TEG. SAED patterns, with indexed reflections characteristic of fcc Pt and NiAs-type PtSn, are shown in the inset.

3.4 Converting supported Pt nanoparticles into intermetallics

Pre-formed nanocrystalline Pt can clearly be converted into nanocrystalline Pt-based alloys and intermetallics by reactions with metal salt solutions under reducing conditions. However, the intermetallic nanoparticle products are severely coalesced and significantly larger than the Pt precursor, which is expected because of the reaction temperature and reaction conditions, as well as the fact that no surface stabilizers were used. In catalyst systems, immobilizing metal nanoparticles on a thermally-stable high surface-area support minimizes their aggregation during heating, provides more accessible surface-area, and facilitates the metal-support interactions that play crucial roles in catalysis. By using supported Pt nanoparticles as precursors, intermetallic nanoparticles can still be formed using reactions with metal salt solutions under reducing conditions. However, in this case, particle

growth during the reaction is minimized, and no deliberately-added surface stabilizers are necessary.

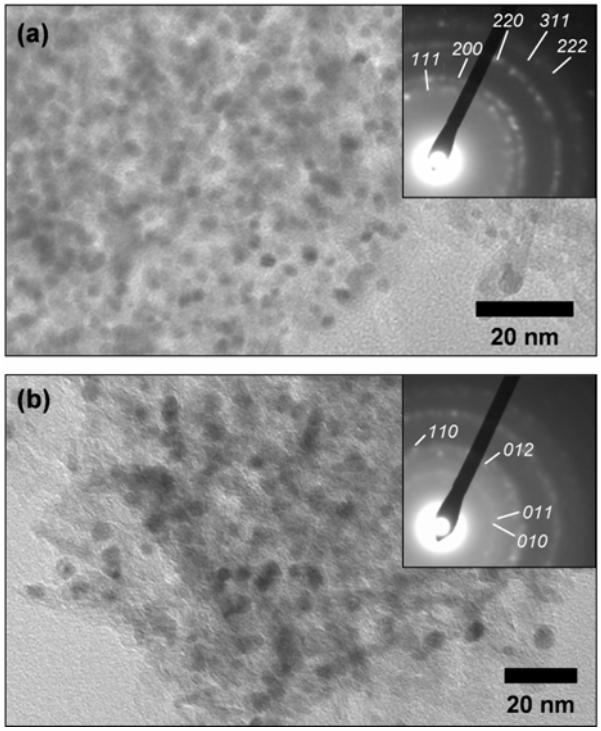

Figure 3.6. TEM micrographs showing (a) supported Pt/Al_2O_3 (3.2 wt% Pt) and (b) supported $PtSn/Al_2O_3$ formed by reacting Pt/Al_2O_3 with a solution of $SnCl_2$ in TEG. SAED patterns, with indexed reflections characteristic of fcc Pt and NiAs-type PtSn, are shown in the insets.

Figure 3.6a shows a representative TEM image of Pt nanoparticles (3.2 wt%) supported on γ-Al_2O_3 (Pt/Al_2O_3) made by heating K_2PtCl_6 in ethylene glycol in the presence of the Al_2O_3 support. The resulting Pt nanoparticles are well dispersed and have an average diameter of 3.3 ± 0.5 nm, and XRD (Figure 3.7) confirms the presence of nanocrystalline Pt. After this Pt/Al_2O_3 sample was added to a TEG solution of $SnCl_2$ and heated to 235 °C for 1 h, the Pt was converted to PtSn to form

$PtSn/Al_2O_3$. The supported PtSn nanoparticles, shown in Figure 3.6b, remain well dispersed. The particle sizes grew to an average of 5.2 ± 1.0 nm, which is close to that expected for the addition of Sn to Pt via an additive, diffusion-based mechanism. The XRD data (Figure 3.7) and SAED pattern (Figure 3.6b, inset) both show a hexagonal NiAs-type pattern consistent with that of PtSn. This confirms the formation of intermetallic PtSn supported on Al_2O_3 and shows that the reaction does indeed succeed at the on-support conversion of Pt to PtSn with retention of the general size and size dispersity defined by the Pt precursor.

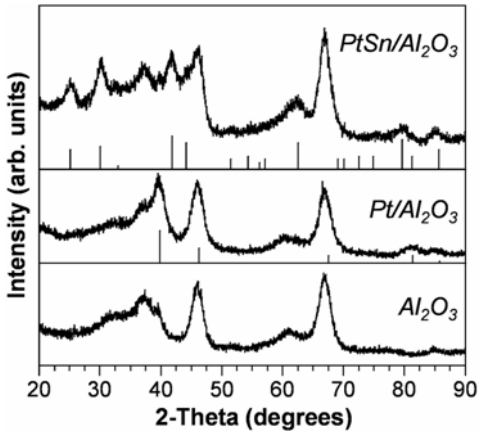

Figure 3.7. Powder XRD patterns for γ-Al_2O_3 (support), Pt/Al_2O_3 (synthesized by heating γ-Al_2O_3 with a solution of K_2PtCl_6 in EG), and intermetallic/Al_2O_3 formed by reacting Pt/Al_2O_3 with a solution of $SnCl_2$ in TEG. Standard reference patterns showing peak positions and relative intensities for Pt and PtSn and shown below the experimental data.

This approach for converting supported Pt nanoparticle catalysts into supported intermetallics is quite versatile for a variety of alloy, intermetallic and support systems. For example, the powder XRD patterns in Figure 3.8 show

$PtPb/CeO_2$ (prepared from 3.2 wt% Pt), $PtSn/CeO_2$ (prepared from 3.2 wt% Pt), Pt_3Sn/Vulcan (prepared from 20 wt% Pt), and Cu_3Pt/Al_2O_3 (prepared from 3.2 wt% Pt). All of these supported nanoparticle systems were derived from supported Pt nanoparticles (e.g. Pt/CeO_2, Pt/Vulcan, Pt/Al_2O_3) after reactions with metal salt

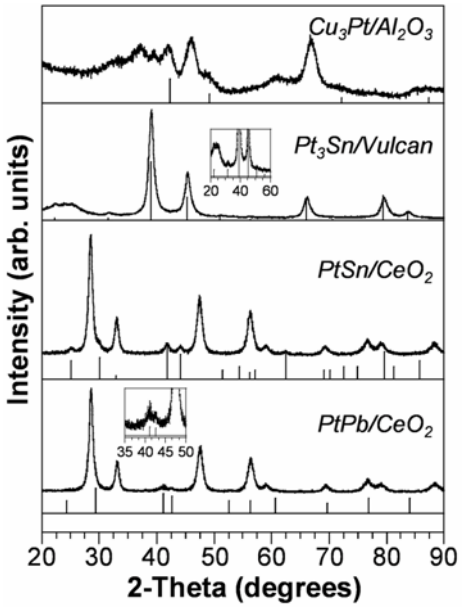

Figure 3.8. Powder XRD patterns showing supported Pt-based catalysts formed by reacting supported Pt nanoparticles with appropriate metal salt solutions under reducing conditions: intermetallic $PtPb/CeO_2$, $PtSn/CeO_2$ and Pt_3Sn/Vulcan XC-72, and Cu-Pt alloy (Cu_3Pt/Al_2O_3). The insets show enlarged views that highlight the key peaks characteristic of the intermetallic phase.

solutions under reducing conditions. Interestingly, we find that intermetallic $AuCu_3$-type Pt_3Sn forms at temperatures as low as 285 °C without the need for high-temperature annealing, as is usually necessary for this known catalyst system.[113] (The weak superlattice reflections indicate that atomic ordering into the $AuCu_3$ structure has occurred, but the order is probably incomplete.) In the case of Cu_3Pt,

the XRD pattern shows an fcc structure with peaks that are shifted relative to those of Pt, indicating the formation of a Pt-Cu alloy. The TEM images in Figure 3.9 show the supported alloy and intermetallic nanoparticles, and the SAED patterns confirm the alloy and intermetallic phase formation observed by XRD. The nanoparticles are, on average, slightly larger than their Pt precursors, which is required by the addition of more material to the particles via diffusion. Some sintering is observed (particularly for the Pt_3Sn/C system), but the nanoparticles still remain relatively well dispersed. The support clearly allows the conversion reactions to proceed without significant particle coalescence, as was observed for the unsupported particles (Figure 3.4).

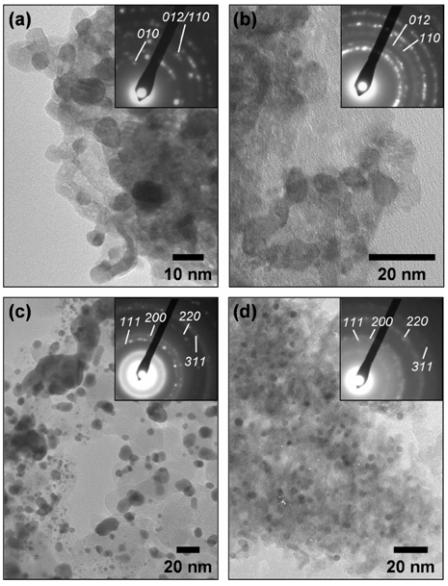

Figure 3.9. TEM micrographs of (a) $PtPb/CeO_2$, (b) $PtSn/CeO_2$, (c) Pt_3Sn/Vulcan, and (d) Cu_3Pt/Al_2O_3. SAED patterns, with indexed reflections characteristic of the intermetallic phase, are shown in the insets.

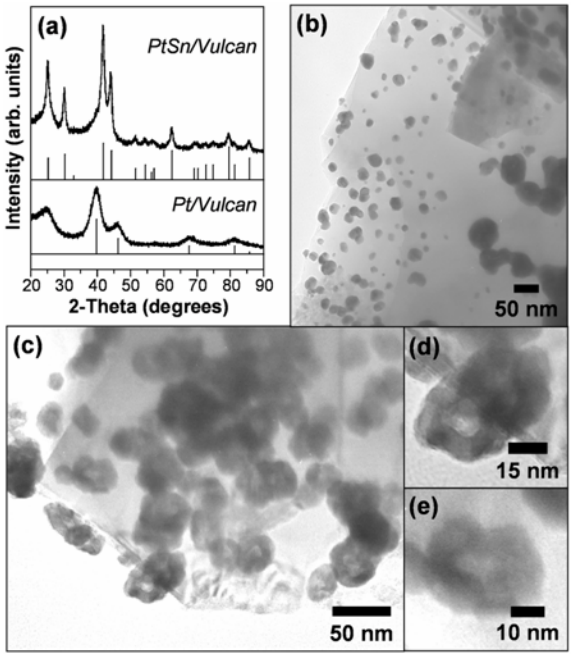

Figure 3.10. (a) Powder XRD pattern of Pt/Vulcan and PtSn/Vulcan formed by reacting Pt/Vulcan with a solution of $SnCl_2$ in TEG. TEM micrographs of (b) Pt/Al_2O_3 (Strem Chemicals, 5%Pt), (c) $PtSn/Al_2O_3$ formed by reacting Pt/Al_2O_3 (Strem) with a solution $SnCl_2$ in TEG, and (d and e) enlarged images from panel (c) showing hollow PtSn nanoparticles.

The supported catalysts shown in Figures 3.8 and 3.9, with the exception of Pt_3Sn/Vulcan, were derived from Pt nanoparticles that were reduced directly onto the supports using a standard polyol process. Commercially-available supported Pt/Vulcan XC-72 (20 wt% Pt, E-TEK) and Pt/Al_2O_3 (5 wt% Pt, Strem Chemicals) can also be converted into intermetallic catalysts, as shown in Figure 3.10(a). TEM images and SAED patterns of Pt/Al_2O_3 (Strem) and $PtSn/Al_2O_3$, formed by reacting Strem Pt/Al_2O_3 with $SnCl_2$ in TEG at 235 °C, are shown in Figures 3.10b and 3.10(c-e), respectively. The supported Pt nanoparticles in Figure 3.10b are significantly larger than those used previously, with diameters ranging from 6 to 71 nm. We[106,

[114, 115] and others[9, 10, 116, 117] have observed that hollow nanoparticles form through similar diffusion-mediated reactions as a result of a nanoscale Kirkendall effect. In some cases, we have observed size effects where smaller metal nanoparticle precursors generate dense products while larger ones will become hollow.[22, 30] A majority of the PtSn nanoparticles derived from the Strem Pt/Al_2O_3 system are hollow, demonstrating that the Kirkendall reactions that generate hollow nanocrystals are also applicable to supported nanocrystal systems.

In addition to the direct reactions that convert metals into intermetallics, we have also shown that binary intermetallic nanoparticles can be cyclically interconverted to form different phases.[26] For example, PtSn nanoparticles can be reacted with a solution of K_2PtCl_6 under reducing conditions to form Pt_3Sn, which can in turn be reacted with a solution of $SnCl_2$ under similar conditions to form PtSn. (These reactions utilize diffusion-based processes, so the nanoparticles grow at each step.) A similar process is successful for modifying supported intermetallic nanoparticle catalysts. For example, Pt/Vulcan can be converted to PtSn/Vulcan as described previously, and the XRD data in Figure 3.11 confirm that this conversion is successful. The PtSn/Vulcan system can then be added to a solution of K_2PtCl_6 in TEG and heated to 280 °C for 1 h. The product of this reaction is Pt_3Sn/Vulcan, as indicated by the XRD pattern shown in Figure 3.11. The superlattice peaks confirm the formation of intermetallic $AuCu_3$-type Pt_3Sn. There are slight Pt and PtSn impurities, which could result from the deposition and conversion of new Pt nanoparticles on the support during the course of the reaction. While Pt_3Sn was also accessible by the direct conversion of Pt/Vulcan via reaction with $SnCl_2$ (Figure

3.8), this result demonstrates that multi-step conversion reactions can indeed be used for supported nanoparticle precursors. This is important because it opens the door for preparing supported nanoparticles of compounds that might be difficult to form using direct methods.

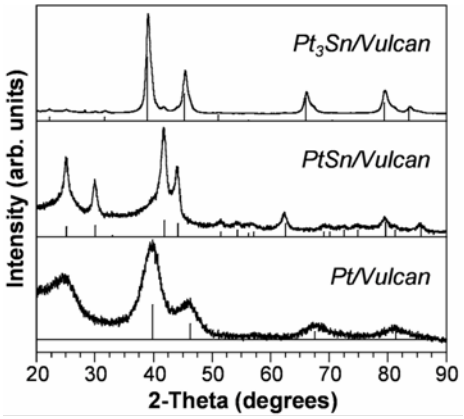

Figure 3.11. Powder XRD patterns showing a multi-step conversion: Pt/Vulcan reacted with a TEG solution of $SnCl_2$ to form NiAs-type PtSn/Vulcan, which is then reacted with a TEG solution of K_2PtCl_6 to form $AuCu_3$-type Pt_3Sn/Vulcan.

3.5 Catalysis studies of supported intermetallic nanoparticles

While the chemistry described thus far clearly generates supported intermetallic nanoparticles, it is useful to explore whether they are active for relevant catalytic reactions and, importantly, whether this chemistry can yield useful catalysts. Pt-based intermetallic nanoparticles are known to be active electrocatalysts for reactions such as formic acid oxidation,[63] but few such studies have been done using *supported* intermetallic nanoparticle catalysts. The electrocatalytic activity of Pt/Vulcan XC-72 (E-TEK), PtRu/Vulcan XC-72 (E-TEK) and PtPb/Vulcan XC-72 catalysts were

analyzed by our calloborater Joy Chen. The cyclic voltammograms of the nanoparticle catalyst in 1 M formic acid with 0.5 M H_2SO_4 as the supporting electrolyte are shown in Figure 3.12 (PtPb/Vulcan XC-72 was formed by reacting

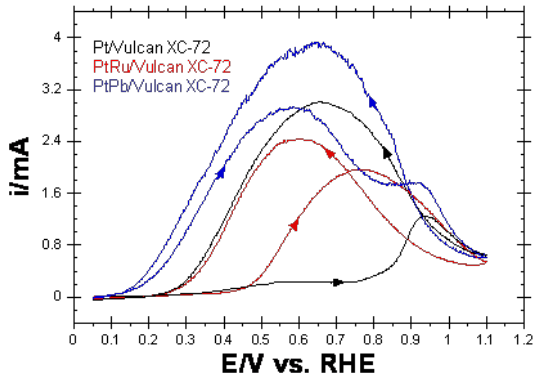

Figure 3.12. Cyclic voltammograms of commercial Pt/Vulcan (20% Pt on Vulcan XC-72), commercial PtRu/Vulcan (20% PtRu/Vulcan XC-72), and PtPb/Vulcan [formed by reacting commercial Pt/Vulcan with a TEG solution of $Pb(C_2H_3O_2)_2$] in 1 M formic acid with 0.5 M H_2SO_4.

Pt/Vulcan XC-72 with $Pb(C_2H_3O_2)_2 \cdot 3H_2O$ in TEG at 190 °C for 1 h). The onset potentials for formic acid oxidation were observed at about 0.8 V, 0.4 V, and 0.1 V (vs. RHE) for Pt/Vulcan, PtRu/Vulcan and PtPb/Vulcan, respectively. As shown in Figure 3.12, PtPb/Vulcan provides a higher current at a significantly lower potential compared to both Pt/Vulcan and PtRu/Vulcan, which makes it a good catalyst for formic acid oxidation. This also compares favorably with electrochemical formic acid oxidation using unsupported intermetallic PtPb nanoparticles, which were reported to have an onset potential as low as -0.2 V vs. Ag/AgCl, or ~0.02 V vs. RHE.[62] The observation of electrocatalytic activity for formic acid oxidation, at a

much lower onset potential than PtRu/Vulcan, confirms that the supported nanoparticle systems synthesized using "conversion chemistry" techniques can indeed serve as active catalysts. It should be noted that pretreating the catalysts at high potentials will likely cause leaching of the non-noble metal (in this case Pb) to form a Pt-rich surface, so the catalytically active surface may be different from the bulk composition and structure. DiSalvo, Cabrera and Abruña studied the surface stability of PtBi and PtPb by ex-situ X-ray photoelectron spectroscopy after treatment at various potentials.[60] The results indicated that the surface composition of PtPb was relatively stable up to +0.8 V vs. Ag/AgCl (~1.02 V vs. RHE), while above that potential the Pb oxidizes to produce a Pt rich surface.

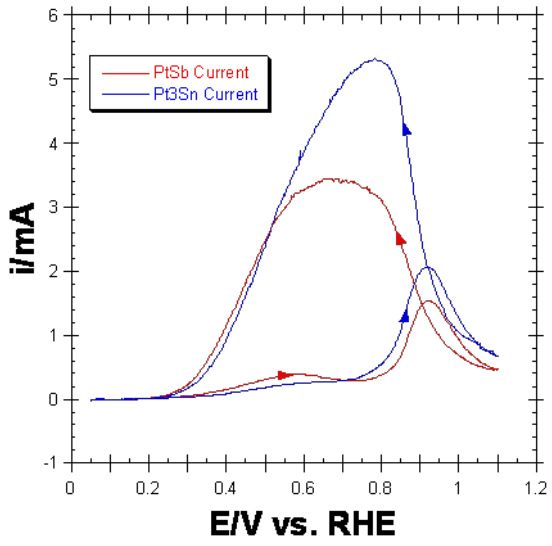

Figure 3.13. Cyclic voltammograms of PtSb/Vulcan and Pt_3Sn/Vulcan [formed by reacting commercial Pt/Vulcan with a TEG solution of $SbCl_3$ or $SnCl_2$] in 1 M formic acid with 0.5 M H_2SO_4.

Additionally, Chen analyzed the formic acid electro-oxidation was tested for the supported intermetallic compounds of Pt_3Sn/Vulcan XC-72 and PtSb/Vulcan XC-72. [(Pt_3Sn and PtSb were formed by reacting Pt/Vulcan XC-72 and $SnCl_2$ (3:1 and 1:1 molar ratio of Pt to $SnCl_2$ and $SbCl_3$ respectively) in TEG at 285 °C for 1h or $SbCl_3$ in TEG at 275 °C for 1h respectively.)] The onset potential, shown in Figure 3.13, for Pt_3Sn/Vulcan XC-72 was ~ 0.75 V and for PtSb it was ~ 0.8 V vs. RHE. PtSb/Vulcan XC-72 and Pt_3Sn/vulcan XC-72 almost mirror the electrocatalytic activity of Pt/Vulcan XC-72 with the exception that Pt_3Sn almost doubles the current at a peak potential of ~ 0.95 V. It can be concluded that Pt_3Sn/Vulcan XC-72 and PtSb/Vulcan XC-72 do not improve the oxidation of formic acid reaction when compared to Pt/Vulcan XC-72.

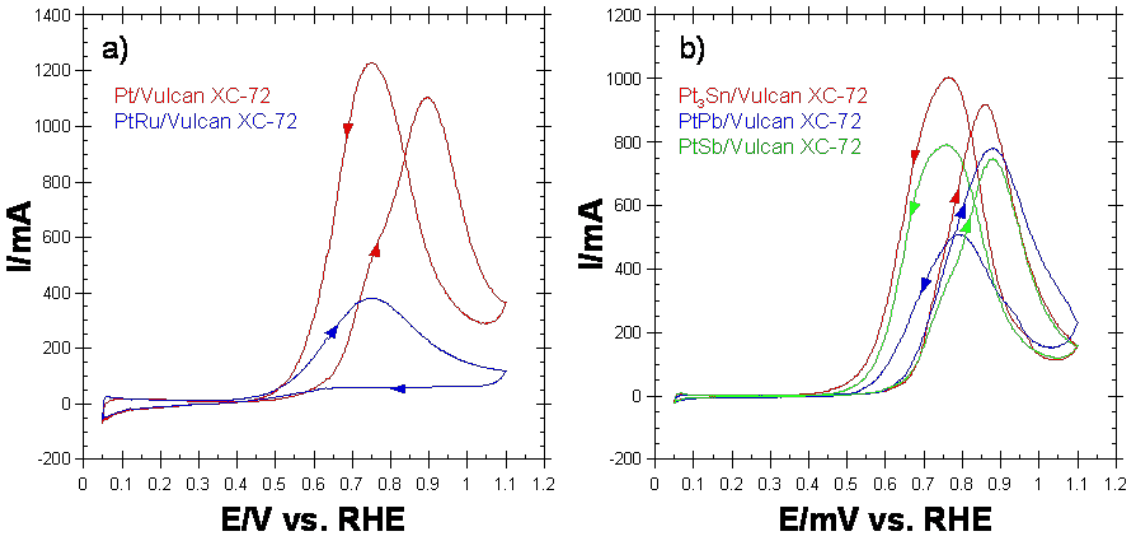

Figure 3.14. Cyclic Voltammograms of (a) commercial Pt/Vulcan (20 % Pt on Vulcan XC-72) and commercial PtRu/Vulcan (20 % PtRu on Vulcan XC-72) and (b) Pt_3Sn/Vulcan, PtPb/Vulcan, and PtSb/Vulcan [formed by reacting commercial Pt/Vulcan in TEG with $SnCl_2$, $Pb(C_2H_3O_2)_2{\cdot}3H_2O$, and $SbCl_3$]. Both experiments were done in 1 M methanol with 0.5 M H_2SO_4.

Cyclic votametry experiments using the same nanoparticle catalysts as listed above (Pt, PtRu, PtPb, Pt_3Sn, and PtSb supported on Vulcan XC-72) for methanol oxidation were perfomed as well by our callaborator Chen. Methanol is considered a desirable source of fuel for fuel cells (even though it is considered toxic) because its easy ability to store and handle (compared to H_2 gas) and its high energy density. The electrocatalytic activity of the nanoparticle catalysts was studied using 1 M methanol with 0.5 M H_2SO_4 as the supporting electrolyte. As shown in Figure 14a,

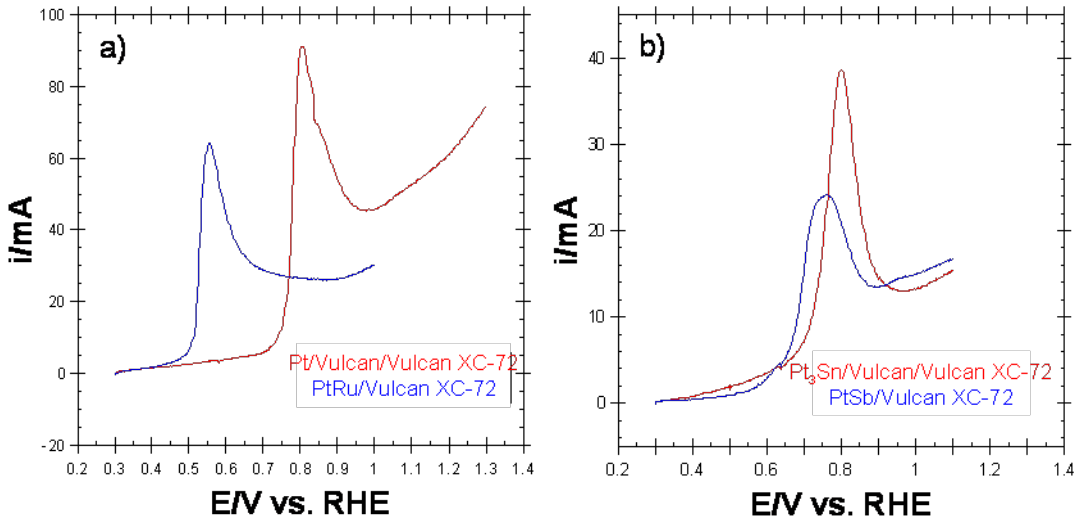

Figure 3.15. CO stripping voltammograms of (a) commercial Pt/Vulcan (20 % Pt on Vulcan XC-72) and PtRu/Vulcan (20 % PtRu on Vulcan XC-72) (top) and (b) Pt_3Sn/Vulcan and PtSb/Vulcan [formed by reacting commercial Pt/Vulcan in TEG with $SnCl_2$ or $SbCl_3$] in CO saturated 0.5 M H_2SO_4.

The onset potntial for Pt/Vulcan XC-72 and PtRu/Vulcan XC-72 was 0.4 V and 0.6 V, respectively. The Pt and PtRu catalysts out perfomed the intermetallic catalysts of PtPb/Vulcan XC-72, Pt_3Sn/Vulcan XC-72, and PtSb/Vulcan XC-72 whose onset

potentials were 0.65 V vs. RHE in all three cases shown in the bottom of Figure 3.14.

Multimetallic catalysts for alcohol oxidation reactions are generally known to enhance electrocatalytic reactions by lowering the onset potential and increasing the tolarence of carbon monoxide and thiol poisoning due to electronic conributions from the second metal[118, 119] and surface geometry.[63] For example, Bi and Pb increase the fermi energy (for the intermetallic sructures) which causes the anti-bonding orbitals of the CO to be filled and weakens the Pt-CO interaction. Also, the addition of Bi or Pb increases the distance between the Pt atoms so the more stable brigded or 3-fold bonding positions with CO are less accessible leaving the least stable lineraly bonded position as the preferred arrangment. The CO tolerance of the catalysts tested for methanol and formic acid oxidation were studied by CO stripping voltammetry (carried out by our callaborator) using CO saturated 0.5 M H_2SO_4 and the results can be found in Figure 3.15. CO oxidation occurred at ~0.55 V and 0.80 V for PtRu/Vulcan XC-72 and Pt/Vulcan XC-72. Pt_3Sn/Vulcan XC-72 and PtPb/Vulcan XC-72 showed similar results to Pt and oxidized CO at ~0.80 V vs. RHE. PtSb/Vulcan XC-72 showed a slightly improved CO tolerance relative to Pt/Vulcan XC-72 with a broad CO stripping peak at ~0.75 V vs. RHE.

Many of these intermetallic systems are also used in gas phase reactions for CO oxidation. In particular, Pt_3Sn is able to catalyze CO oxidation at low temperatures while still maintaining a high selectivity and activity.[108, 120] Theoretical and experimental studies have shown that the reaction rate of Pt_3Sn/C (*111* surface) is two orders of magnitude higher at 300 K than on Pt/Al_2O_3 (*111* surface).[108-110, 121]

As a preliminary screening of their ability to serve as CO oxidation catalysts, a simple gas-phase CO oxidation experiment was performed (with the assistance of Qingsheng Liu) on Cu_3Pt/Al_2O_3 and Pt_3Sn/Vulcan prepared by conversion of polyol-derived Pt/Al_2O_3 and Pt/Vulcan. It was found that Cu_3Pt/Al_2O_3 and Pt_3Sn/Vulcan started to catalyze the reaction at ~175 °C and 160 °C, respectively. These catalysts show an improvement when compared to their Pt/Al_2O_3 and Pt/Vulcan precursors, which began to catalyze the reaction at 200 °C. While these are clearly not the most active catalysts for CO oxidation, they are measurably improved relative to pure Pt and serve as a preliminary indication that these supported intermetallic nanoparticles can also catalyze gas-phase reactions.

The experiment (shown in Figure 3.16) was extended to further study the affects of CO oxidation with additional intermetallic systems (PtPb, PtSn, and PtSb) in combination with various supports (Vulcan XC-72, graphite, Al_2O_3, and CeO_2). It was found that Pt/Al_2O_3 and Pt/graphite started to catalyze the reaction at 200 °C while Pt/CeO_2 oxidized CO at ~140 °C. Jin et al. reported that Temperature-Programmed Disorption experiments indicate the in Pt/CeO_2, lattice oxygen at the interface play an important role in the formation of CO_2; supposedly the lattice oxygens are at an accessible site which permit oxidation of CO at a lower temperature in our experiments.[122] The effect of lowering the CO oxidation temperature by supporting Pt on ceria is a common observation brought on by strong-metal-support-interactions (SMSI).[123] Common explanations as to why the SMSI effect can affect the CO oxidation reaction are that the Pt and Ce can form an

alloy,[124; 125] partially reduced ceria can decorate or encapsulate Pt,[126; 127] and electronic interactions between Pt and Ce.[128]

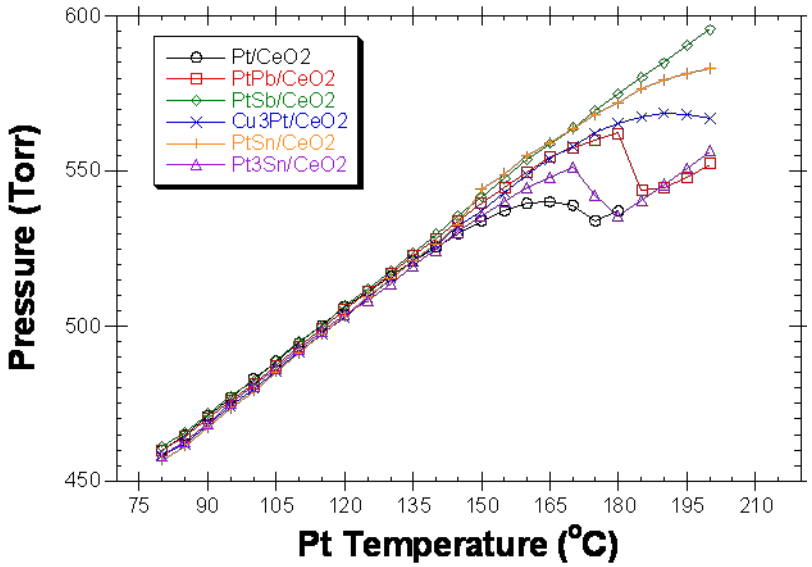

Figure 3.16. Estimation of CO oxidation onset temperature by reacting O_2 and CO gas (O_2:CO = 6) with Pt, PtPb, PtSb, Cu_3Pt, PtSn, and Pt_3Sn supported on ceria.

Pt/CeO_2 was converted into supported intermetallic nanoparticle catalysts that were tested for the oxidation of CO. As seen in Figure 3.16, the intermetallic catalysts required higher reaction temperatures (PtPb, 175 °C; PtSn, 180 °C; PtSb, 220 °C; Pt_3Sn, 175 °C; and Cu_3Pt (alloy), 185 °C) to catalyze the reaction than pure Pt. It is believed that the CO oxidation reaction may happen at the interface between Pt and ceria.[129] It has even been demostrated that Pt can even be fully encapsulated with a thin film of ceria and still show better catalytic activity than a clean surface of Pt.[129] One accepted mechanism for this process is that Pt can transfer some of its electron density and partially reduce the ceria support ($Ce^{4+} \rightarrow Ce^{3+}$).[129] In situations

where the Pt nanoparticles are not fully encapsulated the CO molecule may absorb onto the Pt nanoparticle and migrate to the Pt/ceria interface.[122] The ceria support can then donate an oxygen atom from its lattice to oxidize CO to CO_2.[122]

It is clearly seen that alloying a new metal to Pt supported on CeO_2 causes CO oxidation to occur at higher temperatures. However, when carbon or γ-Al_2O_3 are used the intermetallic nanoparticles catalyzes the reaction at a lower temperature than Pt. Therefore, the reduced catalytic effects of the intermetallic nanoparticles supported on CeO_2 are most likely caused by electronic interaction between the catalyst and support. Considering the proposed electronic interaction between Pt and ceria, one would expect that the binding energy on Pt 4d would increase and while it would decrease on the lattice O 1s. Investigating the electronic structures of the intermetallic compound of PtPb shows a narrowing of the d-orbital band, lowering of the d-orbital away from the Fermi energy, and that the s and p orbitals (from Pb) have an increasing interaction with the absorbant.[119] XPS measurments also indicate, in the case of Pt_3Sn, the binding energy of the Sn 3d peak shifts 0.3 eV toward a higher energy which is typical of alloying (increasing electron density on Pt).[130] It may be reasonable to assume that Pt-based intermetallic compounds with similar elements follow a similar trend. One may expect to expect that the increased electron density on Pt may enhance the Pt/ceria effect. However, the Pt/ceria interface where CO oxidation occurs might be impeded by the presence of the foreign metal in the intermetallic nanoparticle; oxidation would then require higher temperatures. XPS experiments should be conducted in the future to further

understand the interaction between the Pt-based intermetallic nanoparticle and the ceria support.

3.6 Conclusion

We have shown that low-temperature solution chemistry strategies that are being developed for transforming metal nanoparticles into derivative alloys and intermetallic compounds are also applicable to supported nanoparticle systems. This strategy makes it possible to use supported single metal nanoparticles (e.g. Pt/Al_2O_3), either made by literature methods or purchased commercially, as templates that help to define the size, size dispersity, morphology, and spatial dispersity of the product alloy and intermetallic nanoparticles, which remain on the support during the chemical conversion reaction. While the final alloy and intermetallic nanoparticles are larger than the supported metal nanoparticle precursors (since the synthetic process involves a diffusion-based mechanism), the support helps to minimize aggregation and sintering, which is typical for intermetallic catalysts prepared by other solution-phase and high-temperature annealing methods. As such, no deliberately added surface stabilizers are needed to maintain nanocrystallinity in the alloy and intermetallic products. The supported alloy and intermetallic nanoparticles are catalytically active for chemical transformations such as formic acid oxidation (PtPb/Vulcan) and CO oxidation (Pt_3Sn/graphite and Cu_3Pt/Al_2O_3), providing evidence that this synthetic strategy can yield useful catalytic materials.

4. THE CONVERSION OF SUPPORTED Pd NANOPARTICLES TO ALLOY AND INTERMETALLIC CATALYSTS FOR ORGANOCOUPLING REACTIONS

4.1 Introduction

Suzuki-Miyaura cross-coupling[131] is one of the most important and widely used organic reactions because it is able to form carbon-carbon bonds and is routinely used in the synthesis of pharmaceuticals, polymers, and agrochemicals. The Suzuki reaction usually initiates carbon coupling between electrophiles (aryls, alkyls, alkenyls and alkynyls) and organoboranes over a Pd catalyst. The mechanism for this reaction, shown in Figure 4.1,

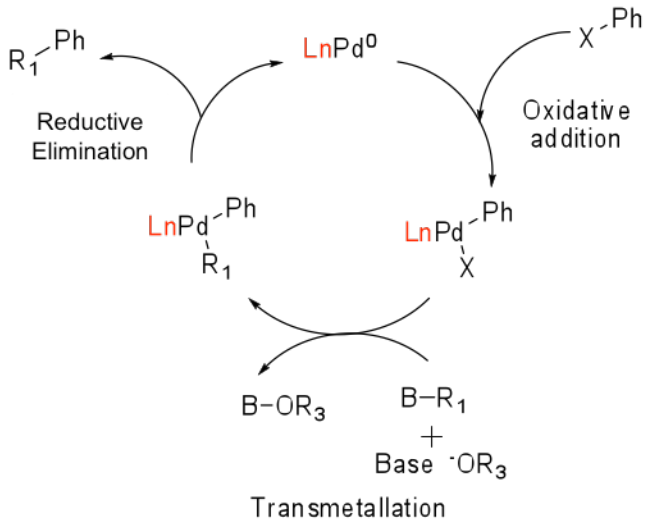

Figure 4.1. General reaction mechanism for the Suzuki coupling reaction. The first step is oxidative addition, followed by transmetallation and finally ends with the product forming via reductive elimination.

begins with the oxidative addition of the alkyl halide onto the Pd^0 to make the Pd^{2+} complex, as shown. In the next step, the base aids the transmetallation process, in which the halide from the Pd^{2+} intermediate is exchanged for the alkyl group or the organoboron species after it has been activated by the base. The transmetallation yields another Pd^{2+} (organopalladium) intermediate. The product is then formed as a result of reductive elimination of the organopalladium and the Pd^0 catalyst is recycled to its original state.

Another type of an important carbon-coupling reaction is called the Heck reaction where aryl or vinyl halides are reacted with activated alkenes in the presence of

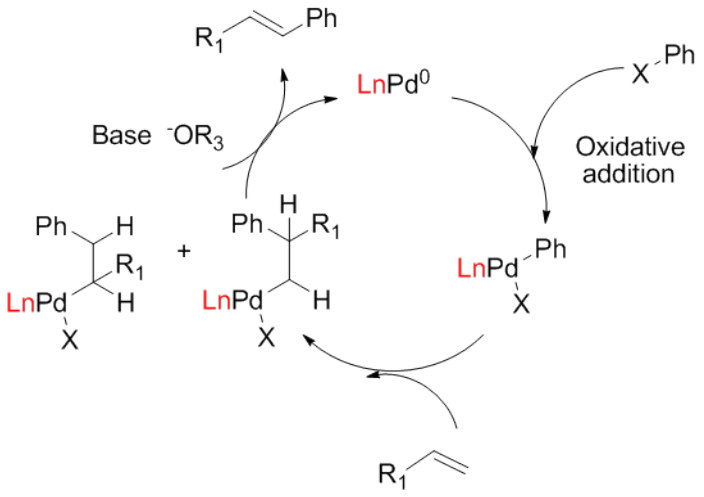

Figure 4.2. Reaction mechanism of the Heck reaction where the phenyl halide is added to Pd by oxidative addition, the alkene is inserted and the product is formed through reductive elimination.

a strong base and a Pd catalyst to form substituted alkenes. [132] In some cases this process can begin by reducing a Pd^{2+} source with triphenylphosphine (PPh_3) to reduce to

Pd^0 [$Pd(PPh_3)_2$]. Next, an aryl or vinyl halide is added to the Pd complex through oxidative addition. An alkene is then added to the complex to initially form a π-complex with Pd followed by an insertion forming a σ-complex as seen in Figure 4.2. The product is formed through β-hydride elimination and then the base removes the "H" and the halide by reductive elimination to regenerate the Pd catalyst.

Suzuki and Heck reactions are traditionally carried out in organic solvents with homogenous Pd systems. The homogenous Pd catalysts are highly reactive, but have several drawbacks that can limit their use. One drawback is that expensive and air-sensitive phosphine ligands are generally required and they can restrict the use to only expensive bromo- and iodoarenes. Another problem is that homogenous catalysts are difficult to separate and as a result products can be contaminated with Pd metal even after the purification step. The Pd contamination becomes an issue when biologically active compounds are synthesized. On the other hand, heterogeneous Pd catalysts can be easily removed from the reaction by filtration or centrifugation and contamination of the final product can be prevented. The catalysts can also be recycled through the reaction several times and does not require air-sensitive and toxic phosphines.

Instead of using the traditional homogenous catalysts that often required difficult conditions, the Suzuki reaction can be carried out over the surface of Pd nanoparticles. However, since nanoparticles contain a large fraction of their atoms on the surface (high surface-area to volume ratio) many unpassivated bonds are present resulting in the instability of the small size of the particles. Therefore, it becomes necessary to use

surface stabilizers to prevent the particles from agglomerating and growing to maximize the surface-area.

El-Sayed and coworkers reported that Pd nanoparticles stabilized with PVP could successfully be used as catalysts for the Suzuki coupling reaction between phenyl boronic acid and iodobenzene.[133] They found that the average size of the Pd nanoparticles increased due to Ostwald ripening and eventually precipitated out of solution thus lowering the catalytic activity every cycle. Additional PVP was added to the Suzuki reaction and the small sizes of the Pd nanoparticles were preserved, but the catalytic activity still decreased and this was attributed to the PVP's increased binding to the nanoparticle's surface. In a separate study, El-Sayed compared polystyrene-poly(sodium acrylate) block copolymers, PVP and second generation (G2), third generation (G3) and fourth generation (G4) stabilized hydroxyl-terminated poly(amido-amine) (PAMAM) dendrimers as capping agents for Pd nanoparticle catalysts for the Suzuki reaction.[134] It was observed that Pd nanoparticles stabilized by G4 dendrimers were the most stable but less reactive while lower generation dendrimers were less stable, but showed the most activity. PVP stabilized Pd nanoparticles showed the highest activity, but formed carbon-black powder in the solution while block copolymer stabilized particles were more stable and showed comparable activity.

Using Pd nanoparticles as catalysts for the Heck reaction has also been studied. A few early studies were done using Pd colloids for catalysts and using various stabilizing agents with mixed results.[135-138] The main issue was that the Pd nanoparticles were not very stable and tended to exhibit signs of metal leaching that eventually caused

particle growth and loss of surface area that led to a decrease of catalytic activity. In one specific case, the authors observed that even when $Pd(OAc)_2$ (OAc – acetate) was used as the catalyst; Pd colloids were precipitated out during the reduction process of the Heck reaction and they even functioned as catalysts.[139] Crooks reported that using poly(propyleneimine) (PPI) dendrimers modified on the periphery with perfluorinated polyether chains were efficient as stabilizers for the Heck reaction of n-butul-acrylate with aryl halides and lowered the reaction temperature required to obtain the desired product with 100% yield.[140] Using the dendrimers in liquid and supercritical CO_2 however, gave high yields of the byproducts of the Heck coupling reaction.[141] An additional study was done involving G4-PAMAM Pd dendrimers for the coupling of aryl halides and acrylic acid and it was found that 200-400 times less catalyst was required, but the particles were not stable through the reaction conditions in view of the fact that Pd leaching was observed.[142] The concern of nanoparticle stability becomes apparent through the previously mentioned work and it appears that the more the particles are stabilized with a capping agent the less reactive the catalysts become. The diminished reactivity may be attributed to the capping agents blocking the catalytically active sites.

Stabilizing agents can be avoided if the nanoparticles are immobilized on a solid support. Introducing Pd nanoparticles supported on a solid support may perhaps be ideal because it is already in the form of solid crystals and one would expect that the formation of carbon black should be reduced. The idea of using supported Pd nanoparticles for the Heck reaction has been around since 1973 when Julia and co-workers catalyzed cross-coupling reaction of styrene with aromatic chlorides (usually

less reactive than the more expensive iodides) using Pd/C with about 50 % conversion to the product.[143] However, the first report of the use of Pd/C for the Suzuki reaction is fairly recent (1994) and was done by Marck *et. al.* for the coupling of phenylboronic acids with aryl halogens and triflates.[144] Since Pd/C is a well-known hydrogenation catalysts, it should be expected to be relevant for the catalysis of both Suzuki and Heck coupling reactions.[37, 145] Pd nanoparticles have also been supported on carbon nanotubes,[146] as well as a variety of oxide supports including, titania[147], silica[148], and alumina[149]. All examples cited in literature describe how Pd nanoparticle catalysts can be stable even after recycling through the reaction several times while preserving a relatively small particle size distribution. In the same way, for the Heck reaction Pd nanoparticles have been supported on MgO, SiO_2, Al_2O_3, TiO_2, ZrO_2, and ZnO.[37] The most reactive catalysts from the published studies appear to be Pd/C, however, the oxide supports proved to generate the most stable Pd nanoparticles which were less susceptible to metal leaching. The stability of Pd on reducible metal oxide supports can possibly be attributed to strong metal support interactions (SMSI) that can affect the electron density on the metal and help prevent particle sintering.[37]

In an effort to explore the potential improvement on the catalytic activity for further reaction systems, a second metal can be added to synthesize bimetallic or alloy nanoparticle catalysts for coupling reactions such as hydrogenation[33], CO oxidation[150], and small organic molecules (SOM's) oxidation.[40] Common reasoning as to why multi-metal catalyst surfaces often improve catalytic activity or selectivity can be explained by the surface composition that effects the relative positioning of the surface atoms.

Theoretical studies have concluded that the bonding of a second metal raises the Fermi energy to fill anti-bonding orbitals and weaken the Pt – adsorbate interaction in the cases of BiPt[118] and PtPb.[119] Surprisingly, there has been little published research on exploring multi-metallic nanoparticles as catalysts for the Suzuki and Heck reactions even though they are some of the most widely used reactions. Reetz and coworkers prepared Pd/Ni nanoparticles stabilized by tetraalkylammonium salts or PVP and found it to be more active compared to Pd for Suzuki coupling and active for Heck coupling.[151] In a further study, 15 combinations of multi-metallic catalysts containing Cu, Pd, Ru, and Pt were used for Suzuki coupling reactions.[152] It was observed that Pd was the most active, however, Cu/Pd colloids were comparable, which means not as much expensive Pd is required. Trimetallic colloids were also tested for the Suzuki reaction and the most active combinations were Cu/Pd/Ru > Cu/Pd/Pt > Pd/Pt/Ru.[152] Even a tetrametallic (Cu/Pd/Pt/Ru) catalyst was made and even though it showed a low activity it was stable.[152] These two instances reveal that the presence of an additional metal can provide stable and active catalysts, comparable to pure Pd nanoparticles. However, even though it was reported that forming ordered alloy Pd nanoparticles can improve the activity or selectivity for hydrogenation,[153] NO_x reduction,[154] and oxidative acetoxylation[155] reactions, there is virtually no published study on the effect of the catalytic ability of them for carbon-coupling reactions.

In designing a synthesis for new nanoparticle catalysts, especially multi-metal nanoparticles, there are numerous parameters to simultaneously control (size dispersity, shape, structure, composition, and how the particles are stabilized) and the task can

become challenging. As discussed in section 3, a pioneer method was developed to convert supported Pt nanoparticles to alloy and intermetallic nanocrystals while maintaining control over the size dispersion, structure, and composition. To investigate this hypothesis, we decided to employ the same technique to synthesize supported Pd-based alloy and intermetallic nanoparticles to explore the reactivity of them as potential new catalysts for the Suzuki and Heck coupling reactions.

4.2 Experimental

4.2.1 Chemicals

The following metal reagents were used: $Pd(C_5H_7O_2)_2$ (35.07 % Pd), $Pb(C_2H_3O_2)_2 \cdot 3H_2O$ (ACS, 99.0-103.0%), $SnCl_2$ (anhydrous, 99% min.), $Ga(NO_3)_3 \cdot xH_2O$ (99.9%), $In(NO_3)_3 \cdot xH_2O$ (99.9%), $Cu(NO_3)_2 \cdot 3H_2O$ (ACS, 98.0-102.0%), and $AgNO_3$ (ACS, 99.9+ %). Commercial supports were used: MISC Milled Vulcan XC-72 Carbon support in powder form (E-TEK) and gamma Alumina, 97.7 % (Strem Chemicals). Organic reagents used were: iodobenzene (Sigma-Aldrich, 98%), 1-octene (Sigma-Aldrich, 98 %), and 9-borabicyclo[3.3.1]nonane (9-BBN; Sigma-Aldrich, 0.5 M solution in tetrahydrofuran). Solvents were tetraethylene glycol (TEG, 99+%), *N,N*-dimethylformamide (DMF anhydrous, Sigma-Aldrich, ACS, 99.8%), Benzene (Sigma-Aldrich, ACS, 99%), and tetrahydrofuran (THF; EMD^{TM}, ACS, 99+%). The bases used were NaOH (EMD^{TM}), K_3PO_4 (anhydrous), and K_2CO_3 (Sigma-Aldrich, ACS reagent, >99.0%). All chemicals were purchased from Alfa Aesar unless otherwise noted.

4.2.2 Conversion of Pd nanoparticles to intermetallic nanocrystals

Alloy and intermetallic Pd nanoparticles were synthesized in a similar manner to the Pt intermetallic nanocrystals in the previous section but the procedure was adapted to a one-pot synthesis. In this case, $Pd(C_5H_7O_2)_2$ (16 mg, 0.071 mmol) was dissolved in 25 mL of TEG. After purging with Ar for 15 min, the temperature was raised to 125 °C for 1.5 h and the color turned from yellow to black forming Pd nanoparticles. The conversion from Pd nanoparticles to intermetallic compounds was carried out by injecting the appropriate metal salt dissolved in 3 mL of TEG into the reaction. The reaction mixture was maintained at 125 °C for 15 min and then the temperature was increased to the necessary temperature to form the desired product. Specifically, Pd_2Sn (1:2 Pd:$SnCl_2$ molar ratio) was heated to 190 °C for 90 min; Pd_2Ga [1:1 Pd:$Ga(NO_3)_3{\cdot}xH_2O$ (molar ratio assuming that the compound was a fully hydrated octahydrate)] was heated to 255 °C for 60 min; PdIn [1:1.2 Pd:$In(NO_3)_3{\cdot}xH_2O$ molar ratio] was heated to 260 °C for 60 min; Pd_3Pb [3:1 Pd:$Pb(C_2H_3O_2)_2{\cdot}3H_2O$ molar ratio] was heated to 160 °C for 1 h; Cu_3Pd [1:3 Pd:$Cu(NO_3)_2{\cdot}3H_2O$ molar ratio] was heated to 310 °C for 60 min. The final product was collected by centrifugation, washed with ethanol, and air-dried.

4.2.3 One pot synthesis of supported Pd nanoparticles and conversion to intermetallic catalysts

Supported Pd intermetallic nanoparticles (Pd_2Sn, Pd_2Ga, Pd_3Pb, PdIn, Cu_3Pd, and AgPd) were synthesized adapting to the procedure mentioned above. In this procedure, a one-pot synthesis was developed where Pd nanoparticles nucleated to a support and a metal

salt solution was injected to the reaction for the alloy or intermetallic conversion to occur. The procedure began with supporting Pd nanoparticles (3 or 5 wt% loading) on γ-Al_2O_3 or Vulcan XC-72 using the polyol method. The γ-Al_2O_3 and Vulcan XC-72 supports were purchased from Strem Chemicals and E-TEK respectively and were used as received. The support (Vulcan XC-72, 300 mg; Al_2O_3, 300 mg) was added and stirred into a solution of $Pd(C_2H_3O_2)_2$ (26.6 mg or 45.2 mg, to obtain 3 wt% 5 wt% Pd respectively) in 25 mL of TEG. The mixture was purged with Ar for 20 min and the temperature was increased to 125 °C for 2 h. In a separate solution a metal salt was dissolved in 3 mL of TEG and added to the supported Pd nanoparticle mixture. The reaction was maintained at 125 °C for 15 min and then the temperature was increased to the necessary temperature to obtain the alloy or intermetallic product. The final product was separated from the solution by filtration, washed with at least 200 mL of acetone and air-dried. The supported intermetallic nanoparticles were made as follows: Pd_2Sn [1:6 Pd:$SnCl_2$ molar ratio] was heated to 190 °C for 1 h; Pd_2Ga [1:1 Pd:$Ga(NO_3)_3 \cdot xH_2O$ molar ratio] was heated to 255 °C for 2 h; Pd_3Pb [3:1 Pd:$Pb(C_2H_3O_2)_2 \cdot 3H_2O$ molar ratio] was heated to 160 °C for 1 h; PdIn [1:1.2 Pd:$In(NO_3)_3 \cdot xH_2O$ molar ratio] was heated to 260 °C for 1 h; Cu_3Pd alloy [1:3 Pd:$Cu(NO_3)_3 \cdot 3H_2O$ molar ratio] was heated to 280 °C for 1 h in 20 mL of TEG.

For AgPd, Ag nanoparticles were supported on Vulcan XC-72 [0.017 $AgNO_3$, 0.100 mmol; 0.204 g Vulcan XC-72; 5 wt% Ag] by dissolving $AgNO_3$ in 30 mL of TEG heating to 105 °C for 1 h after purging the reaction system with Ar for 15 min. Then $Pd(C_2H_3O_2)_2$ (30.5 mg, 0.100 mmol) was dissolved in 4 mL of TEG and added to the

105 °C reaction dropwise. The reaction was maintained at this temperature for 90 min and then filtered, washed with 200 mL of acetone and air-dried.

4.2.4 Catalytic testing

The alloy and intermetallic compounds were tested as potential catalysts for the Suzuki-Miyaura cross-coupling reaction. The general experimental procedure was followed as published, where the Pd salts and complexes from the originally designed procedure were used but in this case it was adapted to use Pd nanoparticles as the catalysts.[156]

4.2.4.1 Formation of octylborane

A 50 mL single-neck round-bottom flask was purged with Ar for 20 min. Then 9-borabicyclo[3.3.1]nonane (9-BBN) (5 mmol) was added to the flask via syringe, followed by the addition of 1-octene (5 mmol). The reaction was stirred for 1 h under an Ar atmosphere.

4.2.4.2 Formation of phenyloctane by Suzuki coupling

A general procedure for the formation of phenyloctane began with purging a 50 mL single-neck round-bottom flask and condenser, from the oven, with Ar for 20 min. The catalysts (3 mol%) and base (NaOH, 3.3 mmol) were added to the flask. After additional purging with Ar iodobenzene (1.1 mmol), octylborane (1.1 mmol) and benzene (5 mL) were added. The reaction flask was placed in an oil bath and heated to 80 °C for 25 h. After the reaction cooled to room temperature the catalyst could be removed by filtration through Celite®. The product was washed with distilled water, hexanes, dried with $MgSO_4$, filtered, and the solvent was evaporated to afford the

desired phenyloctane. The reaction was also carried out in glass sealed tubes. All reaction conditions were left the same except the sealed tubes were inserted into an oil bath heated at 110 °C for 25 h under an Ar atmosphere.

Additional solvents and bases were used to study the effects on the reaction. In all cases 3 mol% catalyst, 5 mL of solvent and the same reactants were used in the Suzuki reaction; however, the molar ratio of base was changed. When *N,N*-Dimethylformamide (DMF) was used for the solvent and K_2CO_3 (2.2 mmol) or K_3PO_4 (1.1 mmol) as base the reaction was heated at 50 °C for 25 h. In another example, a mixture of tetrahydrofuran (THF) and distilled water (5:1 volumetric ratio) was used with NaOH (3.3 mmol) as the base and was heated to 65 °C for 25 h.

4.2.4.3 Formation of 1-phenyloctene by Heck coupling

Pd/Al_2O_3 and Pd_3Pb/Al_2O_3 were also used as catalysts for the heck reaction and the procedure used by Berthoil was followed.[157] In a typical experiment, a 50 mL single-neck round-bottom flask connected to a condenser was flushed with Ar for 20 min after being dried in an oven. Then the nanoparticle catalyst (5 mol%), iodobenzene (0.2469 g, 1.1 mmol), 1-octene (0.2468 g, 2.2 mmol), and K_2CO_3 (0.3041 g, 2.2 mmol) were added with 5 mL of DMF. The reaction was heated in an oil bath at 130 °C under an Ar atmosphere for 31.5 h. The catalyst was removed by centrifugation and the product was washed in distilled water, extracted with hexane, and dried with $MgSO_4$.

4.3 Conversion of unsupported and supported Pd intermetallic nanoparticles

The formation of alloy and intermetallic compounds by conversion of unsupported Pd nanoparticles was studied using methods discussed in Section 3 to form Pt-based intermetallic compounds.[158] The polyol process[112] was used to form Pd nanoparticles by reducing $Pd(C_5H_7O_2)_2$ at 125 °C without the use of PVP as a stabilizing agent. The next step began by dissolving a stoichiometric amount of a metal salt [$Cu(NO_3)_2$, $SnCl_2$, $Ga(NO_3)_3 \cdot xH_2O$, $Pb(C_2H_3O_2)_2 \cdot 3H_2O$, and $In(NO_3)_3 \cdot xH_2O$) in 3 mL of TEG. The metal

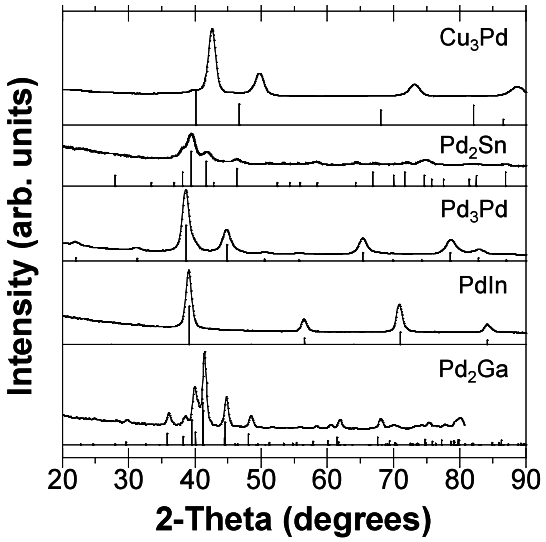

Figure 4.3. Powder XRD patterns for Pd based face-centered cubic alloy of Cu_3Pd and the intermetallic phases of Co_2Si-type Pd_2Sn and Pd_2Ga, $AuCu_3$-type Pd_3Pb, and CsCl-type PdIn nanoparticles by the reaction of Pd nanoparticles in TEG with the appropriate metal salt at a specific temperature. Standard reference patterns showing peak positions and relative intensities are shown below the experimental data.

salt solution was slowly added (dropwise) to the Pd nanoparticle reaction and the temperature was increased to form the final alloy or intermetallic product. Figure 4.3 shows the XRD pattern after reacting the Pd nanoparticles with the respective metal salt

at specific temperatures to yield alloy (Cu_3Pd, 310 °C) and intermetallic (Pd_2Sn, 190 °C; Pd_2Ga, 255 °C; PdIn, 260 °C; Pd_3Pb, 160 °C) compounds. The XRD pattern for Cu_3Pd shows a face centered cubic pattern shifted away from the pure Pd reference peaks at 40.1 °2θ to 42.2 °2θ and no super lattice peaks are present indicating that the alloy formed has no ordering, though it is expected to form slightly above 300 °C. Vegard's law approximates that the alloy is composed of about 66% Cu, which is consistent with the stoichiometric proportions of Pd nanoparticles reacted with $Cu(NO_3)_2$. It should be noted that this sample is not pure due to the existence of a small 111 peak of Pd (40.1 °2θ). Intermetallic compounds were also formed through the conversion of Pd nanoparticles to generate Pd_2Sn, Pd_2Ga (Co_2Si structure-type), Pd_3Pb ($AuCu_3$ structure-type), and InPd (CsCl structure-type). The short and broad peaks in the XRD pattern of Figure 4.3 are attributed to the small size of the crystal domains (instrumental broadening is also a contributing factor) and affirm the alloy and intermetallic nanoparticles are on the nanoscale. Pd nanoparticles were converted into alloy and intermetallic nanocrystals in solution, however; no surface stabilizers were added and it can be expected, based off previous studies of converting Pt nanoparticles into intermetallics,[158] that the particles sintered together lowering the surface-area. Generally the use of surface stabilizers produces dispersed particles, but can block the catalytically active sites on the surface of the catalyst and lower the catalytic activity. Pd nanoparticles supported on a solid support were converted into alloy and intermetallic nanoparticles that were small, dispersed and did not have any added surface stabilizers to hinder access to the catalytically active sites on the surface of the catalyst.

Supported alloy (Cu_3Pd) and intermetallic (Pd_2Sn, Pd_2Ga, Pd_3Pb, and PdIn) nanoparticle catalysts were prepared using the same procedure as described for the unsupported nanoparticles. The procedure began by reducing $Pd(C_5H_7O_2)_2$ in the presence of a solid-support (Vulcan XC-72, E-TEK) in TEG. Depending on the alloy or intermetallic compound desired the appropriate metal salt ($Cu(NO_3)_2 \cdot 3H_2O$, $SnCl_2$, $Ga(NO_3)_3 \cdot xH_2O$, $Pb(C_2H_3O_2)_2 \cdot 3H_2O$, or $In(NO_3)_3 \cdot xH_2O$) was dissolved in 3 mL of TEG and injected into the Pd/Vulcan XC-72 reaction mixture slowly (dropwise). The reaction was heated to specific temperatures for 1-2 h to form the desired product (same conditions to synthesize unsupported nanoparticles were used). The XRD patterns in Figure 4.4 show the alloy and intermetallic nanocrystals of Cu_3Pd, Pd_2Sn, Pd_2Ga, Pd_3Pb, and PdIn made by the conversion of carbon (Vulcan XC-72) supported Pd nanoparticles, which are compared to the referenced peak positions and relative intensities. The sharp and intense peaks (indicated by the arrows) in the Pd_2Ga sample are a result of the diffraction of the stainless steel plate used to hold the sample. The peaks mark with an asterisk in the Pd_2Ga and Pd_3Pb samples mark the face-centered cubic pattern of pure Pd, indicating incomplete conversion.

The synthesis of AgPd/Vulcan XC-72 was not carried out in the normal procedure described to this point. In this case, Ag nanoparticles were first reduced in TEG at 105 °C in the presence of Vulcan XC-72 support and a 3 mL solution of $Pd(C_5H_7O_2)_2$ was added. A galvanic replacement reaction occurred where Ag^0 spontaneously oxidized to Ag^+ (Ag^+/Ag = 0.8 V vs. SHE) and reduced Pd^{2+} ions to Pd^0 (Pd^{2+}/Pd = 0.95 V vs. SHE) at 105 °C to form a AgPd alloy. As seen in the XRD pattern

in Figure 4.4, a fcc pattern was shifted 0.2 °2θ away from the referenced Pd peak positions which corresponds to a AgPd alloy with a composition of 19% Ag and 81% Pd according to Vegard's law. As the arrows indicate in Figure 4.4 the 111 and 200 peaks of pure Pd are still present indicating that the full conversion to AgPd was not complete.

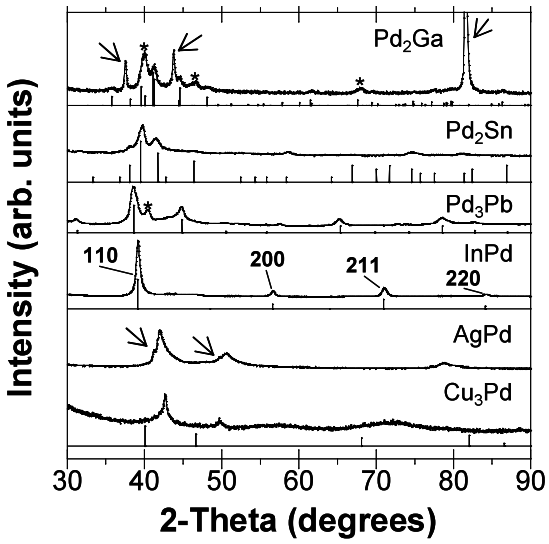

Figure 4.4. Powder XRD pattern after reacting supported Pd nanoparticles with a metal salt to obtain supported alloy Cu_3Pd ($Cu(NO_3)_2{\cdot}3H_2O$, 310 °C) and intermetallic nanocrystals of Pd_2Ga ($Ga(NO_3)_3{\cdot}xH_2O$, 255 °C), Pd_2Sn ($SnCl_2$, 190 °C), Pd_3Pb ($Pb(C_2H_3O_3)_2{\cdot}3H_2O$, 160 °C), and PdIn ($In(NO_3)_3{\cdot}xH_2O$, 260 °C). AgPd was made by a galvanic replacement reaction of supported Ag nanoparticles with $Pd(C_5H_7O_2)_2$ at 105 °C (arrows indicate presence of pure Pd 111 and 200 peaks). Standard reference patterns showing peak positions and relative intensities are shown below the experimental data. PdIn was indexed to the body-centered CsCl structure.

In another example, commercially available γ-Al_2O_3 (Strem Chemicals) was used as a high surface-area support and as seen in the XRD pattern in the bottom of Figure 4.5 the broad peaks indicate that it was slightly amorphous with a small crystal domain size. $Pd(C_5H_7O_2)_2$ was reduced in TEG with γ-Al_2O_3 to form supported Pd nanoparticles as

seen in the middle of Figure 4.5. A 3 mL solution of $Pb(C_2H_3O_2)_2 \cdot 3H_2O$ was added to the reaction and heated to 160 °C to form $Pd_3Pb/\gamma\text{-}Al_2O_3$. The top of Figure 4.5 shows $AuCu_3$-type pattern of $Pd_3Pb/\gamma\text{-}Al_2O_3$.

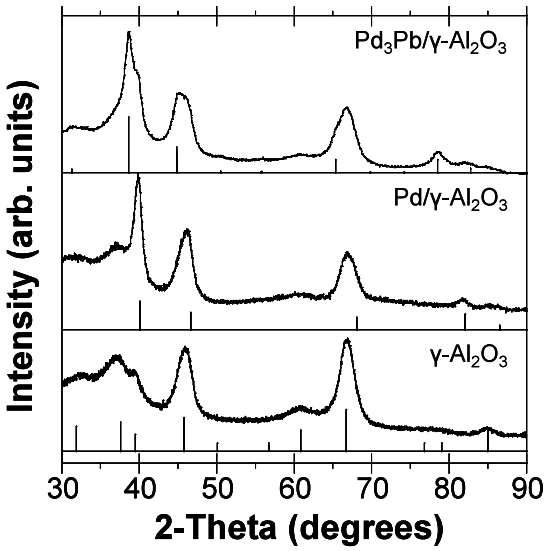

Figure 4.5. Powder XRD of $\gamma\text{-}Al_2O_3$ (bottom), $Pd/\gamma\text{-}Al_2O_3$ made by reducing $Pd(C_5H_7O_2)_2$ in TEG (middle), and $Pd_3Pb/\gamma\text{-}Al_2O_3$ synthesized by reacting $Pd/\gamma\text{-}Al_2O_3$ with $Pb(C_2H_3O_2)_2 \cdot 3H_2O$ in TEG at 160 °C (top). Standard reference patterns showing peak positions and relative intensities are shown below the experimental data.

Supported Pd nanoparticles could be reacted with a metal salt to form Pd-based alloy or intermetallic nanoparticles in a solution of TEG. Representative TEM samples of PdIn, Cu_3Pd, and Pd_2Sn supported on Vulcan XC-72 are shown in Figure 4.6. PdIn nanoparticles (average diameter of 18.4 nm) and Pd_2Sn (average diameter of 9.4 nm) were relatively small and dispersed as seen in Figure 4.6a and d, respectively. It should be noted that while the Pd_2Sn nanoparticles were all relatively small there were some portions of the PdIn sample that contained sintered particles and may be responsible for

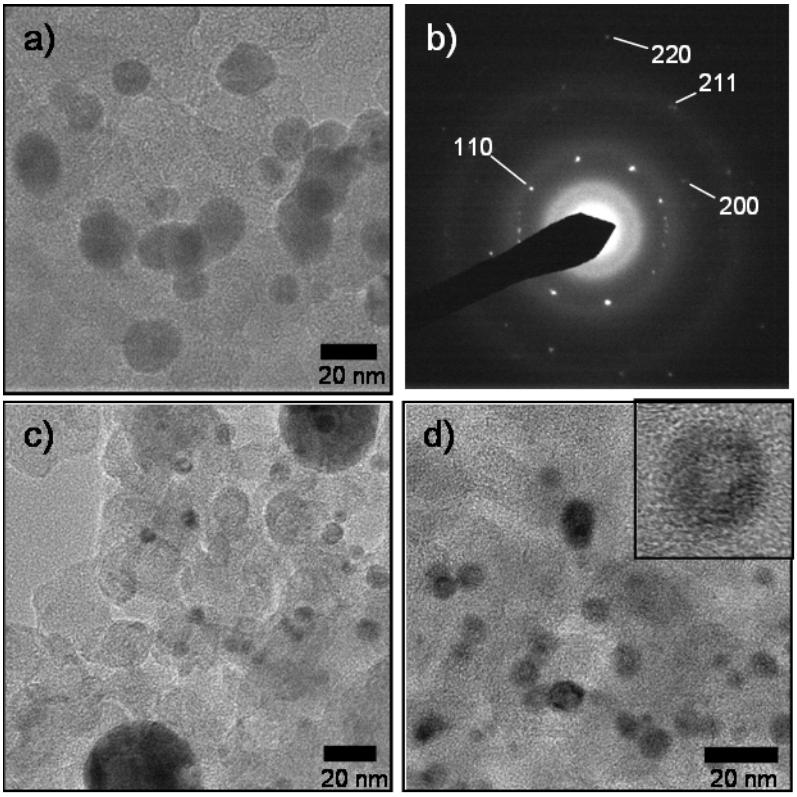

Figure 4.6. TEM images of (a) PdIn/Vulcan XC-72, (b) SAED pattern of PdIn/Vulcan XC-72 showing the CsCl-type structure, (c) Cu_3Pd/Vulcan XC-72, and (d) Pd_2Sn/Vulcan XC-72 with an inset image showing a hollow Pd_2Sn nanoparticle.

the sharper peaks in the XRD pattern in Figure 4.5. The SAED pattern in Figure 4.6b shows a pattern consistent with a body-centered cubic CsCl-type structure (B_2) confirming the XRD patterns reported above. The short and broad XRD peaks observed in Figure 4.4 were analyzed by the Scherrer equation and the particle size was calculated to be 11.7 nm in diameter. The powder XRD and TEM results are relatively consistent with the small size of the nanocrystals. On the other hand, Cu_3Pd showed a mixture of large particles (46.4 nm in diameter) and smaller nanoparticles (9.7 nm in diameter) and may explain why the XRD peaks are sharper than the other intermetallic samples. In the

inset of Figure 4.6d a representative Pd_2Sn nanoparticle is shown with a lighter contrast in the center. This points to a hollow interior that is formed due to different diffusion rates[9] of Pd and Sn and this phenomenon is known as the Kirkendall effect. Similar examples of the hollow nanoparticles formed from this effect have been reported elsewhere.[9, 10, 22, 30, 116, 117, 158]

4.4 Supported alloy and intermetallic nanoparticle catalysts for the Suzuki coupling reaction

Pd-based intermetallic nanoparticle catalysts have been synthesized on a solid support (Vulcan XC-72, or Al_2O_3) via the conversion of Pd nanoparticles in a metal salt solution of TEG. These supported intermetallic nanoparticle catalysts were then studied to explore their catalytic potential toward Suzuki coupling reactions. It has been shown that supported intermetallic nanoparticle catalysts can increase the catalytic activity and selectivity of certain reactions such as; hydrogenation,[153] NO_x reduction,[154] and oxidative acetoxylation[155] reactions. There are also some examples of Pd-based multi-metal (bimetallic and alloy) catalysts that have shown increased reactivity and stability when used for carbon-coupling reactions such as Suzuki,[152] Heck,[141] and Sonogashira.[159, 160] Intermetallic catalysts may potentially be good candidates for carbon-coupling reactions due to the uniform surface composition, increased stability and the fact that multi-metal catalysts have shown improvements for these types of reactions. To this date we are not aware of any study using intermetallic nanoparticles as catalysts for Suzuki, Heck, or any other type of carbon-coupling reaction. Intermetallic alloys containing Ag, Sn, and Cu were selected because it is known that they are reactive for

transmetallation reactions with organoboranes, as are the other common metal catalysts (Pd, Ni, and Pt). For this reason the combination of these metals with Pd would possibly make interesting catalysts for the Suzuki cross-coupling reaction. They could possibly have a potential to participate in the mechanism and facilitate the formation of the desired cross-coupled product. The transmetallation step is important in this reaction because the faster the transmetallation occurs between the first catalyst complex and the organoborane the least byproduct or homocoupled product is observed.

On the other hand, Ga, In, and Pb are not known to be active toward transmetallation, but they are known to affect the electronic structure of Pd as well as the surface geometry and it may be interesting to study the influence on the coupling mechanism. XPS measurements have shown that a higher shift in binding energy occurs (Pd 3d) in InPd[161] and Ga-Pd[162] intermetallic compounds. One may expect that a more positive Pd center may aid in increasing the reaction kinetics in the transmetallation process where a nucleophilic organo-group will bond with Pd. Also, the oxidative addition step in the mechanism of the Suzuki coupling reaction is considered the rate-limiting step and activating aryl and alkyl halides with a variety of electron withdrawing groups can increase the reactivity. It is also possible to make sterics and electronic adjustments to the Pd center to affect the outcome of the reaction. For instance, phosphine ligands are varied to more bulky or fewer than four phosphines making the saturated Pd center more reactive for oxidative addition. In cases where phosphine ligands are used the rate-limiting step can often be their (phosphine ligands) dissociation from the catalyst complex. When metallic nanoparticles are used, phosphine ligands are

no longer required. However, alloying Pd with different metals can affect the electronic structure, which may influence the rate-limiting step.

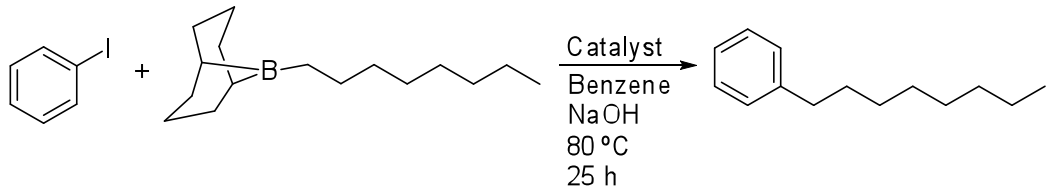

Scheme 4.1. Reaction with iodobenzene and octyl-9BBN to yield phenyloctane.

A Suzuki coupling reaction between iodobenzene and octylborane (formed by the hydroboration of 1-octene and 9-BBN) was done using $Pd(PPh_3)_4$, Pd/C, or PdIn/C as catalysts using benzene as the solvent and NaOH as the base. As can be seen in Table 4.1, $Pd(PPh_3)_4$ gave the best results with a 90% conversion of the desired phenyloctane product while Pd/Vulcan XC-72 gave a conversion of about 28% and PdIn/Vulcan XC-72 gave a 13% conversion. A high conversion of iodobenzene to biphenyl (homocoupled product) was generally obtained when nanoparticle catalysts were used and is one of the reasons for the lower conversions for the desired product. Interestingly, doubling the amount of Pd/Vulcan XC-72 caused the yield of phenyloctane to increase from 28.9% to 73.7% as well as the selectivity. Doubling the amount of PdIn/Vulcan XC-72 consumed a similar amount of iodobenzene (7.2% remaining), however, biphenyl consisted of 82.7% of the product. When the amount of octylborane was doubled the selectivity for PdIn improved, but the overall yield of phenyloctane was low (32.3% iodobenzene, 36.6% biphenyl, and 31.1% phenyloctane).

Table 4.1. Suzuki coupling reaction between iodobenzene and octylborane.

Entry	Catalysts	Iodobenzene (%)	Biphenyl (%)	Phenyloctane (%)
1	$Pd(PPh_3)_4$	4.4	6.0	90.0
2	Pd/C	22.6	48.5	28.9
3	PdIn/C	50.4	36.6	13.1
4	Pd/C[a]	3.7	22.6	73.7
5	PdIn/C[a]	7.2	82.7	10.1
6	PdIn/C[b]	32.3	36.6	31.1

Table 4.1. Suzuki coupling reaction between iodobenzene and octylborane. The reaction was carried out in 5 mL of benzene with 3 mol% catalyst, 3.3 mmol NaOH, 1.1 mmol of iodobenzene, and 1.1 mmol of octylborane at 80 °C for 25 h. [a] 6 mol% catalysts was used. [b] The amount of octylborane was doubled to 2.2 mmol octylborane.

Overall, the amount of iodobenzene that was consumed using the intermetallic PdIn/Vulcan XC-72 catalysts was significantly less than or equal to the Pd/Vulcan XC-72 catalysts and generally showed a preference to forming biphenyl (the homocoupled product).

As it was mentioned before, in the Suzuki coupling reaction the oxidative addition of an alkyl halide is the rate-limiting step,[131] however, using alkyl boranes, with β-hydrides (sp^3 alkyl groups) can reduce the rate of transmetallation (ligand exchange). This step also depends a lot on bases, ligands, and transition metal complexes to proceed well. For example, in cases where Pd is used, NaOH or alkhoxide bases give the desired cross-coupled product, while bases like triethylamine give abnormal products. The combination of the intermetallic structure of PdIn, using an alkyl borane, and the current reaction conditions may influence the rate of oxidative addition of iodobenzene and the transmetallation process. Therefore, the iodobenzene molecules may have a higher chance to react

and form biphenyl before the transmetallation step between the organoborane and the organopalladium is complete. As mentioned, the transmetallation step is facilitated by a base activating the organo group on the boron making it more nucleophilic through quaternization.[131] Perhaps, the activating power of the base is not quite enough to propagate the transmetallation process or maybe the reaction conditions need to be harsher to facilitate this step. It is also possible that a stronger interaction between Pd and In (as indicated by 0.8 eV shift to higher binding energy exhibited by the Pd $3d_{5/2}$ peak by XPS measurments[161]) may stabilize the structure and reduce Pd leaching. Some speculate that under certain reaction conditions a Pd^{2+} (after oxidative addition) species is leached from the Pd nanoparticles and it may be the catalytically reactive component.

It was found that if the reaction was carried out in a sealed tube at 110 °C the yield of phenyloctane was increased to ~80% for Pd/Vulcan XC-72 (~ 90% for

Table 4.2. Suzuki coupling reaction between iodobenzene and octylborane in a sealed tube.

Entry	Catalysts	Iodobenzene (%)	Biphenyl (%)	Phenyloctane (%)
1	Pd/C	6.9	12.6	80.6
2	$PdIn/Al_2O_3$	99.1	0.3	0.6
3	Pd_2Sn/Al_2O_3	91.5	3.6	4.9
4	Pd_2Sn/C	7.2	85.3	7.5
5	Pd_2Sn/C	6.3	83.1	10.6
6	PdIn/C	8.6	36.5	54.9
7	PdIn/C (650 °C)	1.2	98.7	0.1
8	Pd_3Pb/C	6.3	92.2	1.4
9	Pd_2Ga/C	51.1	17.7	31.2
10	Cu_3Pd/C	100	0	0

The reaction was carried out in 5 mL of benzene with 3 mol% catalysts, 3.3 mmol of NaOH, 1.1 mmol of iodobenzene, and 1.1 mmol of octylborane at 110 °C for 25 h using a sealed pressure tube.

$Pd(PPh_3)_4$). The sealed tube allowed the reaction to approach harsher conditions that are otherwise out of reach do to the solvent's boiling point limitation. Due to the improved yield of the product under these conditions other alloy and intermetallic nanoparticle catalysts were tested. When γ-Al_2O_3 support was used for Pd_2Sn and PdIn the activity of the catalyst was very low. However, Table 4.2 shows that when Pd_2Sn, Pd_3Pb, and PdIn, were supported on Vulcan XC-72 most of the iodobenzene was consumed (comparable to pure Pd), but the selectivity toward phenyloctane product was not optimal with Pd. Given that Cu^+ salts and CuO have been used as co-catalyst for carbon-coupling and carbon-nitrogen coupling reactions, it was thought that alloying Cu with Pd would be a good choice of catalyst. However, the alloy of Cu_3Pd/Vulcan XC-72 did not react at all. As table 4.2 depicts, the reactivity of the reaction is greatly increased when carried out in sealed tubes though the intermetallic catalysts still produce a large yield of biphenyl. The effectiveness of the transmetallation step could still be responsible for the low phenyloctane yield.

Oxidative addition and reductive elimination steps are well-studied and common fundamental processes in the Suzuki coupling reaction; however, the transmetallation mechanism is less understood because it is highly dependent on the organometallics and reaction conditions used for coupling. In fact, it is common to report that a mixture of desired and undesired products formed through transmetallation depend a lot on the base and catalysts used. Studies on the effect of the yield and selectivity of phenyloctane

were done by using different bases and more polar solvents. As depicted in Table 4.3, the consumption of iodobenzene from Pd (22.9%) and PdIn (45.8%) supported on Vulcan XC-72 using *N,N*-dimethylformamide (DMF) and K_2CO_3 was relatively similar to their counterparts under the reaction conditions in Table 4.1 (entries 1 and 4). However, the combination of DMF and K_2CO_3 afforded a higher percent yield of phenyloctane (Pd, 64.9%; PdIn, 41.5%) and lower yield of biphenyl (Pd, 12.3%, PdIn, 12.7%) thereby, improving the selectivity. Published results show that the catalyst $PdCl_2$(dppf) (dppf - 1,1'-Bis(diphenylphosphino)ferrocene) can obtain a 98% yields of phenyloctane under similar reaction conditions.[156] When the base was changed from K_2CO_3 to K_3PO_4 it appeared that the amount of iodobenzene consumed in the reaction was slightly diminished but the formation of phenyloctane was slightly more favored. The improved selectivity toward phenyloctane could be explained by the fact that a polar aproctic solvent (DMF) dissociates K_2CO_3 so the CO_3^{2-} anion quaternizes octylborane and increases it nucleophilicity (more than NaOH in benzene) to initiate transmetallation. In fact, it is known that aprotic solvent can increase nucleophilicity of an anion.[163] A solvent mixture of THF and H_2O (5:1, THF:H_2O) and NaOH as the base resulted in 50% and 100% conversion of iodobenzene for Pd/Vulcan XC-72 and PdIn/Vulcan XC-72 respectively. Unfortunately, the homocoupled product was favored with a ~95% yield in the case of PdIn. Clearly it can be seen that the combination of solvents and bases with these catalysts has a tremendous effect on the product mixtures. The reason may be due to the effect the solvents have over the nature in which the base and octylborane interact to initiate the transmetallation step or on the rate of the other

steps such as the oxidative addition. Various combinations of solvent and base as well as the reaction conditions are needed in order to completely explore the optimal conditions to switch the selectivity on these catalysts.

Table 4.3. Suzuki coupling reaction of iodobenzene and octylborane.

Entry	Catalysts	Reaction Conditions	Iodobenzene	Biphenyl	Phenyloctane
1	Pd/C	DMF, K_2CO_3, 50 °C	22.9	12.3	64.9
2	PdIn/C	DMF, K_2CO_3, 50 °C	45.8	12.7	41.5
3	Pd/C	DMF, K_3PO_4, 50 °C	33.5	4.5	62
4	PdIn/C	DMF, K_3PO_4, 50 °C	54.7	9.3	35.9
5	Pd/C	THF-H_2O (5:1), NaOH, 65 °C	49.0	35.5	15.6
6	PdIn/C	THF-H_2O (5:1), NaOH, 65 °C	0	94.7	5.3

The reaction was carried out in 5 mL of solvent with a base (2.2 mmol of K_2CO_3, 1.1 mmol of K_3PO_4, or 3.3 mmol of NaOH), 1.1 mmol of iodobenzene, and 1.1 mmol of octylborane for 25 h.

4.5 Supported alloy and intermetallic nanoparticle catalysts for Heck coupling

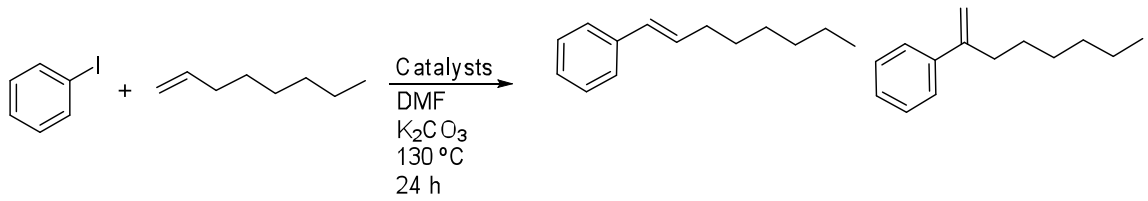

Scheme 4.2. Reaction of iodobenzene with 1-octene to produce a mixture of products: 1-phenyloctene and 2-phenyloctene. The reaction was carried out using Pd/γ-Al_2O_3 or Pd_3Pb/γ-Al_2O_3 as catalysts.

Some of the supported intermetallic nanoparticle catalysts were tested as potential catalysts for the Heck reaction as well. It is believed that the Heck reaction may be less complicated than the Suzuki coupling reaction and offer fewer problems. For instance, there is no transmetallation step, which we believe to be responsible for

causing a high yield of the homocoupled product in the Suzuki coupling reaction. Heck coupling reactions are also more robust in the since that the base and catalysts selections tend to have the most effect on the product yield and selectivity. In our example, the Heck reaction was studied by the reaction of iodobenzene and 1-octene, using common reaction conditions reported[157], in DMF with K_2CO_3 at 130 °C for 31.5 h to form two isomers: 1-phenyloctene and 2-phenyloctene. After the product was washed and extracted, GC results indicated that the Pd/γ-Al_2O_3 catalyst produced 15% 1-phenyloctene and 85% 2-phenyloctene. The Pd_3Pb/ γ-Al_2O_3 gave slightly better results (in terms of selectivity) showing a 21.2% and a 78.8% conversion to 1-phenyloctene and 2-phenyloctene, respectively. Pd_3Pb/γ-Al_2O_3 appears to be slightly more selective toward 1-phenyloctene and further optimization of this reaction can be explored since the base and the nature of the substrate can help improve the yield and selectivity. The reaction can be optimized by adding various functional groups to the substrate as was demonstrated by Berthiol who found that less reactive arylbromides with electron-withdrawing groups can improve the selectivity of the reaction as compared to iodobenzene.[157]

4.6 Conclusion

The same "conversion chemistry" techniques used to synthesize Pt-based alloy and intermetallic nanocrystals supported on alumina or carbon (Vulcan XC-72) has been applied to supported Pd nanoparticle catalysts. The carbon and alumina supports stabilized the nanoparticles (in most cases) to remain small and dispersed without the need for a surface stabilizer. As a result, it was shown that multi-metal nanoparticles can

be designed for potential catalytic applications with relative control over the size, particle dispersion, composition, and free of added surface stabilizers that can hinder access to the catalytically active sites. The simultaneous control over many of these parameters can offer a higher degree of control and may be applied to a variety of multi-metallic nanoparticles through conversion chemistry methods to potentially discover new catalytic materials that may provide more selectivity and better conversion rates.

In this work supported Pd nanoparticle catalyst were converted into alloy and intermetallic compounds and for the first time their catalytic potential for the Suzuki and Heck coupling reactions were explored. We have also not seen any published studies on the 9-BBN mediated Suzuki coupling reported using unsupported or supported Pd nanoparticle catalysts. We have chosen to use 9-BBN as our main example since it is the most used reagent for the Suzuki-cross coupling in the field of organic synthesis and we felt it needed to be explored for a series of reaction conditions that can potentially be useful for chemist in other fields. It was found that the intermetallic catalysts supported on carbon (Vulcan XC-72) were active towards Suzuki coupling of octylborane and iodobenzene, however, they tended to show a higher affinity toward the homocoupled product under the current reaction conditions. In this case, the possibility of improving the reaction still needs to be explored by changing the alkyl groups on the organoboron to a more reactive group or simply by inverting the reagent hybridization to accelerate the transmetallation step in comparison to the oxidative addition to possibly reduce the formation of the byproduct. It was also shown that there was very low activity when the disordered alloy Cu_3Pd/Vulcan XC-72 was used as the catalyst, or when γ-Al_2O_3 was

used as the support. Varying the bases and switching to more polar solvents can reduce the percentage of the homocoupled product that is formed. $Pd_3Pb/\gamma\text{-}Al_2O_3$ was shown to be active for the Heck reaction and was more selective toward 1-phenyloctene than $Pd/\gamma\text{-}Al_2O_3$, which is a very interesting result to further explore. Supported Pd-M (M = Sn, Ga, In, and Pb) intermetallic nanoparticles show catalytic activity toward Suzuki and Heck coupling reactions that is comparable (in some cases) to pure Pd and it has been shown that further optimization of the reaction conditions could potentially improve the selectivity toward the desired products.

5. INVESTIGATING THE USE OF PLATINUM NANOCUBES AS TEMPLATES FOR THE CONVERSION INTO INTERMETALLIC NANOCRYSTALS

5.1 Introduction

Developments in nanoparticle synthesis have come a long way over the last two decades. Today, a variety of synthetic methods exist to form a vast library of nanoparticles. Solution methods are particularly interesting because not only are they versatile in forming various types of nanoparticles, but they can offer a large degree of control. For instance, it is possible to form nanoparticles with tight control over the crystallite size[164-167] and the particle morphology.[166, 168, 169] However, these are not considered general and each nanoparticle system requires different conditions which can make the development of these materials time consuming and difficult. In some cases, the properties of a nanocrystal, such as ferromagnetism in FePt,[170] can be affected by physical characteristics, such as size, crystal structure, shape, and composition.

There has been an effort to advance the capacity of high-density magnetic storage media over the last few years from 100 Gbit/in^2 to a magnitude on the terabit/in^2 range.[174] In order to achieve this goal, new synthetic methods combined with new materials may need to be developed. Recently, a lot of research has focused on the nanoparticle synthesis of the ordered face-centered tetragonal (fct) $L1_0$ phase of FePt due to its high uniaxile magnetocrystalline anisotropy ($K \sim 7 \times 10^6$ j/m^3).[174] The nanoparticles should be uniform in size to prevent interference from each other, caused

by poorly defined grain shape and size. However; if the particles are too small their magnetic properties become unstable.

One problem that exists in the synthesis of FePt nanoparticles is that a face-centered cubic alloy forms, with superparamagnetic properties, and a post-annealing step is required to obtain the fct structure. FePt nanoparticles were originally synthesized by forming nanoparticle films by vacuum deposition techniques[171-173] to obtain the disordered fcc alloy followed by annealing to get the fct structure. This process produces particles with a broad range in size accompanied by agglomeration of the particles during the annealing step. To improve the quality of the FePt nanoparticle samples, solution methods were investigated to obtain much greater control over the size distribution and particle dispersion.

The first example of producing nearly monodisperse FePt nanoparticles was done by Sun and co-workers at IBM.[174] They demonstrated that platinum(II) acetylacetonate ($Pt(acac)_2$) could be reduced by hexadecanediol and nucleate to Pt-rich particles while iron pentacarbonyl $Fe(CO)_5$ could simultaneously thermally decompose in the presence of oleic acid and oleyl amine for the formation of FePt. The as-synthesized particles were on the order of 4 nm in diameter and consisted of the disordered fcc structure and could be self assembled into superlattice structures. The FePt superlattice assembly could be transformed from the fcc to the fct structure at 500-600 °C which then show ferromagnetic behavior. Unfortunately, the post-annealing step required to obtain the high magnetic anisotropic ordered fct phase induces particle sintering.

Many similar methods have since been developed where $Pt(acac)_2$ was reduced and $Fe(CO)_5$ was thermally decomposed.[175-180] Sun and co-workers also showed that a superhydride ($LiBEt_3H$) could be used for the co-reduction of $Pt(acac)_2$ and $Fe(acac)_2$ salts in a phenylether solution.[181] $Pt(acac)_2$ and $Fe(acac)_3$ could also be co-reduced to the fcc alloy of FePt in a polyol solution to eventually assemble into superlattice structures where additional annealing was required for the ordered fct transformation.[182-183]

In the procedures mentioned above, it appears that the FePt disordered fcc alloy forms around 200 °C and the full transformation to the ordered fct phase occurs above 500 °C. Some research groups have discovered that $Pt(acac)_2$ and $Fe(acac)_3$ can be co-reduced and refluxed in high-boiling point solvents, such as tetraethylene glycol (TEG; b.p. ~ 310 °C), to directly synthesize partially ordered fct FePt nanoparticles.[184-191] It is believed that adjustments to the reaction kinetics can help to directly synthesize the fct phase of FePt. For example, Hinotsu was able to synthesize nanoparticles containing the more unstable hcp phase (actually a mixture of hcp and fcc) of Ni and fcc, the metastable phase ε-Co, and hcp phases of Co by increasing the reaction kinetics.[187] He believes that the fcc structure of FePt is an unstable phase caused by faster reaction kinetics.[184; 186; 187] The authors were able to control certain parameters of the reaction such as, the type of polyol, reaction temperature, and Fe:Pt ratio, to control the kinetics and favor the fcc or the partially ordered fct phases.[186] A similar approach was taken by Nguyen and co-workers who were able to directly form the ordered fct $L1_0$ or transform the unordered

fcc FePt in solution by using octylether, decylether, 18-crown-6, nonadecane, docosane, or tetracosane as solvents, all of which have boiling points in the area of 300 - 380 °C.[192]

There are many more novel synthetic methods that deal with forming the ordered $L1_0$ fct phase of FePt that reduce particle sintering. Some have added additional metal impurities into FePt systems which result in a reduction in the temperature required for the transformation from the unordered fcc to the ordered fct phase.[193-195] The reduction in the phase transformation temperature is believed to occur due to the formation of defects created as the impurity metal is being excreted from the FePt system during annealing.[196] Other techniques involve forming the disordered fcc FePt alloy and encasing the particles in TiO_2 matrix,[197] SiO_2,[198] or Fe_3O_4 shell[199] which aid in protecting the nanoparticles from sintering during the annealing step.

The majority of the synthetic methods discussed thus far produce spherical FePt nanoparticles. When these spherical particles are assembled on a substrate, their easy magnetic axes are not aligned and as a consequence are arranged in all different directions. An electron beam evaporation method was used to epitaxially grow oriented FePt nanoparticles with high coercivity onto MgO(111) and NaCl(111) surfaces to improve alignment.[200] Jia and co-workers were able to directly synthesize ordered fct FePt nanoparticles and aligning them in a magnetic field.[201]

It was realized that a simpler way to improve the alignment of the easy magnetic axes was to control the shape of the nanoparticles. One such way was to form FePt nanocubes that could easily be aligned along the [001] direction where the magnetocrystalline anisotropy constant is measured in the $L1_0$ FePt structure. FePt

nanocubes have been formed through solution methods that involve the co-reduction of $Pt(acac)_2$ and $Fe(acac)_3$ under reducing conditions in the presence of certain combinations of surface-stablizers.[2, 3, 202] Margeat and co-workers used similar conditions to form nanocubes of the disordered fcc phase of $FePt_3$ nanocubes.[203] Additionally, FePt can exhibit different magnetic properties when confined in one dimension and which can be accomplished by manipulation of the components in the reaction[4, 5, 204] or even use the mosaic tobacco virus as a template to form CoPt and $FePt_3$ nanowires.[205] Unfortunately, these methods only produce the disordered fcc phase and still require additional annealing to reach the $L1_0$ phase. Another problem with these methods is that the procedure is difficult and specific conditions must be met exactly to obtain uniform size and shape of the particles. In the event that additional shapes are required or a mixture of shapes and sizes are desired, it would be very difficult to find the synthetic conditions to meet those specifications. For example, the surface of Pt tetrahedral nanoparticles consist mainly of (111)[206] facets which also happens to be the most catalytically active surface for Pt_3Sn.[207] It may be more convenient to convert Pt tetrahedral nanoparticles to the intermetallic phase (Pt_3Sn) than to find the exact reaction conditions to directly synthesize the product.

The syntheses of some single metal nanoparticles have been studied in detail and a certain degree of controlling their physical parameters (size and shape) is becoming easier. For instance, Pt nanocrystals can be synthesized in many different anisotropic shapes including cubes[110, 208-214], multipods[215-217] and wires[216-221] while maintaining a monodisperse size distribution. It now becomes practical to synthesize Pt nanoparticles

with uniform shape and size to be used as reactive templates for the transformation into intermetallic FePt nanoparticles. In this work, we will investigate the possibility of adapting conversion chemistry methods to directly form disordered fcc and partially ordered alloys of magnetically relevant materials (e.g. $FePt_3$, CoPt, and NiPt) using Pt nanoparticle clusters or Pt nanocubes. This technique may eventually open the way to align fct FePt nanocubes along their magnetically easy access.

5.2 Experimental

5.2.1 Synthesis of Pt nanoparticles (with no surface stabilizers)

K_2PtCl_6 (60 mg, 0.124 mmol) was dissolved in 20 mL of ethylene glycol. After purging with Ar for 15 min, the temperature was raised to 160 °C (the color turned from yellow to dark brown), and the solution was removed from the heat. The Pt nanoparticles were collected by centrifugation and washed with ethanol.

5.2.2 Synthesis of PVP-stabilized Pt nanocubes

The synthesis of Pt nanocubes stabilized by PVP was adapted from the published procedure of Peidong Yang and is briefly described.[214] A typically procedure began by refluxing 2.5 mL of ethylene glycol (EG) for 5 min. Then 0.5 mL of 2 x 10^3 M solution of $AgNO_3$ dissolved in EG glycol was added and the solution's color turned slight yellow. Separate solutions of 0.375 M of PVP/EG and 0.0625 M H_2PtCl_6/EG were made. Aliquots of 94 μL of PVP/EG and 47 μL of H_2PtCl_6/EG solutions were added simultaneously every 30 s for 16 min. The color of the reaction started to turn brown within the first minute after the first addition of H_2PtCl_6 indicating that Pt^{4+} was reduced to Pt^0. After the addition of the reagents was completed the reaction refluxed for an

additional 5 min before being removed from the heat. The reaction mixture was centrifuged at 5,000 rpm for 15 min. The supernatant was separated and diluted in 24 mL of acetone. Then the mixture was centrifuged at 3,000 rpm for 5 min. The precipitant was collected and dispersed in 3 mL of ethanol and mixed with 9 mL of hexane. The mixture was centrifuged for 5 min. at 3,000 rpm and the resulting Pt nanocubes were re-dispersed into 3 mL of ethanol.

5.2.3 Synthesis of Pt nanocubes stabilized by 1-adamantanecarboxylic acid and 1-hexadecylamine

In the synthesis of Pt nanocubes stabilized by 1-adamantanecarboxylic acid (ACA and 1-hedadecylamine HDA) the experimental procedures were adapted from Yang and co-workers.[202; 204] The procedure begins by adding $Pt(acac)_2$ (100 mg, 0.25 mmol), ACA (137.5 mg, 0.76 mmol), 1,2-hexadecanediol (HDD) (1.6 g, 6.2 mmol), HDA (2 g, 8.2 mmol), and diphenyl ether (DPE) (1 mL, 6.3 mmol) to a 50-mL single neck round bottom flask with a magnetic stirrer. The reaction was carried out under slowly flowing Ar gas and was placed in a preheated oil bath at 130 °C to melt all of the components. When the $Pt(acac)_2$ was dissolved and the solution started to turn to a clear-yellow, the reaction flask was transferred to another preheated oil bath at 160 °C. The color of the solution turned to dark brown as the reaction progressed, indicating the reduction of Pt^{4+} to Pt^0, and was heated for 2.5 h. Since the solution solidifies at room temperature it was only allowed to cool down to 60 °C. The reaction solution (0.2 mL) was added to a mixture of chloroform (0.8 mL) and ethanol (1.0 mL) and the mixture was centrifuged at 5,000 rpm for 5 min. The samples were washed with the same mixture three times before re-dispersing the Pt nanocubes in 3 mL of ethanol.

5.2.4 Conversion of Pt nanoparticles into $FePt_3$, CoPt, and NiPt

Pt nanoparticles synthesized by the reduction of a Pt salt in an EG solution without the use of capping ligands were directly converted into the partially ordered $L1_2$ phase of $FePt_3$ in the presence of an iron salt. The typical synthesis began by dispersing Pt nanoparticles (3.2 mg, 0.016 mmol) into 1.5 mL of TEG by sonication. The dispersion mixture was then added to 20 mL of TEG in a 3-neck round bottom flask equipped with a condenser and magnetic stir bar. $FeCl_3 \cdot 6H_2O$ (29.6 mg, 1.1 mmol) was dissolved in 5 mL of TEG before being added to the Pt nanoparticle mixture. The mixture was stirred under fast flowing Ar for at least 2 h. The temperature was increased to 310 °C for 3.5 h before the reaction was removed from the heat. The $FePt_3$ nanoparticles were collected by centrifugation at 14,000 rpm for 10 min. The samples were washed with ethanol 3 times.

CoPt and NiPt fcc alloy nanoparticles were synthesized in a similar manner. In the case of CoPt, Pt nanoparticles (3.7 mg, 0.02 mmol) were reacted with $Co(acac)_2$ (4.9 mg, 0.02 mmol) in TEG at a temperature of 310-320 °C for 3.5 h. NiPt was formed by reacting Pt nanoparticles (5 mg, 0.03 mmol) with $Ni(acac)_2$ (6.9 mg, 0.03 mmol) in TEG at 310-320 °C for 2 h.

5.2.5 Attempts at conversion of Pt nanocubes to $FePt_3$ nanocubes

The process of converting Pt nanocubes directly into a fcc FePt alloy or the partially ordered $L1_2$ phase involved a similar process as was required for the conversion of Pt nanoparticles. In one typical example, Pt nanocubes stabilized by PVP (3.8 mg, 0.02 mmol) were reacted with $FeCl_3 \cdot 6H_2O$ (34.8 mg, 128.7 mmol) or $Fe(acac)_3$ (0.02-128.7

mmol) in TEG at 310 °C for ~3 h. The reaction was centrifuged at 13,500 rpm for 10 min and the sample was washed with ethanol three times. In the case of using $Fe(acac)_3$, Fe_3O_4 was a by-product when high molar ratios (Fe:Pt) were used. In an effort to decrease the effects of particle sintering and to increase the dispersion of the particles a new solvent system was used. HDA (5.1 g, 0.021 mol), HDD (113.7 mg, 0.4 mmol), and Pt nanocubes (3.6 mg, 0.018 mmol), were added to a 3-neck round bottom flask with a condenser and a magnetic stir bar. After purging the reaction flask with Ar for 2 h the temperature was increased to 160 °C and $FeCl_2 \cdot xH_2O$ (4.8 mg, 0.023 mmol) (dissolved in 0.5 mL of ethanol) was injected. The reaction temperature was maintained for an additional hour. The temperature was finally increased to 350 °C for 3.5 h. The reaction mixture was dissolved in a 1:1 mixture of ethanol and hexane. The products were collected by centrifugation at 13,000 rpm for 10 min and washed with ethanol 3 times before being re-dispersed into 3 mL of ethanol.

Pt nanocubes stabilized by ACA and HDD were also used as reactive templates for the synthesis of $FePt_3$ nanocubes. After the Pt nanocubes were formed following the already mentioned procedure, the reaction temperature was lowered to 95 °C. $Fe(CO)_5$ (2:1 molar ratio of Fe:Pt) was added by injection and the temperature was slowly increased to a range of temperatures (300-350 °C) for 3.5 h. The solid reaction mixture was dissolved in 10 mL of chloroform and 10 mL of ethanol and centrifuged at 13,000 rpm for 5 min. After the particles were washed with ethanol three times they were suspended in 3 mL of ethanol.

The Pt nanocubes (4.6 mg, 0.024 mmol) that were stabilized by ACA and HDD were also transferred to a solution of TEG where they were reacted with $FeCl_3 \cdot 6H_2O$ (44.8 mg, 165.7 mmol) at 310 °C for 3 h under flowing Ar. The nanoparticles were collected by centrifugation at 13,000 rpm for 10 min and washed three times with ethanol before being re-dispersed into 3 mL of ethanol.

5.2.6 Conversion of Pt nanocubes into intermetallic PtSn nanocubes

ACA and HDD stabilized Pt nanocubes could also be used as templates for the synthesis of intermetallic PtSn (NiAs structure-type) in a modified reaction method mentioned above. The procedure began by adding HDD (1.6 g, 6.2 mmol), HDA (2.3 g, 9.4 mmol), DPE (1.1 mL, 6.9 mmol), and $SnCl_2$ (10.5 mg, 0.055 mmol) in a 3-neck round-bottom flask attached to a condenser and a stir bar. After purging with fast flowing Ar for 2 h the temperature was slowly increased to 235 °C for ~ 30 min. The reaction product was dissolved in 10 mL of chloroform and 10 mL of ethanol. The mixture was centrifuged at 13,000 rpm for 10 min and washed three times with ethanol before being re-dispersed in 3 mL of ethanol.

5.3 Direct conversion of Pt nanoparticles into Co and Ni alloys and the partially ordered $L1_2$ phase of $FePt_3$

Generally, the synthesis of FePt nanoparticles usually yields the unordered fcc phase which are accompanied by superparamagnetic properties. To obtain the ordered $L1_0$ or $L1_2$ phases of the Fe-Pt system a post-annealing step (above 500 °C) is required which can lead to particle sintering. Several studies have shown that controlling the reaction parameters (Fe/Pt ratio and reducing power of the solvent) can slow down the reaction

kinetics to form the ordered phases of FePt.[186] Here, we show that it is possible to directly convert preformed Pt nanoparticles into the partially ordered $L1_2$ phase of $FePt_3$ in solution.

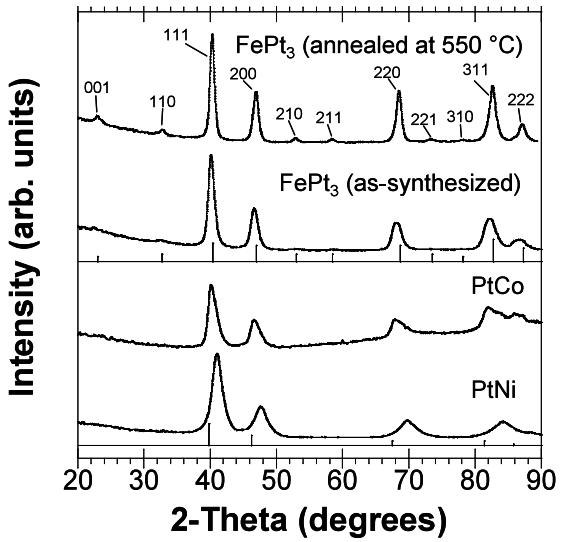

Figure 5.1. Powder XRD pattern showing unordered face-centered cubic alloys of PtNi and PtCo (compared to the Pt reference peaks) made by reacting $Ni(acac)_2$ and $Co(acac)_2$ with Pt nanoparticles (1:1 molar ratio of Pt to Ni or Co) at 310 °C. XRD pattern of an as-synthesized partially ordered $L1_2$ phase of $FePt_3$ (compared to the $FePt_3$ reference peaks) formed by reacting $FeCl_3 \cdot 6H_2O$ (1:6 molar ratio of Pt to Fe) in TEG at 310 °C for 3.5 h and an annealed sample at 550 °C for 30 min are also shown.

Pt nanoparticles were prepared through the reduction of K_2PtCl_6 in ethylene glycol without the use of any capping ligands as was done in our previous study.[155] In this study, TEM images revealed that the Pt nanoparticles were small (~5 nm in diameter) and were aggregated in clusters (50 - 100 nm). The as-prepared Pt nanoparticles were dispersed in a solution of TEG followed by the addition of $FeCl_3 \cdot 6H_2O$ (1:6 molar ratio of Pt to Fe). The solution was heated to a temperature of 310 °C for 3.5 h under flowing Ar. Figure 5.1 shows the powder XRD pattern of the

partially ordered as-synthesized $FePt_3$. The XRD pattern shows that very weak superlattice peaks are present (001, 110, 210, and 211) which coincides with the $L1_2$ ($AuCu_3$ structure-type) phase of $FePt_3$. Additional annealing of the sample at 550 °C for 30 min under flowing Ar increased its crystallinity, making the superlattice peaks more pronounced. Disordered alloys of PtNi and PtCo were made by reacting Pt nanoparticles in TEG with $Ni(acac)_2$ and $Co(acac)_2$ at 310 °C for 2 and 3 h, respectively. The powder XRD pattern in Figure 5.1 also shows that both PtNi and PtCo are disordered alloys with an fcc pattern that is shifted away from the Pt reference peaks, indicating a contraction in the lattice constants.

5.4 Using Pt nanocubes as templates for the conversion into $FePt_3$ nanocubes

Pt nanocubes were synthesized to study the possibility of using them as templates to form intermetallic $FePt_3$ nanocubes ($L1_2$ phase) by the diffusion of iron. Pt nanocubes were synthesized using a procedure developed by Song and co-workers[214] where they used trace amounts of Ag (1.1 mol%) and the PVP : Pt ratio to influence the growth rates along [100]. It should be noted that this particular procedure gives a mixture of Pt nanocubes (80-90%) and tetrahedral (10-20%) particles with an average size of 5 nm (edge length), as seen in Figure 5.2(a and e). A second procedure to develop Pt nanocubes was taken from Yang[215, 217] who synthesized Pt nanocubes and tripods by reducing $Pt(acac)_2$ in HDD and DPE using ACA and HDA as surface-stabilizers. The Pt nanocubes, in Figure 5.2(i), have defined edges and corners with an average size around 19 nm (edge length). The insets in Figure 5.2(a, e, and i) show the SAED pattern of an fcc structure corresponding to Pt.

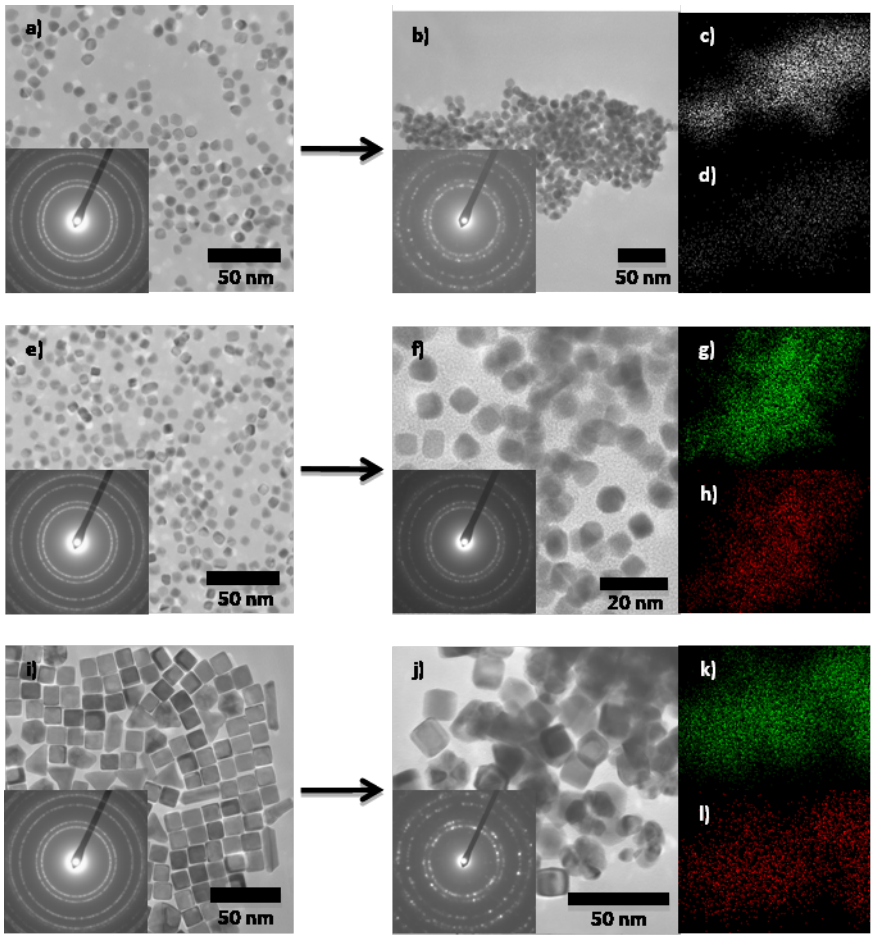

Figure 5.2. TEM images of (a and e) Pt nanocubes stabilized by PVP, (b) Pt nanocubes reacted with $FeCl_3 \cdot 6H_2O$ in TEG at 310 °C for 2.5 h under Ar, (f) Pt nanocubes reacted with $FeCl_2 \cdot xH_2O$ in HDA and HDD at 340 °C for 3.5 h under Ar, (i) Pt nanocubes stabilized by ACA and HDA, (j) Pt nanocubes reacted with $FeCl_3 \cdot 6H_2O$ in TEG at 310 °C for 3.5 h under Ar, (c,d, g, h, k, and l) are electron mapping images of the reacted Fe-Pt cube samples showing that Fe and Pt are present at the same location. Insets are SAED images of the Pt and reacted Fe-Pt nanocubes.

The Pt nanocubes were used as templates to preserve the shape during the conversion reaction to generate intermetallic $FePt_3$ nanocubes. Based off previous studies, we have shown that the metal to intermetallic transformation is a diffusion-based process.[21-23, 26, 158] The experiment began with Pt nanocubes, in Figure 5.2(a), that were

reacted with $FeCl_3 \cdot 6H_2O$ (Pt:Fe molar ratio of 1:6.6) in TEG at 310 °C for 3.5 h. The resulting product, in Figure 5.2(b), showed relatively unchanged particles that still had an edge length of ~5 nm with a cubic morphology except the only difference was they were aggregated. The SAED pattern in the inset of Figure 5.2(b) corresponded to a fcc structure adopted by Pt and was confirmed by powder XRD as well. Though SAED and XRD only confirm the face-centered cubic structure of Pt; electron mapping confirmed that Pt and Fe were simultaneously present in Figure 5.2(c and d), respectively. It should be observed that the mapping signal for Pt is much more intense than the signal for Fe which agrees well with EDS results (Pt – 70% and Fe – 30 %).

Pt nanoparticles in Figure 5.2(e) were added to a reaction system containing HDA and HDD. An iron source was added ($FeCl_2 \cdot xH_2O$ in a 2:1 molar ratio of Fe to Pt) and the temperature was raised to 350 °C for 3.5 h under Ar. Figure 5.2(f) shows that the particles maintained their cubic shape and size after being reacted with $FeCl_2 \cdot xH_2O$. The SAED pattern in the inset shows a fcc structure indicating that the Pt nanocubes did not transform into an ordered $L1_2$ phase and XRD experiments confirmed that Pt was the only crystalline phase present. Interestingly, electron-mapping experiments in Figure 5.2(g and h) indicated that both Pt and Fe were present (Pt showing the highest intensity) over the area occupied by the nanocubes. EDS measurements also confirm these findings showing that the sample contains 76% Pt and 24% Fe.

Experiments were done using Pt nanocubes in Figure 5.2(i), stabilized by ACA and HDA, that were also reacted with $FeCl_3 \cdot 6H_2O$ in a solution of TEG at 310 °C for 3.5 h. After the reaction the resulting particles, which were slightly aggregated, still

maintained their cubic shape and size. The SAED in the inset of Figure 5.2(j) shows a fcc pattern and agrees well with powder XRD experiments that showed pure Pt. However, electron mapping, in Figure 5.2(k and l) shows that both Pt and Fe (Pt showing a higher intensity) were present in the nanocubes sample, which is also confirmed by EDS experiments (Pt- 91% and Fe – 9%).

In these experiments mentioned in Figure 5.2, it appears that any significant amount of Fe failed to diffuse into the Pt nanocubes. Although in all cases, EDS and electron mapping experiments did show that Fe was indeed present either near or on the surface of the Pt nanocubes. Interestingly, earlier experiments showed that aggregated Pt nanoparticles, with no added capping ligands, did transform into the $L1_2$ $FePt_3$ intermetallic phase in the presence of excess $FeCl_3 \cdot 6H_2O$ in TEG (as shown in Figure 5.1). Work done by Shinoda and co-workers investigated the pathway to the formation of $L1_0$ FePt nanoparticles in TEG.[222] They concluded that small Pt rich particles formed with a thin Fe rich amorphous shell and the particles begin to aggregate. Upon heating at higher temperatures (~ 300 °C) the particles begin to sinter at the amorphous interface and crystallization along with ordering occurred to induce the formation of ordered $L1_0$ polycrystalline FePt nanoparticles. It could be that the preformed nanoparticles followed a similar process where an amorphous coating surrounded the aggregated particles. Since the particles were already in close contact the possibility that sintering could occur more easily to induce crystallization of $FePt_3$ could be possible, which Shinoda thought facilitated partial ordering. Possibly the larger size of the Pt nanocubes, the capping

ligands, or shape may contribute to the hindrance of the formation of FePt that was proposed by Shinoda.[222]

Experiments to convert Pt nanocubes into disordered fcc or ordered $L1_2$ alloys were also attempted by using $Fe(CO)_5$. The procedure began by forming ACA and HDA stabilized Pt nanocubes (average edge length ~19 nm) in the presence of HDD and DPE at 160 °C. After the Pt nanocubes were formed the reaction temperature was decreased to 95 °C under flowing Ar. The temperature was slowly raised to reach 310 °C for 3.5 h. As seen in Figure 5.3(a), the powder XRD pattern indicated that pure Pt (as compared to the reference peaks) was still present with Fe_3O_4 (as indicated by the *). The SAED pattern in Figure 5.3(d) confirms the XRD results and shows the indexed rings corresponding to fcc Pt. Figure 5.3(b) shows Fe_3O_4 nanoparticles formed that are poly-dispersed in size and are highly crystalline. It is possible that the $Fe(CO)_5$ decomposed too quickly and failed to nucleate on the Pt nanocubes and instead formed Fe nanoparticles that oxidized to form Fe_3O_4 on exposure to air. Interestingly, after the Pt nanocubes went through the attempted conversion reaction with $Fe(CO)_5$ they appeared relatively unchanged in terms of maintaining a similar size (~19 nm) and still had well defined edges and corners, which gives us some insight about the stability of the starting material.

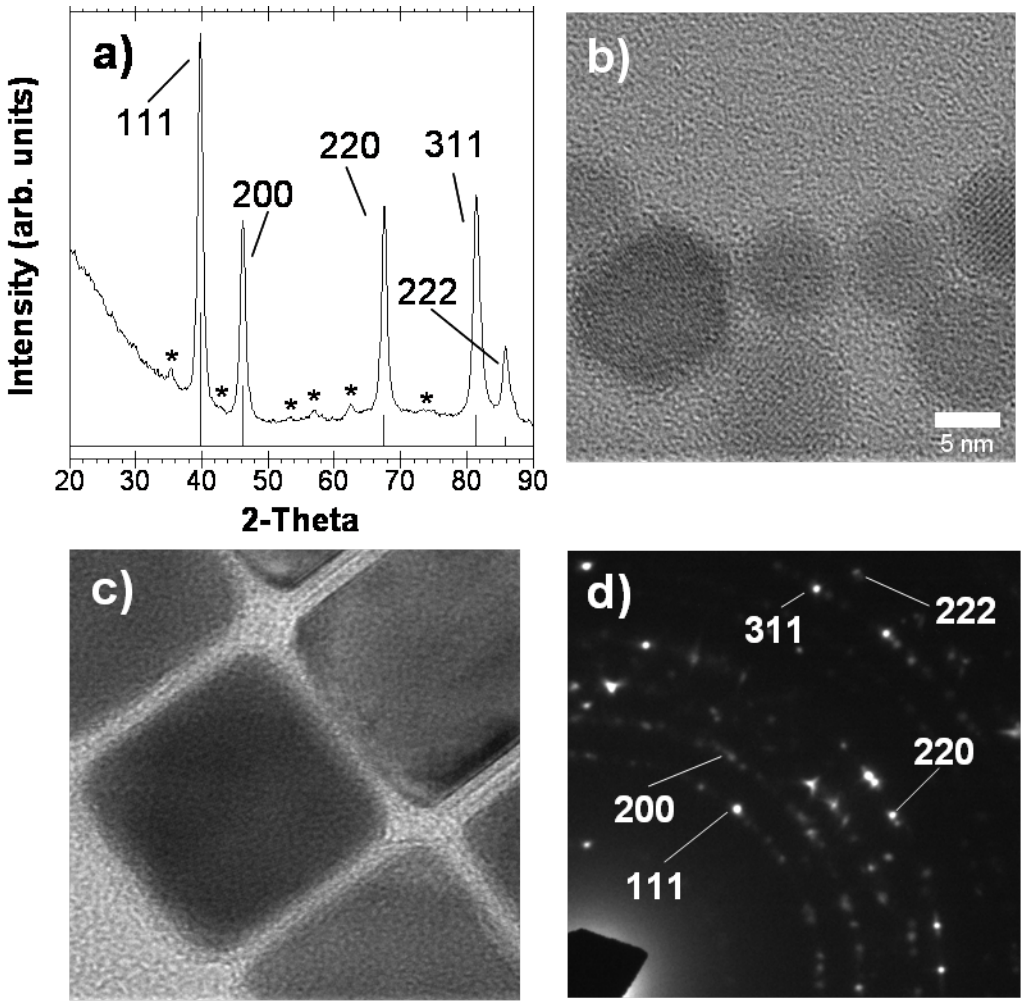

Figure 5.3. (a) Powder XRD pattern showing a mixture of Fe_3O_4 (marked by *) and the fcc pattern of Pt (indexed peaks) after reacting as-synthesized Pt nanocubes with $Fe(CO)_5$ in the presence of HDD, HDA, and DPE at 350 °C. TEM micrographs showing (b) Fe3O4 nanoparticles, (c) Pt nanocubes after the addition of $Fe(CO)_5$, and (d) SAED showing the indexed fcc pattern of Pt and Fe_3O_4 (not indexed).

5.5 Conversion of Pt nanocubes into intermetallic PtSn nanocubes.

It has been shown that various Pt nanoparticle shapes have the ability to affect the catalytic activity in some types of reactions such as, ethylene hydrogenation[110], electro-oxidation of formic acid and ethanol,[223] and many more.[224] It is well known now that Pt-based intermetallic compounds have excellent potential as catalysts.[41, 57-62] It may be

worth combining both concepts to design an intermetallic nanoparticle catalyst that has a surface made primarily of its most catalytically reactive facets.

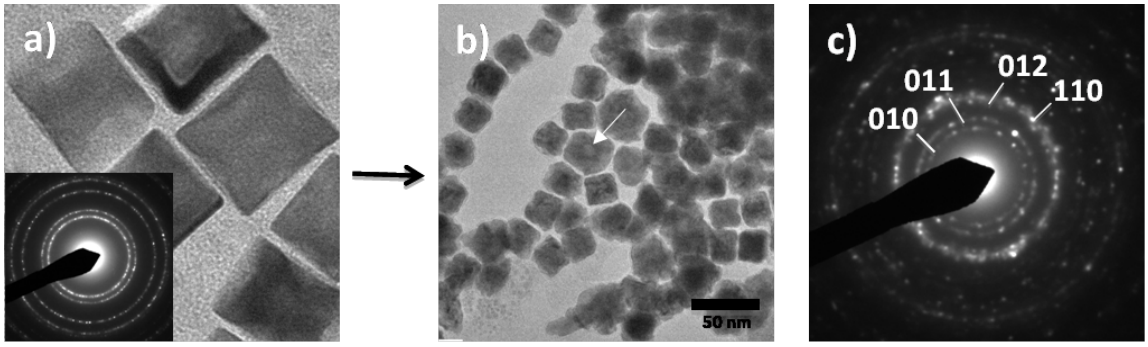

Figure 5.4. TEM micrographs showing (a) Pt nanocubes stabilized by ACA and HDD in the presence of HDD and DPE, (b) PtSn nanocubes after reacting Pt nanocubes with $SnCl_2$ (1:4.3 molar ratio of Pt to Sn) at 235 °C (Arrow indicates that larger particles have hollow centers), and (c) SAED pattern of the PtSn nanocubes indexed to the hexagonal NiAs structure-type indicating an ordered PtSn phase.

In an effort to begin a proof of concept approach in designing such materials, Pt nanocubes were used as templates that were made by stabilizing the surface with ACA and HDA with a solvent mixture of HDD and DPE at 160 °C, as shown in Figure 5.4(a). The as-prepared cubes were then added to the reaction flask with HDD, HDA, DPE, and $SnCl_2$ (added in a 1:4.3 molar ratio of Pt to Sn). After flushing the reaction flask with Ar the temperature was increased to 235 °C for 30 min. After the reaction, the nanocubes were analyzed by TEM in Figure 5.4(b) and it was shown that cubic morphologies were present. However, the nanocubes were not dispersed and there was a large degree of sintering. The nanocubes grew from an average size of ~19 nm to a range of about 23-27 nm along the edge (only considering particles that maintained the cubic shape). Some particles completely lost their cubic shape and instead had irregular morphologies.

As pointed out by the arrow in Figure 5.4(b) some larger particles exhibited hollowing which is indicative of the Kirkendall effect and is consistent with what we have observed in other studies.[22, 23, 32, 158] According to the SAED pattern shown in Figure 5.4(c), the crystal structure is consistent with the hexagonal NiAs structure-type of an intermetallic PtSn compound. It can be concluded that Pt nanocubes were converted into intermetallic PtSn nanocubes with a hexagonal structure.

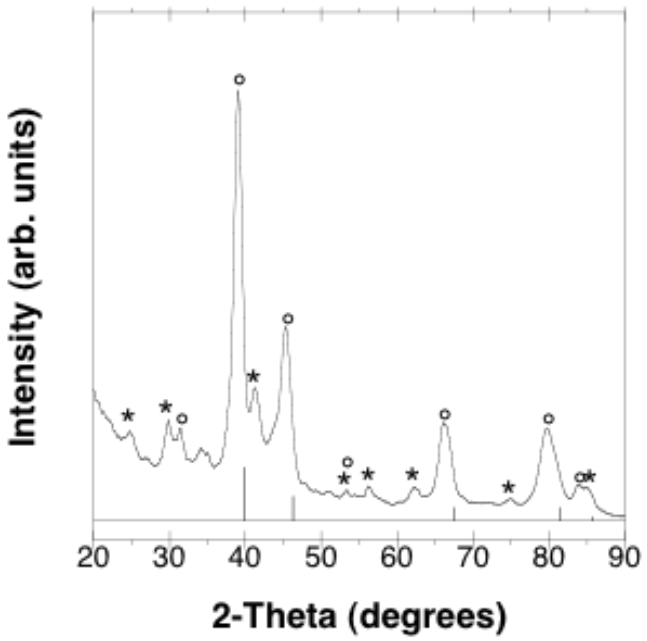

Figure 5.5. Powder XRD pattern of Pt nanocubes reacted with $SnCl_2$ (3:1 molar ratio) in the presence of HDA, HDD, and DPE at 300 °C for ~45 min. The (*) and (°) indicates the NiAs structure-type PtSn and the $AuCu_3$ structure-type phase formations. The XRD pattern is referenced to Pt simulated XRD peaks.

The molar ratios of Pt (nanocubes) and $SnCl_2$ were adjusted to a 3:1 molar ratio respectively and the reaction was heated to 300 °C for 45 min under Ar in the presence of HDA, HDD, and DPE in an attempt to form Pt_3Sn nanocubes. According to the

powder XRD pattern in Figure 5.5 Pt_3Sn ($AuCu_3$ structure-type) was the main phase, however, the NiAs structure-type PtSn was also present. The XRD pattern was referenced to Pt simulated peaks and Pt was not observed. The TEM image in Figure 5.6 reveals that some of the resulting particles maintained a cubic morphology and similar size after the reaction. However, some particles have irregular shapes and increased in size

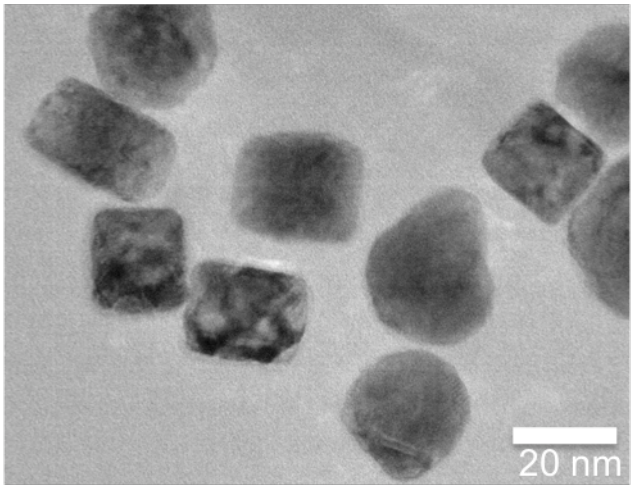

Figure 5.6. TEM image of Pt_3Sn/PtSn nanocube mixture after reacting Pt nanocubes with $SnCl_2$ (3:1 molar ratio of Pt to $SnCl_2$) in the presence of HDA, HDD, and DPE at 300 °C for ~45 min.

5.6 Conclusion

It has been demonstrated that preformed Pt nanoparticles can be converted directly into a partially ordered $L1_0$ intermetallic phase of $FePt_3$ in the presence of $FeCl_3 \cdot 6H_2O$ in a polyol solution. Furthermore, it is possible to convert Pt nanoparticles with Co and Ni salts into disordered fcc alloys of CoPt and NiPt in solution. These solution techniques used to convert single metal nanoparticles into alloy and intermetallic compounds were

applied to more complex nanostructures (e.g. Pt nanocubes instead of spherical particles) with the hope to further enhance their physical properties.

A variety of experiments were employed with the goal of converting Pt nanocubes either stabilized by PVP or ACA and HDA to FePt or $FePt_3$ intermetallic compounds by using a variety of Fe sources. It was found by powder XRD and SAED experiments that Fe did not diffuse into Pt to make any significant change to its crystal structure. TEM micrographs also showed no physical changes (shape or size) to the nanocubes. Electron mapping did show, however, that the Fe signal overlapped the coverage area of the Pt nanocubes. This was also confirmed by EDS that showed Fe was present and may indicate that a thin amorphous Fe shell encapsulates the Pt nanocubes, though none was visible by TEM. The reasoning for the lack of Fe diffusing into the Pt nanocubes is not well understood at this time. When $Fe(CO)_5$ thermally decomposes it appears that small Fe nanoparticles quickly form and prevent any significant amount of Fe from nucleating onto the surface of the Pt nanocubes. It is believed that these Fe nanoparticles quickly oxidize when exposed to air after the reaction. XRD, SAED, and TEM experiments confirm the mixture of Pt nanocubes and Fe_3O_4 nanoparticles.

Pt nanocubes stabilized by ACA and HDD were also used as templates to form PtSn nanocubes and offer potential as being a viable method in the future to obtain such structures. The PtSn nanocubes do show sintering and some do completely loose the "cube" shape, but the Pt nanocubes still preserve their shape. Some cubes did show evidence of hollowing and grew 4 – 8 nm indicating a diffusion process may be involved.

6. SUMMARY AND CONCLUSIONS

In Section 2, the concept of using nanoparticles as reactive precursors toward the formation of more complex materials was investigated. The method takes advantage of the fact that the high surface-area to volume ratio of nanoparticles puts the majority of the atoms on the surface. When the nanoparticles were mixed in solution to form a "nanoparticle composite", a high level of interface contact was achieved. This decreased the distance the elements needed to diffuse into each other and essentially eliminated solid-solid diffusion as a rate-limiting step. As a result, materials such as alloys and intermetallic compounds, that usually require extreme annealing conditions, can be synthesized at relatively low-temperatures and short reaction times. By mixing single-metal nanoparticles into binary metal composites and annealing in an inert atmosphere it was shown that for most systems studied, the alloy and intermetallic phase would form under heating to 600 °C as compared to ~ 1000 °C for the synthesis of their bulk counterparts.

The work of using nanoparticles to achieve shorter diffusion distance was also extended toward making ternary and quaternary oxide materials. In this case metal salts were reduced in solution with a capping ligand, PVP, and allowed to oxidize in air, or a metal isopropoxide was made to undergo a hydrolysis reaction. The oxide nanoparticles were mixed into nanocomposites, mixed according to the stoichiometric proportions that were desired for the compound, and after annealing, the desired multi-metal oxide was formed. Using nanoparticle composites to reduce the diffusion distance proved to be an

extremely versatile method in obtaining many alloy, intermetallic compound and multi-metal oxide powders while requiring less energy.

Section 3 took the concept of using metal nanoparticles as reactive precursors one step further. In this case, Pt nanoparticles were transformed into Pt-M (M = Sn, Pb, and Bi) intermetallic compounds in the presence of a metal salt in solution at relatively low-temperatures. Pt could also be converted into a disordered FePt alloy and further annealing under an Ar atmosphere yielded the intermetallic compound $FePt_3$. However, no capping agent was used in the synthesis of Pt nanoparticles and as a result the converted intermetallic nanoparticle products were highly sintered. Since these intermetallic compounds are often used in catalysis, it would be disadvantageous to use capping agents to stabilize the nanoparticles when access to the surface could potentially be inhibited.

Capping ligands can be avoided by immobilizing nanoparticles on a solid-support because they are able to remain stable with a relatively clean surface. However, the synthesis of alloy and intermetallic compounds becomes complicated because high-temperature annealing is often required that may result in particle aggregation and loss in surface-area. To overcome this dilemma, preformed nanoparticles supported on γ-Al_2O_3, CeO_2, and Vulcan XC-72 were added to a polyol solution with a metal salt ($SnCl_2$, $SbCl_3$, $Pb(C_2H_3O_2)_2 \cdot 3H_2O$ and $CuCl_2$). After heating to a specified temperature in solution, intermetallic compounds of PtSn, Pt_3Sn, PtSb, and PtPb and a disordered alloy of Cu_3Pt would form on the supports. It was decided that the formation of intermetallic compounds was diffusion-based due to presence of hollow PtSn

nanoparticles, which we attributed to the Kirkendall effect. The relatively low temperatures allow the nanoparticles to remain small with a high surface-area giving them great potential in catalysis.

The intermetallic nanoparticles supported on Vulcan XC-72 were tested for methanol and formic acid electro-oxidation. It was found that PtRu/Vulcan XC-72 out-preformed all intermetallic nanoparticles for methanol electro-oxidation. However, PtPb/Vulcan XC-72 showed the lowest onset potential (0.1 V vs. RHE) with a relatively equal current as PtRu/Vulcan XC-72 making it a very efficient catalyst. Cyclic voltammetry CO stripping experiments were performed and it was found that PtSb/Vulcan XC-72 was the only intermetallic compound that had an improved CO tolerance compared to Pt/Vulcan XC-72, ~0.80 V vs. RHE, (PtRu/Vulcan XC-72, ~0.55 V vs. RHE, still showed the best performance). Pt_3Sn and Cu_3Pt supported on Vulcan XC-72 also showed a lower CO oxidation temperature (160 °C and 175 °C, respectively) compared to Pt (200 °C) showing that they are viable catalysts for gas phase reactions as well.

The subject of Section 4 was the possibility of using the "conversion chemistry" technique described in Section 3 to create supported intermetallic systems for new catalytic reactions. More specifically, Pd nanoparticles that were supported on Vulcan XC-72 and γ-Al_2O_3 were converted to Pd-based intermetallic compounds (Pd_2Sn, Pd_2Ga, PdIn, and Pd_3Pb) and alloys (AgPd and Cu_3Pd). It was found that Pd_2Sn nanoparticles as small as 5 nm showed hollowing most likely due to the Kirkendall effect, as seen with PtSn in Section 3.

The Pd-based intermetallic nanoparticles were tested for catalytic activity toward the Suzuki and Heck coupling reactions. Pd complexes or salts traditionally catalyze these reactions; however, Pd nanoparticles are becoming a popular new approach toward coupling reactions. Even though bimetallic nanoparticles have been used as catalysts for the Heck reaction, or similar carbon-coupling reactions, to the best of our knowledge, the effects of using an intermetallic catalyst have never been reported.

The effects of using Pd-based intermetallic nanoparticle catalysts were studied with reacting octylborane with iodobenzene to form phenyloctane. It was found that the intermetallic nanoparticle catalysts were active; however, they tend to prefer the homocoupled product, biphenyl, as opposed to the cross-coupled product (phenyloctane). Changing the reaction conditions, such as changing to more polar solvents, can induce a higher selectivity toward the cross-coupled product. When $Cu_3Pd/\gamma\text{-}Al_2O_3$ where used, the Suzuki coupling reaction did not occur. It did turn out that intermetallic Pd_3Pb/Vulcan XC-72 was active toward the Heck reaction (reacting 1-octene with iodobenzene to form 1-phenyoctene) and showed comparable selectivity to pure Pd.

Section 5 dealt with the possibility of extending the "conversion chemistry" concept to transforming preformed Pt nanocubes into intermetallic nanostructures. Our initial work investigated study began by experimenting with the conditions necessary for the formation the Fe-Pt based intermetallic compounds. We found that when Pt nanoparticles with no capping-ligands (aggregates) are reacted with $FeCl_3 \cdot 6H_2O$ in a

TEG solution, the partially ordered $L1_2$ phase of $FePt_3$ is formed. The disordered alloys of CoPt and NiPt could also be formed under similar conditions.

Pt nanocubes were synthesized by two different methods where they were either stabilized by PVP, or ACA and HDD. The nanocubes were reacted with $FeCl_3 \cdot 6H_2O$ in TEG or HDA and HDD. In either case, it was shown that the Pt nanocubes did not react at all; however, elemental mapping and EDS did show that the nanocubes were present with Fe. It could be possible that the cubes have an amorphous Fe shell, but diffusion into Pt was not favored. When $Fe(CO)_5$ was used as the Fe source, it was found that small Fe_3O_4 nanoparticles were found amongst the un-reacted Pt nanocubes. This may be attributed to the fact that $Fe(CO)_5$ may decompose and nucleate to form small Fe nanoparticles quickly not leaving very much Fe to nucleate onto the surface of the Pt nanocubes. Exposure of the sample to air caused the Fe nanoparticles to oxidize. When Pt nanocubes, stabilized by ACA and HDA, were reacted with excess $SnCl_2$ it was found that they transformed into Pt nanocubes with the NiAs structure.

The small size of nanoparticles and the fact that most atoms are located on the surface, make them ideal solid-state reaction precursors for the synthesis of more complex multi-element materials. It has been shown that they can be so effective in reducing diffusion distance in a solid-state reaction that the temperature normally required for the formation of a product can be significantly reduced. Furthermore, the small size allows the diffusion of metal atoms into the particles, forming more complex structures, while preserving many physical attributes (size, shape, etc.). The less harsh reaction conditions will hopefully allow for more control over the final form of

nanostructures for greater access into new or enhanced physical properties. Using nanoparticles as reactants may prove to be a viable way to discover new metastable phases that are difficult to synthesize, or are not yet discovered.

REFERENCES

(1) Westbrook, J. H., Ed. *Intermetallic Compounds* John Wiley & Sons, Inc., New York, 1967.

(2) Chen, M.; Kim, J.; Liu, J. P.; Fan, H.; Sun, S. *J. Am. Chem. Soc.* **2006**, *128*, 7132-7133.

(3) Shukla, N.; Liu, C.; Roy, A. G. *Mater. Lett.* **2006**, *60*, 995-998.

(4) Chen, M.; Pica, T.; Jiang, Y.-B.; Li, P.; Yano, K.; Liu, P.; Datye, A. K.; Fan, H. *J. Am. Chem. Soc.* **2007**, *129*, 6348-6349.

(5) Wang, C.; Hou, Y.; Kim, J.; Sun, S. *Angew. Chem. Int. Ed.* **2007**, *46*, 6333-6335.

(6) Maksimuk, S.; Yang, S.; Peng, Z.; Yang, H. *J. Am. Chem. Soc.* **2007**, *129*, 8684-8685.

(7) Yang, S.; Peng, Z.; Yang, H. *Adv. Funct. Mater.* **2008**, *18*, 2745-2753.

(8) Hyeon, T.; Lee, S. S.; Park, J.; Chung, Y.; Na, H. B. *J. Am. Chem. Soc.* **2001**, *123*, 12798-12801.

(9) Yin, Y.; Rioux, R. M.; Erdonmez, C. K.; Hughes, S.; Somorjai, G. A.; Alivisatos, A. P. *Science* **2004**, *304*, 711-714.

(10) Yin, Y.; Erdonmez, C. K.; Cabot, A.; Hughes, S.; Alivisatos, A. P. *Adv. Funct. Mater.* **2006**, *16*, 1389-1399.

(11) Khanna, P.; Jun, K. -W.; Hong, K. B.; Baeg, J.-O.; Mehrotra, G. K. *Mater. Chem. Phys.* **2005**, *92*, 54-58.

(12) Singh, N.; Khanna, P. K. *Synth. React. Inorg. Met.* **2007**, *37*, 367.

(13) Chiang, R.-K.; Chiang, R.-T. *Inorg. Chem.* **2007**, *46*, 369-371.

(14) Chen, J.; Wiley, B.; McLellan, J. M.; Xiong, Y.; Li, Z.-Y.; Xia, Y. *Nano Lett.* **2005**, *5*, 2058-2062.

(15) Chen, J.; Mclellan, J. M.; Siekkinen, A.; Xiong, Y.; Li, Z.-Y.; Xia, Y. *J. Am. Chem. Soc.* **2006**, *128*, 14776-1477.

(16) Sun, Y.; Xia, Y. *Adv. Mater.* **2004**, *16*, 264-268.

(17) Sun, Y.; Tao, Z.; Chen, J.; Herricks, T.; Xia, Y. *J. Am Chem. Soc.* **2004**, *126*, 5940-5941.

(18) Lu, X.; Tuan, H.-Y.; chen, J.; Li, Z.-Y.; Korgel, B. A.; Xia, Y. *J. Am. Chem. Soc.* **2007**, *129*, 1733-1742.

(19) Vasquez, Y.; Sra, A. K.; Schaak, R. E. *J. Am. Chem. Soc.* **2005**, *127*, 12504-12505.

(20) Leonard, B. M.; Bhuvanesh, N. S. P.; Schaak, R. E. *J. Am. Chem. Soc.* **2005**, *127*, 7326-7327.

(21) Leonard, B. M.; Schaak, R. E. *J. Am. Chem. Soc.* **2006**, *128*, 11475-11482.

(22) Chou, N. H.; Schaak, R. E. *J. Am. Chem. Soc.* **2007**, *129*, 7339-7345.

(23) Chou, N. H.; Schaak, R. E. *Chem. Mater.* **2008**, *20*, 2081-2085.

(24) Cable, R. E.; Schaak, R. E. *Chem. Mater.* **2007**, *19*, 4098-4104.

(25) Anderson, M. E.; Buck, M. R.; Sines, I. T.; Oyler, K. D.; Schaak, R. E. *J. Am. Chem. Soc.* **2008**, *130*, 14042-14043.

(26) Cable, R. E.; Schaak, R. E. *J. Am. Chem. Soc.* **2006**, *128*, 9588-9589.

(27) Dawood, F.; Leonard, B. M.; Schaak, R. E. *Chem. Mater.* **2007**, *19*, 4545-4550.

(28) Chen, J.-H.; Tai, M.-F.; Chi, K.-M. *J. Mater. Chem.* **2004**, *14*, 296-298.

(29) Schmidt, F. K.; Belykh, L. B.; Cherenkova, T. V. *Kinet. Catal.* **2001**, *42*, 163.

(30) Henkes, A. E.; Vasquez, Y.; Schaak, R. E. *J. Am. Chem. Soc.* **2007**, *129*, 1896-1897.

(31) Henkes, A. E.; Schaak, R. E. *Chem. Mater.* **2007**, *19*, 4234-4242.

(32) Henkes, A. E.; Schaak, R. E. *Inorg. Chem.* **2008**, *47*, 671-677.

(33) Choudhary, T. V.; Sivadinaryana, C.; Datye, A. K.; Kumar, K.; Goodman, D. W. *Catal. Lett.* **2003**, *86*, 1-8.

(34) Kidwai, M.; Bansal, V.; Saxena, A.; Shankar, R.; Mozumbar, S. *Tetrahedron Lett.* **2006**, *47*, 4161-4165.

(35) Yang, C.-m.; Kalwei, M.; Schuth, F.; Chao, K.-j. *Appl Catal. A: General* **2003**, *254*, 289-296.
(36) Tang, Y.; Zhang, L.; Wang, Y.; Zhou, Y.; Gao, Y.; Liu, C.; Xing, W.; Lu, T. *J. Power Sources* **2006**, *162*, 124-131.

(37) Biffis, A.; Zecca, M.; Basato, M. *J. Mol Catal A: Chemical* **2001**, *173,* 249-274.

(38) Edvardsson, J.; Rautanen, P.; Littorin, A.; Larsson, M. *J. Am. Oil Chem. Soc.* **2001**, *78*, 319-327.

(39) Salgado, J. R. C.; Antolini, E.; Gonzalez, E. R. *Appl. Catal., B* **2005**, *57*, 283-290.

(40) Antolini, E. *Mater. Chem. Phys.* **2003**, *78*, 563-573.

(41) Casado-Rivera, E.; Volpe, D. J.; Alden, L.; Lind, C.; Downie, C.; Vazquez-Alvarez, T.; Angelo, A. C. D.; DiSalvo, F. J.; Abruna, H. D. *J. Am. Chem. Soc.* **2004**, *126*, 4043-4049.

(42) Sun, S.; Murray, C. B.; Weller, D.; Folks, L.; Moser, A. *Science* **2000**, *87*, 423-438.

(43) Goll, D.; Kronmuller, H. *Naturewissenschaften* **2000**, *87*, 423-438.

(44) Paduani, C. *J. Appl. Phys.* **2001**, *90*, 6251-6254.

(45) Stern, R. A.; Willoughby, S. D.; Maclaren, J. M.; Cui, J.; Pan, Q.; James, R. D. *J. Appl. Phys.* **2003**, *93*, 8644-8646.

(46) Kirchheim, R.; Mutschele, T.; Keininger, W.; Gleiter, H.; Birringer, R.; Koble, T. D. *Mater. Sci. Eng.* **1988**, *99*, 457-462.

(47) Kamakoti, P.; Sholl, D. S. *J. Membr. Sci.* **2003**, *225*, 145-154.

(48) Lopez, M. F.; Escudero, M. L. *Electrochim. Acta* **1998**, *43*, 671-678.

(49) Salamon, M. B.; Jaime, M. *Rev. Mod. Phys.* **2001**, *73*, 583-628.

(50) Gavaler, J. R.; Janocko, M. A.; Bradinski, A. I.; Rowland, G. W. *IEEE Trans. Magn.* **1975**, *2*, 192-196.

(51) Cava, R. J.; Takagi, H.; Zandergen, H. W.; Krajewski, J.; Peck, W. F.; Siegrist, T.; Batlogg, B.; Vandover, R. B.; Felder, R. J.; Mizuhashi, K.; Lee, J. O.; Eisaki, H.; Uchida, S. *Nature* **1994**, *367*, 252-253.

(52) Nagamatsu, J.; Makagawa, N.; Muranaka, T.; Zenitani, Y.; Akimitsu, J. *Nature* **2001**, *410*, 63-64.

(53) Cava, R. J. *J. Am. Ceram. Soc.* **200**, *83*, 5-28.

(54) Halasyamani, P. S.; Poeppelmeier, K. R. *Chem. Mater.* **1998**, *10*, 2753-2769.

(55) Boivin, J. C.; Mairesse, G. *Chem. Mater.* **1998**, *10*, 2870-2888.

(56) Roucoux, A.; Schulz, J.; Patin, H. *Chem. Rev.* **2002**, *102*, 3757-3778.

(57) Casado-Rivera, E.; Gal, Z.; Angelo, A. C. D.; C. Lind, F. J. D.; Abruna, H. D. *Chem. Phys. Chem.* **2003**, *4*, 193-199.

(58) Alden, L. R.; Han, D. K.; Matsumoto, F.; Abruna, H. D.; DiSalvo, F. J. *Chem. Mater.* **2006**, *18*, 5591-5596.

(59) Alden, L. R.; Roychodhury, C.; Matsumoto, F.; Han, D. K.; Zeldovich, V. B.; Abruna, H. D.; DiSalvo, F. J. *Langmuir* **2006**, *22*, 10465-10471.

(60) Blasini, D. R.; Rochefort, D.; Fachini, E.; Alden, L. R.; DiSalvo, F. J.; Abruna, C. R. C. H. D. *Surface Science* **2006**, *600*, 2670-2680.

(61) Roychowdhury, C.; Matsumoto, F.; Mutlol, P. F.; Abruna, H. D.; DiSalvo, F. J. *Chem. Mater.* **2005**, *17*, 5871-5876.

(62) Roychowdhury, C.; Matsumoto, F.; Zeldovich, V. B.; Warren, S. C.; Mutolo, P. F.; Ballesteros, M.; Wiesner, U.; Abruna, H. D.; DiSalvo, F. J. *Chem. Mater.* **2006**, *18*, 3365-3372.

(63) Volpe, D.; Casado-Rivera, E.; Alden, L.; Lind, C.; Hagerdon, K.; Downie, C.; Korzeniewski, C.; DiSalvo, F. J.; Abruna, H. D. *J. Electrochem. Soc.* **2004**, *151*, A971-A977.

(64) Pena, M. A.; Fierro, J. L. G. *Chem. Rev.* **2001**, *101*, 1981-2017.

(65) Froes, F. H. S. *Materials Science and Engineering* **1995**, *193*, 612-623.

(66) Paris, S.; Gaffet, E.; Bernard, F.; Munir, Z. A. *Scrip. Mater.* **2004**, *50*, 691-696.

(67) Gauthier, V.; Bernard, F.; Gaffet, E.; Munir, Z. A.; Larpin, J. P. *Intermetallics* **2001**, *9*, 571-580.

(68) Paris, S.; Valot, C.; Gosmain, L.; Gaffet, E.; Bernard, F.; Munir, Z. *J. Mater. Res.* **2003**, *18*, 2331-2338.

(69) Rehbein, M.; Epple, M.; Fischer, R. D. *Soid State Sci.* **1996**, *2*, 473-488.

(70) Onda, A.; Komatsu, T.; Yashima, T. *J. Catal.* **2001**, *201*, 13-21.

(71) Haubold, T.; Bohn, R.; Birringer, R.; Gleiter, H. *Mater. Sci. Eng.* **1992**, *A153*, 679-683.

(72) Withers, J. C.; Loutfy, H. C.; Wang, P. *Miner. Met. Mater. Soc.* **1991**, *43*, 36-39.

(73) Rao, C. N. R.; Gopalakrishman, J., *New Directions in Solid State Chemistry*; Cambridge University Press: Cambridge, (1989).

(74) Feng, S.; Xu, R. *Acc. Chem. Res.* **2001**, *34*, 239-247.

(75) Schaak, R. E.; Mallouk, T. E. *J. Am. Chem. Soc.* **2000**, *122*, 2798-2803.

(76) Schaak, R. E.; Mallouk, T. E. *Chem. Mater.* **2002**, *14*, 1455-1471.

(77) Wright, J. D.; Sommerdijk, A. J. M., *Sol-gel materials: chemistry and applications*; Gordon and Breach: Amsterdam, **2001**.

(78) Feldmann, C. *J. Mater. Res.* **2000**, *15*, 2244-2248.

(79) Bhuvanesh, N. S. P.; Reibenspies, J. H. *J. Appl. Crystallogr.* **2003**, *36*, 1480-1481.

(80) Bhuvanesh, N. S. P.; Reibenspies, J. H.; Zhang, Y.; Lee, P. L. *J. Appl. Crystallogr.* **2005**, *38*, 632-638.

(81) Schaak, R. E.; Sra, A. K.; Leonard, B. M.; Cable, R. E.; Bauer, J. C.; Han, Y.; Means, J.; Teizer, W.; Vasquez, Y.; Funck, E. S. *J. Am. Chem. Soc.* **2005**, *127*, 3506-3515.

(82) Zhang, F. X.; Manoun, B.; Saxena, S. K.; Zha, C. S. *J. Solid State Chem.* **2006**, *4*, 1202-1207.

(83) Zhang, J.; Liu, J.; Peng, Q.; Wang, X.; Li, Y. *Chem. Mater.* **2006**, *18*, 867-871.

(84) Popov, S. G.; Levitskii, V. A. *J. Solid State Chem.* **1981**, *38*, 1-9.

(85) Singh, R. S.; Bhimasankaram, T.; Kumar, G. S.; Suryanarayana, S. V. *Solid State Commun.* **1994**, *91*, 567-569.

(86) Srinivas, A.; Suryanarayana, S. V.; Kumar, G. S.; Kumar, M. M. *J. Phys. Condens. Matter* **1999**, *11*, 3335-3340.

(87) Srinivas, A.; Kim, D.-W.; Hong, K. S.; Suryanarayana, S. V. *Mater. Res. Bull.* **2004**, *39*, 55-61.

(88) Henkes, A. E.; Bauer, J. C.; Sra, A. K.; Johnson, R. D.; Cable, R. E.; Shcaak, R. E. *Chem. Mater.* **2006**, *18*, 567-571.

(89) Yori, J. C.; Manuale, D. L.; Marchi, A. J.; Grau, J. M. *Appl. Catal., A* **2004**, *275*, 221-226.

(90) Joubert, E.; Courtoi, X.; Marecot, P.; Duprez, D. *Appl. Catal., B* **2006**, *64*, 103-110.

(91) Marques, P.; Ribeiro, N. F. P.; Schmal, M.; Aranda, D. A. G.; Souza, M. M. V. M. *J. Power Sources* **2006**, *158*, 504-508.

(92) Suh, D. J.; C. K., J. Kim, S. M. Kwon and T. -J. Park, *J. Power Sources*, **2005**, 142, 70-74.

(93) Wasmus, S.; Kuver, A. *J. Electroanal. Chem.* **1999**, *461*, 14-31.

(94) Leger, J.-M. *Electrochim. Acta* **2005**, *50*, 3123-3129.

(95) Iwasita, T. *Electrochim. Acta* **2002**, *47*, 3663-3674

(96) Bahia, A.; Caga, I. T.; M.Winterbottom, J.; Brown, J. M.; King, C. E.; Harris, I. R. *Appl. Catal., A* **1986**, *25*, 199-206.

(97) Barrault, J.; Duprez, D.; Guilleminot, A. *Appl. Catal., A* **1983**, *5*, 99-107.

(98) Takeshita, T.; Wallace, W. E.; Craig, R. S. *J. Catalysis* **1976**, *44*, 236-243.

(99) Baglin, E. G.; Atkinson, G. B.; Nicks, L. F. *Ind. Eng. Chem. Prod. Res. Dev.* **1981**, *20*, 87-90.

(100) Beard, B. C.; Ross, P. N. *J. Electrochem. Soc.* **1986**, *133*, 1839-1845.

(101) Onda, A.; Komatsu, T.; Yashima, T. *J. Catalysis* **2003**, *221*, 378-385.

(102) Komatsu, T.; Inaba, K.; Uezono, T.; Onda, A.; Yashima, T. *Appl. Catal., A* **2003**, *251*, 315-326.

(103) Xia, D.; Chen, G.; Wang, Z.; Zhang, J.; Hui, S. R.; Ghosh, D.; Wang, H. *Chem. Mater.* **2006**, *18*, 5746-5749.

(104) Dubeau, L.; Coutanceau, C.; Garnier, E.; Leager, J. M.; Lamy, C. J. *J. Appl. Electrochem.* **2003**, *33*, 419-429.

(105) Sra, A. K.; Ewers, T. D.; Schaak, R. E. *Chem. Mater.* **2005**, *17*, 758-766.

(106) Cable, R. E.; Schaak, R. E. *Chem. Mater.* **2005**, *17*, 6835-6841.

(107) Cable, R. E.; Schaak, R. E. *Chem. Mater.* **2007**, *19*, 4098-4104.

(108) Narayanan, R.; El-Sayed, M. A. *J. Am. Chem. Soc.* **2004**, *126*, 7194-7195.

(109) Narayanan, R.; El-Sayed, M. A. *Nano Lett.* **2004**, *4*, 1343-1348.

(110) Lee, H.; Habas, S. E.; Kweskin, S.; Butcher, D.; Somorjai, G. A.; Yang, P. *Angew. Chem. Int. Ed.* **2006**, *45*, 7824-7828.

(111) Davis, S. M.; Zacra, F.; Somorfai, G. A. *J. Catal.* **1984**, *85*, 206-223.

(112) Bonet, F.; Delmas, V.; Grugeon, S.; Urbina, R. H.; Silvert, P.-Y. *Nanostruct. Mater.* **1999**, *11*, 1277-1284.

(113) Jones, J. E.; Milne, S. B.; B. Gurau, E. S. S.; Stock, S. R.; Lukehart, C. M. *J. Nanosci. Nanotech.* **2002**, *2*, 81-87.

(114) Bock, C.; Paquet, C.; Couuillard, M.; Botton, G. A.; MacDougall, B. R. *J. Am. Chem. Soc.* **2004**, *126*, 8028-8037.

(115) Bock, C.; MacDougall, B.; LePage, Y. *J. Electrochem. Soc.* **2004**, *151*, A1269-A1278.

(116) Cao, H.; Qian, X.; Zai, J.; Yin, J.; Zhu, Z. *Chem. Commun.* **2006**, *43*, 4548-4550.

(117) Belova, I. V.; Murch, G. E. *J. Phase Equilib.* **2005**, *26*, 430-434.

(118) Oana, M.; Hoffmann, r.; Abruna, H. D.; DiSalvo, F. J. *Surface Science* **2005**, *574*, 1-16.

(119) Ranjan, C.; Hoffmann, R.; DiSalvo, F. J.; Abruna, H. D. *J. Phys. Chem. C* **2007**, *111*, 17357-17369.

(120) Schubert, M. M.; Kahlich, M. J.; Feldmeyer, G.; Huttner, M.; Hackenberg, S.; Gasteiger, H. A.; Behm, R. J. *Phys. Chem. Chem. Phys.* **2001**, *3*, 1123-1131.

(121) Dupont, C.; Jugnet, Y.; Loffreda, D. *J. Am. Chem. Soc.* **2006**, *128*, 9129-9136.

(122) Jin, T.; Okuhara, T.; Mains, G. J.; White, J. M. *J. Phys. Chem.* **1987,** *91*, 3310-3315.

(123) Bernal, S.; Calvino, J. J.; Cauqui, M. A.; Gatica, J. M.; Larese, C.; Omil, J. A. P. Pintado, J. M. *Catal. Today* **1999**, *50*, 175-206.

(124) Meriaudeau, P.; Dutel, J. F.; Dufaux, M.; Naccache, C. *Stud. Surf. Sci. Catal.* **1982**, *11*, 94-104.

(125) Bernal, S.; Calvino, J. J.; Gatica, J. M.; Larese, C.; Lopez-Cartes, C.; Perez-Omil, J. A. *J. Catal.* **1997**, *169*, 510-515.

(126) Gounski, S. E.; Hatcher, H. A.; Ragaram, R. R.; Truex, T. J. *Appl Catal.B* **1995**, *5*, 367-376.

(127) Graham, G. W.; Hen., H. W.; Chun, W.; McCabe, R. W. *J. Catal.* **1999**, *182*, 228-233.

(128) Mullins, D. R.; Zhang, K. Z. *Surf. Sci.* **2002**, *513*, 163-173.

(129) Hardacre, C.; Ormerod, R. M.; Lambert, R. M. *J. Phys. Chem.* **1994**, *98*, 10901-10905.

(130) Galeotti, M.; Atrei, A.; Bardi, U.; Rovida, G.; Torrini, M. *Surf. Science*, **1994**, *313*, 349-354.

(131) Miyaura, N.; Suzuki, A. *Chem. Rev.* **1995**, *95*, 2457-2483.

(132) Meijere, A. D.; Meyer, F. E. *Angew. Chem. Int. Ed. Engl.* **1994**, *33*, 2379-2411.

(133) Narayanan, R.; El-Sayed, M. A. *J. Am. Chem. Soc.* **2003**, *125*, 8340-8347.

(134) Li, Y.; El-Sayed, M. A. *J. Phys. Chem. B* **2001**, *105*, 8938-8943.

(135) Klingelhofer, S.; Heitz, W.; Greiner, A.; Oestreich, S.; Forster, S.; Antonietti, M. *J. Am. Chem. Soc.* **1997**, *119*, 10116-10120.

(136) Reetz, M. T.; Lohmer, G. *Chem. Commun.* **1996**, 1921-1922.

(137) Beller, M.; Fischer, H.; Kuhlein, K.; Reisinger, C. -P.; Herrman, W. A. *J. Organomet. Chem* **1996**, *520*, 257-259.

(138) Bars, J. L.; Specht, U.; Bradley, J. S.; Blackmond, D. G. *Langmuir* **1999**, *15*, 7621-7625.

(139) Reetz, M. T.; Westermann, E. *Angew. Chem. Int. Ed.* **2000**, *39*, 165-168.

(140) Yeung, L. K.; Crooks, R. M. *Nano Lett.* **2001**, *1*, 14-17.

(141) Yeung, L. K.; Lee, C. T.; Johnston, K. P.; Crooks, R. M. *Chem. Commun.* **2001**, *2001*, 2290-2291.

(142) Rahim, E. H.; Kamounah, F. S.; Frederiksen, J.; Christensen, J. B. *Nano Lett.* **2001**, *1*, 499-501.

(143) Julia, M.; Duteil, M. *Bull. Soc. Chim. Fr.* **1973**, 2790.

(144) Marck, G.; Villiger, A.; Buchecker, R. *Tetrahedron Lett.* **1994**, *35*, 3277-3280.

(145) Felpin, F.-X.; Ayad, T.; Mitra, S. *Eur. J. Org. Chem.* **2006**, 2679-2690.

(146) Chen, X.; Hou, Y.; Wang, H.; Cao, Y.; He, J. *J. Phys. Chem. C* **2008**, *112*, 8172-8176.

(147) Zhong, L. S.; Hu, J. S.; Cui, Z. M.; Wan, L. J.; Song, W. G. *Chem. Mater.* **2007**, *19*, 4557-4562.

(148) Das, D. D.; Sayari, A. *J. Catal.* **2007**, *246*, 60-65.

(149) Choudary, B. M.; Madhi, S.; Chodari, N. S.; Kantam, M. L.; Sreedhar, B. *J. Am. Chem. Soc.* **2002**, *124*, 14127-14136.

(150) Cai, Y.; Jr., H. G. S.; Lyman, C. E. *J. Catal.* **1996**, *161*, 123-131.

(151) Reetz, M. T.; Breinbauer, R.; Wanninger, K. *Tetrahedron Lett.* **1996**, *37*, 4499-4502.

(152) Thathager, M. B.; Beckers, J.; Rothenberg, G. *J. Am. Chem. Soc.* **2002**, *124*, 11858-11859.

(153) Kovnir, K.; Osswald, J.; Armbruster, M.; Giedigkeit, R.; Ressler, T.; Grin, Y.; Schlogl, R. *Scientific Bases for the Preparation of Heterogenous Catalysts* **2006**, *162*, 481-488.

(154) Hirano, T.; Kazahaya, Y.; Nakamura, A.; Miyao, T.; Naito, S. *Catal. Lett.* **2007**, *117*, 73-78.

(155) Komatsu, T.; Inaba, K.; Uezono, T.; Onda, A.; Yashima, T. *Appl Catal. A: General* **2003**, *251*, 315-326.

(156) Miyaura, N.; Ishiyama, T.; Sasaki, H.; Ishikawa, M.; Satoh, M.; Suzuki, A. *J. Am. Chem. Soc.* **1989**, *111*, 314-321.

(157) Berthiol, F.; Doucet, H.; Santelli, M. *Tetrahedron Lett.* **2003**, *44*, 1221-1225.

(158) Bauer, J. C.; Chen, X.; Liu, Q.; Phan, T.-H.; Schaak, R. E. *J. Mater. Chem.* **2008**, *18*, 275-282.

(159) Son, S. U.; Jang, Y.; Park, J.; Na, H. B.; Park, H. M.; Yun, H. J.; Lee, J.; Hyeon, T. *J. Am Chem. Soc.* **2004**, *126*, 5026-5027.

(160) Li, Y.; Zhou, P.; Dai, Z.; Hu, Z.; Sun, P.; Bao, J. *New J. Chem.* **2006**, *30*, 832-837.

(161) Hirano, T.; Kazahaya, Y.; Nakamura, A.; Miyao, T.; Naito, S. *Catal. Lett.* **2007**, *117*, 73-78

(162) Kovnir, K.; Armbruster, M.; Tescher, D.; Venkov, T. V.; Jentoft, F. C.; Knop-, A.; Grin, Y.; Schlogl, R. *Sci. Tech. Adv. Mater.* **2007**, *8*, 420-427.

(163) Carey, F. A.; Sundberg, R. J., Eds. *Advanced Organic Chemistry*. Kluwer Academic / Plenum Publishers, New York, **2000**

(164) Sun, Y.; Xia,Y. *Science* **2002**, *298*, 2176-2179.

(165) Sun, Y.; Mayers, B.T.; Xia, B.T. *Nano Lett.* **2002**, *2*, 481-485.

(166) Chen, J.; Sadki, F.; Wiley, B. J.; Cang, H.; Cobb, M. J.; Li, Z.-Y.; Au, L;. Zhang, H;. Kimmey, M.B.; Li, X.; Xia, Y. *Nano Lett.* **2005**, *5,* 473-477.

(167) B. Wiley, Y. Sun, B. Mayers, Y. Xia *Chem. Eur. J.* **2005**, *11*, 454-463.

(168) Puntes, V. F.; Krishnan, K. M.; Alivisatos, A. P. *Science* **2001**, *291*, 2115-2117.

(169) Scher, E. C.; Manna, L.; Alivisatos, A.P. *Philos. Trans. R. Soc. London A* **2003**, *361*, 241-257.

(170) Sun, S. *Adv. Mater.* **2006**, *18*, 393-403.

(171) Coffey, K. R.; Parker, M. A.; Howard, J. K. *IEEE Trans. Magn.* **1995**, *31*, 2737-2739.

(172) Li, N.Lairson, B. M. *IEEE Trans. Magn.* **1999**, *35*, 1077-1082.

(173) Ristau, R. A.; Barmak, K.; Lewis, L. H.; Coffey, K. R.; Howard, J. K. *J. Appl. Phys.* **1999**, *86*, 4527-4533.

(174) Sun, S.; Murray, C. B.; Weller, D.; Folks, L.; Moser, A. *Science* **2000**, *287*, 1989-1992.

(175) Sun, S.; Fullerton, E. E.; Weller, D.; Murray, C. B. *IEEE Trans. Magn.* **2001**, *37*, 1239-1243.

(176) Chen, M.; Nikles, D. E. *Nano Lett.* **2002**, *2*, 211-214.

(177) Kang, S.; Harrell, J. W.; Nikles, D. E. *Nano Lett.* **2002**, *2*, 1033-1036.

(178) Stahl, B.; Gajbhiye, N. S.; Wilde, G.; Kramer, D.; Ellrich, J.; Ghafari, M.; Hahn, H.; Gleiter, H.; Weissmuller, J.; Wurschum, R.; Schlossmacher, P. *Adv. Mater.* **2002**, *14*, 24-27.

(179) Shevchenko, E.; Talapin, D.; Kornowski, A.; Kotzler, J.; Haase, M.; Rogach, A.; Weller, H. *Adv. Mater.* **2002**, *12*, 287-290.

(180) Stahl, B.; Ellrich, J.; Theissmann, R.; Ghafari, M.; Bhattacharya, S.; Hahn, H.; Gajbhiye, N. S.; Kramer, D.; Viswanath, R. N.; Weissmuller, J.; Gleiter, H. *Phys. Rev. B* **2003**, *67*, 1-12.

(181) Sun, S.; Anders, S.; Thompson, T.; Baglin, J. E. E.; Toney, M. F.; HAmmann, H. F.; Murrary, C. B.; Terris, B. D. *J. Phys. Chem. B* **2003**, *107*, 5419-5425.

(182) Iwaki, T.; Kakihara, Y.; Toda, T.; Abdullah, M.; Okuyama, K. *J. Appl. Phys.* **2003**, *94*, 6807-6811.

(183) Nakaya, M.; Tsuchiya, Y.; Ito, K.; Oumi, Y.; Sano, T.; Teranishi, T. *Chem. Lett.* **2004**, *33*, 130-131.

(184) Jeyadevan, B.; Urakawa, K.; Hobo, A.; Chinnasamy, N.; Shinoda, K.; Tohji, K.; Djayaprawira, D. D. J.; Tsunoda, M.; Takahashi, M. *Jpn. J. Appl. Phys.* **2003**, *42*, L350-L352.

(185) Jeyadevan, B.; Hobo, A.; Urakawa, K.; Chinnasamy, C. N.; Shinoda, K.; Tohji, K. *J. Appl. Phys.* **2003**, *93*, 7574-7576.

(186) Hinotsu, T.; Jeyadevan, B.; Chinnasamy, C. N.; Shinoda, K.; Tohji, K. *J. Appl. Phys.* **2004**, *95*, 7477-7479.

(187) Sato, K.; Jeyadevan, B.; Tohji, K. *J. Magn. Magn. Mater.* **2005**, *289*, 1-4.

(188) Minami, R.; Ktamoto, Y.; Chikata, T.; Kato, S. *Electrochim. Acta* **2005**, *51*, 864-866.

(189) Kitamoto, Y.; Minami, R.; Shibata, U.; Chikata, T.; Kato, S. *IEEE Trans. Magn.* **2005**, *41*, 3880-3882.

(190) Shinoda, K.; Sato, K.; Jeyadevan, B.; Tohji, K.; Suzuki, S. *J. Magn. Magn. Mater.* **2007**, *310*, 2387-2389.

(191) Jeyadevan, B.; Shinoda, K.; Justin, R. J.; Matsumoto, T.; Sato, K.; Takahashi, H.; Sato, Y.; Tohji, K. *IEEE Trans. Magn.* **2006**, *42*, 3030-3035.

(192) Nguyen, H. L.; Howard, L. E. M.; Stinton, G. W.; Giblin, S. R.; Tanner, B. K.; Terry, I.; Hughes, A. K.; Ross, I. M.; Serres, A.; Evans, J. S. O. *Chem. Mater.* **2006**, *18*, 6414-6424.

(193) Platt, C. L.; Wierman, K. W.; Svedberg, E. B.; Veerdonk, R. v. d.; Howard, J. K.; Roy, A. G.; Laughlin, D. E. *J. Appl. Phys.* **2002**, *92*, 6104-6109.

(194) Kitakami, O.; Shimada, Y.; Oikawa, K.; Daimon, H.; Fukamichi, K. *Appl. Phys. Lett.* **2001**, *78*, 1104-1106.

(195) Kang, S.; Harrel, J. W.; Nikles, D. E. *Nano Lett.* **2002**, *2*, 1033-1036.

(196) Kitakami, O.; Shimada, Y.; Oikawa, K.; Daimon, H.; Fukamichi, K. *Appl. Phys. Lett.* **2001**, *78*, 1104-1106.

(197) Sort, J.; Surinach, S.; Baro, M. D.; Muraviev, D.; Dzhardimalieva, G. I.; Golubeva, N. D.; Pomogailo, S. I.; Pomogailo, A. D.; Macedo, W. A. A. *Adv. Mater.* **2006**, *18*, 466-470.

(198) Yan, Q.; Purkayastha, A.; Kim, T.; Kroger, R.; Bose, A.; Ramanath, G. *Adv. Mater.* **2006**, *18*, 2569-2573.

(199) Simeonidis, K.; Mourdikoudis, S.; Tsiaoussis, I.; Dendrinou-Samara, C.; Angelakeris, M.; Kalogirou, O. *J. Magn. Magn. Mater.* **2008**, *320*, 2665-2671.

(200) Sato, E. K.; Hirotsu, Y. *Mater. Trans.* **2003**, *44*, 1518-1522.

(201) Jia, Z.; Kang, S.; Shi, S.; Nikles, D. E.; Harrell, J. W. *J. Appl. Phys.* **2006**, *99*, 08E904-1 - 08E904-3.

(202) Nandwana, V.; Elkins, K. E.; Poudyal, N.; Chaubey, G. S.; Yano, K.; Liu, J. P. *J. Phys. Chem. C* **2007**, *111*, 4185-4189.

(203) Margeat, O.; Tran, M.; Spasova, M.; Farle, M. *Phys. Rev. B* **2007**, *75*, 134410-1 - 134410-7.

(204) Poudyal, N.; Chaubey, G. S.; Nandwana, V.; Rong, C.-B.; Yano, K.; Liu, J. P. *Nanotechnology* **2008**, *19*, 355601-35604.

(205) Tsukamoto, R.; Muraoka, M.; Seki, M.; Tabata, H.; Yamashita, I. *Chem. Mater.* **2007**, *19*, 2389-2391.

206) Narayanan, R.; El-Sayed, M. A. *J. Phys. Chem. B*, **2004**, *108*, 5726-5733.

(207) Céline Dupont, Yvette Jugnet, and David Loffreda *J. Am. Chem. Soc.* **2006**, *128*, 9129–9136

(208) Rioux, R. M.; Song, H.; Grass, M.; Habas, S.; Niesz, K.; Hoefelmever, J. D.; Yang, P.; Somorjai, G. A. *Topics in Catalysts* **2006**, *39*, 167-174.

(209) Ahmadi, T. S.; Wang, Z. L.; Henglein, A.; El-Sayed, M. A. *Chem. Mater.* **1996**, *8*, 1161-1163.

(210) Narayanan, R.; El-Sayed, M. A. *Nano Lett.* **2004**, *4*, 1343-1348.

(211) Wang, C.; Daimon, H.; Lee, Y.; Kim, J.; Sun, S. *J. Am Chem. Soc.* **2007**, *129*, 6974-6975.

(212) Yamada, M.; Kon, S.; Miyake, M. *Chem. Lett.* **2005**, *34*, 1050-1051.

(213) Fu, X.; Wang, Y.; Wu, N.; Gui, L.; Tang, Y. *Langmuir* **2002**, *18*, 4619-4624.

(214) Song, H.; Kim, F.; Connor, S.; Somorjai, G. A.; Yang, P. *J. Phys. Chem. B* **2005**, *109*, 188-193.

(215) Maksimuk, S.; Teng, X.; Yang, H. *Phys. Chem. Chem. Phys.* **2006**, *8*, 4660-4663.

(216) Teng, X.; Yang, H. *Nano Lett.* **2005**, *5*, 885-891.

(217) Maksimuk, S.; Teng, X.; Yang, H. *J. Phys. Chem. C* **2007**, *111*, 14312-14319.

(218) Chen, J.; Herricks, T.; Geissler, M.; Xia, Y. *J. Am Chem. Soc.* **2004**, *126*, 10854-10855.

(219) Chen, J.; Xiong, Y.; Yin, Y.; Xia, Y. *Small* **2006**, *11*, 134-1343.

(220) Shen, Z.; Yamada, M.; Miyake, M. *Chem. Commun.* **2007**, 245-247.

(221) Lee, E. P.; Chen, J.; Yin, Y.; Campbell, C. T.; Xia, Y. *Adv. Mater.* **2006**, *18*, 3271-3274.

(222) Shinoda, K.; Sato, K.; Jeyadevan, B.; Tohji, K. *IEEE Trans. Magn.* **2006**, *42*, 3051-3053.

(223) Tian, N.; Zhou, Z.-Y.; Sun, S.-G.; Ding, Y.; Wang, Z. L. *Science* **2007**, *316*, 732-735.

(224) Xiong, Y.; Wiley, B. J.; Xia, Y. *Angew. Chem. Int. Ed.* **2007**, *46*, 7154-7159.

VITA

John Christopher Bauer received his Bachelor of Arts degree in chemistry at Louisiana Tech University at Ruston Louisiana in May 2004. He entered the Chemistry program at Texas A&M University in August 2004 and received his Ph. D in May 2009. His research interest includes low-temperature synthesis of alloys, intermetallic compounds, and multi-metal oxides using metal and metal oxide nanoparticles as reactive precursors. He is also interested in the low-temperature synthesis of intermetallic nanoparticles (using conversion chemistry methods in solution) for possible application in catalysis such as alcohol electro-oxidation, gas phase CO oxidation, and carbon-carbon coupling reactions. He has also studied the possibility of making intermetallic shape-controlled nanocrystals of magnetic (Fe-Pt systems) and catalytic (Pt-Sn system) materials.

Chris Bauer may be reached at the Department of Chemistry, Texas A&M University, PO Box 30012, College Station, TX 77842-3012. His email is: jbauer@mail.chem.tamu.edu.